QUANTUM DOT LABELING OF MEMBRANE ASSOCIATED TARGETS: THE DEVELOPMENT OF SMALL MOLECULE CONJUGATES TO INTERROGATE THE SEROTONIN TRANSPORTER PROTEIN

By

Michael Robert Warnement

Dissertation

Submitted to the Faculty of the

Graduate School of Vanderbilt University

in partial fulfillment of the requirements

for the degree of

DOCTOR OF PHILOSOPHY

in

Chemistry

December, 2008

Nashville, Tennessee

Approved:

Professor Sandra J. Rosenthal

Professor David E. Cliffel

Professor Michael P. Stone

Professor John P. Wikswo

Professor David W. Wright

To my supportive parents, Robert and Joann

and

To my loving wife and best friend, Maria Paula

ACKNOWLEDGEMENTS

My own personal pursuit of this doctoral degree can hardly be classified as an individual endeavor. As such, there are certainly a great number of people and institutions which have played an integral part of my attainment of this high honor. However, following the precedent established by academic institutions in general, I would like to place my initial focus on monetary matters. Therefore, I gratefully acknowledge financial support from both the National Institute of Health (Grants EB003728 and GM72048-02) and the Vanderbilt Institute for Integrative Biosystems Research and Education (VIIBRE). I would also like to acknowledge a fellowship provided through the Vanderbilt Institute for Nanoscale Science and Engineering (VINSE). The generous support of each of these institutions has undoubtedly enhanced my graduate school experience.

I would like to take this opportunity to acknowledge the incredible amount of support and mentoring offered to me by my graduate advisor, Dr. Sandra J. Rosenthal. I initially would like to thank her for just accepting me into the group against the advice of a senior graduate student (who shall remain unnamed). I can recall from my first day as a rotation student when I initially addressed Sandy as ‘Dr. Rosenthal,’ and I was quickly reprimanded by her saying “Call me Sandy, from here on out we are colleagues and you don’t need to address me as ‘Dr. Rosenthal.’” It was immediately apparent to me that she earned respect by giving respect, and I have come to develop a great deal of respect and admiration for her own unique leadership style. I appreciate the challenging, interdisciplinary project which I was given, and the incredible effort which she undertook

to ensure it was funded. I especially appreciate the trust she placed in me by giving me the important job of ensuring the group's fridge was continuously filled with beer, and I sincerely hope I have met or exceeded her expectations in this critical role of malted beverage management.

I would also like to thank my committee members, Professors David Cliffel, David Wright, John Wikswo, and Michael Stone for their support and guidance throughout the course of this research. While committee meetings have a way of being a uniquely terrifying undertaking, they always proved to be constructive and resulted in the focusing of my research to productive ends. Additionally, I would like to thank our collaborators Dr. Randy Blakely and Dr. Dave Piston for their input and insight at numerous points along the way. Meetings with either of these collaborators frequently resulted in new and exciting approaches to tackling difficult research problems.

If I had to blame anybody for my decision to become a chemist and eventually attend graduate school it would certainly be my undergraduate mentors Dr. Jerry Keil and Dr. Howard Knachel. As such, I would like to express my gratitude to both of them for all of their advice and support; they've obviously had a profound impact on the course my life has taken. I consider myself lucky to have learned from both of them at the University of Dayton, and even luckier to know them later in life as friends.

I am well aware that none of this research would have gotten done without the support and assistance of the entire Rosenthal research group. I would especially like to thank Jerry Chang for joining the group and bringing his undeniable excitement and energy to what would otherwise digress into monotonous day-to-day research. Jerry was the first to identify a suitable ligand to specifically target SERT and I am thankful to him

for making this exciting discovery, which obviously has accelerated all research efforts on our side of the group. Additionally, I would like to acknowledge the efforts of Ian Tomlinson in synthesizing the small molecule compounds which my research was critically dependent upon. Anyone who has ever worked with Ian can attest to the character with which he conducts his research. Thanks also go out to all other group members past and present, including James McBride, Michael Bowers, Danielle Garrett, Rebecca Orndorff, Michael Schreuder, Albert Dukes and Nat Smith, for countless informative and/or entertaining discussions and for generally creating a productive and entertaining place to work. Additionally, I also owe a special debt of gratitude to all the past and present members of the Wright research group which was almost like a second group for me.

I consider myself blessed to have met some pretty remarkable friends during my tenure as a graduate student, and for the sake of brevity, I'll just say 'thanks.' You know who you are, and I doubt many of you will even be reading this!

The greatest blessing I have in life has been the love and support of a remarkable family. I would like to thank my incredible parents, Bob and Joann, for, quite simply, everything... love, support, pride, education, character, faith. I am thankful each and every day to have been blessed to have the two of you as my parents. I consider myself lucky to have loving brothers and sisters: Matt, Mary Claire, Mollie, Megan, Bill and Eric. And I have even recently been blessed with the addition of an entirely new family in Costa Rica! I am fortunate to be able to say that I have the best mother-in-law and father-in-law in the entire world, and I am grateful for the way all the *ticos* have accepted me into their family.

Finally, and undoubtedly most importantly, I would like to express my gratitude for my loving wife Maria Paula. I know now that I was meant to come to graduate school to find you, and I am grateful for each and every minute we are able to spend together.

TABLE OF CONTENTS

LIST OF TABLES

LIST OF FIGURES

LIST OF SCHEMES

CHAPTER I

FLUORESCENT IMAGING APPLICATIONS OF QUANTUM DOT PROBES [*1*]

Introduction

Highly fluorescent semiconductor nanocrystals, or quantum dots (QDs), were initially incorporated into biological imaging applications concurrently by two groups in 1998 [*2, 3*]. Since that time, an ever increasing amount of research has been devoted to expanding their use in various biological applications. All of this research's promise is based upon the unique photophysical properties inherent to QDs, which provide numerous advantages over conventional organic dyes in several fluorescent imaging applications. Specifically, QDs have been engineered to have a narrow, size-tunable fluorescent emission which is extremely bright and photostable. These emission properties are characteristically different from organic fluorophores, which generally have broad, log-normal fluorescent spectra subject to rapid photobleaching. Consequently, QDs have been utilized as improved probes for multiplexed, dynamic imaging applications, both *in vitro* and *in vivo*, owing to their narrow, photostable fluorescence. Additionally, their improved brightness even facilitates receptor trafficking experiments with enhanced sensitivities at the single molecule level. Despite the promise of these, and a myriad of other applications, the primary challenge with any QD-based fluorescence assay involves incorporating a suitable QD surface chemistry which will specifically interact with a biological target of interest, without interfering with the nanocrystal's optical properties.

The unique, size-tunable optical properties of QDs result from the quantum confinement of the electron-hole pair, or exciton, formed after the absorption of a photon

by a semiconductor material. Confinement of this exciton leads to the emergence of discrete electronic states in the nanocrystal and size dependent electronic and optical properties. Several excellent review articles are available which discuss, in greater detail, this quantum confinement effect as it relates to biological imaging applications [*4-8*]. Of particular importance is the idea that QDs can be specifically engineered to be highly fluorescent by encapsulating one nanocrystalline semiconductor core within a differing, wider band gap, semiconductor shell. This "core/shell" architecture, illustrated schematically in Figure 1-1A, is routinely used to generate QDs with exceptionally high quantum yields, capable of exceeding 85%. Structural characterization by means of high resolution atomic number contrast scanning transmission electron microscopy (Z-STEM) has been used to illustrate the importance of a uniform, defect free shell coverage in the synthesis of high quantum yield materials (Figure 1-1B) [*9*]. This shell acts to passivate reactive surface states present on the core, eliminating several non-radiative relaxation processes, ultimately allowing for an improved quantum yield. Additionally, the size dependent optical properties permit the fluorescent emission to be tuned across the visible spectrum and into the near infrared (NIR) by varying the QD size or composition. A representative series of fluorescent emission spectra, displayed in Figure 1-1C, clearly demonstrate this optical tunability and narrow fluorescent lineshape. Overall, this bright, stable, narrow, tunable fluorescence has the promise to expand biological imaging applications well beyond current capabilities.

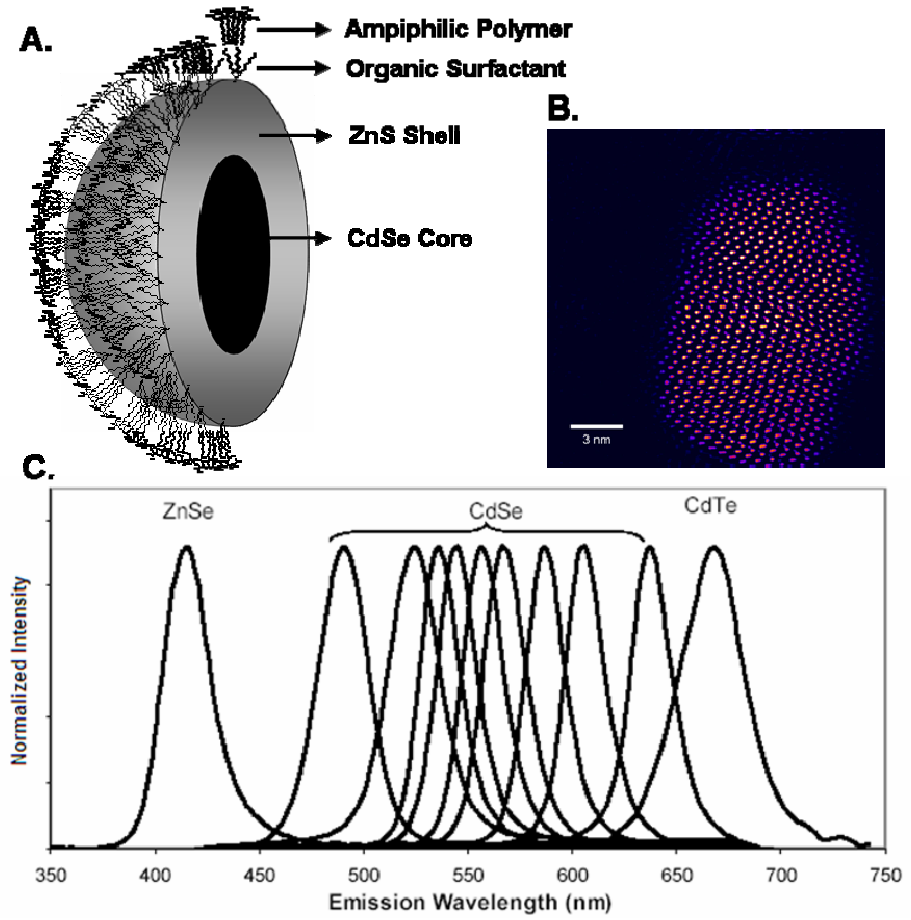

Figure 1-1. Properties of biologically compatible semiconductor quantum dots. (A) Cartoon schematic illustrating core/shell architecture and ampiphilic polymer coating rendering the QD water soluble. (B) High resolution atomic number contrast scanning transmission electron (Z-STEM) micrograph of individual CdSe cores [*9*]. At this resolution it is possible to simultaneously identify both atomic composition and structural information. (C) Fluorescent emission spectra for a series of core/shell nanocrystals. Narrow, gaussian emissions can be tuned across the entire visible spectrum by varying either particle size and/or composition. CdSe nanocrystals are of particular interest for fluorescent imaging applications since their fluorescent emission can be tuned across the entire visible spectrum. Incorporation of CdTe materials allow for the fluorescence to be extended into the near-IR region which is of great interest for *in vivo* imaging applications.

The development of synthetic strategies for surface modifications which enable water solubility, selective targeting, and minimal nonspecific interactions have proven to be a significant challenge facing the application of QDs to biological systems. This chapter will highlight developments in surface modification which have allowed for the specific targeting of cellular targets, followed by a thorough discussion of recent, noteworthy QD

fluorescent imaging applications. The remainder of this chapter will then outline a small molecule targeting strategy for the development of fluorescent QD-conjugates as improved probes for neurotransmitter transporter proteins.

Surface Modification and Biomolecule Attachment

Given the inorganic, hydrophobic nature of these semiconductor nanocrystals, a suitable surface modification which primarily renders the QDs water soluble, and further limits nonspecific cellular interactions, is of critical importance for the development of biologically compatible fluorophores. This section is initially focused on a discussion of methodologies which have been employed to disperse QDs in aqueous solution. Surface modifications which have been designed to limit nonspecific interactions are subsequently described, including covalent attachment mechanisms suitable for biomolecule functionalization. Finally, several applications that employ the high affinity streptavidin-biotin interaction to facilitate the specific cellular targeting of these QD conjugates are discussed.

Water Solubilization

Due to their size dependant optical properties, a monodisperse distribution of QDs is absolutely essential to obtain the narrow fluorescent emission spectra desired for biological applications. The traditional synthetic methodology for maintaining this very narrow size distribution involves the pyrolysis of organometallic precursors at high temperatures in a coordinating surfactant solvent such as trioctylphospine oxide (TOPO) [*10, 11*]. This synthesis yields hydrophobic core/shell nanocrystals which are only soluble in non-polar organic solvents due to the alkyl nature of the TOPO coordinating

surfactant. The development of biocompatible conjugates is primarily dependent upon the ability to render these as-synthesized hydrophobic nanocrystals water-soluble. Initial strategies at water solubilization all employed a ligand exchange strategy to displace the hydrophobic surfactant from the QD surface altogether. This ligand exchange methodology utilizes a reactive free thiol to displace the TOPO coordinating surfactant ligands replacing them, instead, with hydrophilic moieties. Silinazed QDs [*2, 12*], mercaptoacetic acid (MAA) [*3, 13*] mercaptoundecanoic acid (MUA) [*14*] QDs, and dihydrolipoic acid (DHLA) modified QDs [*15-17*] all employ this ligand exchange methodology to stabilize the nanocrystal in aqueous media. Despite several initial advances with these types of nanocrystal, chemical modification directly at the QD surface has been shown to be more likely to have an effect on their desired optical properties. The long term stability of these nanocrystals in aqueous solutions has also been called into question.

In order to overcome these shortcomings, alternate strategies to disperse the QDs in aqueous solutions have been developed which utilize bifunctional hydrophobic/hydrophilic compounds to self assemble onto the hydrophobic QD surface. In this architecture the hydrophobic organic capping ligands are retained, but they are encapsulated in a lipid or bifunctional polymeric material with sufficient hydrophilicity to disperse the QDs in aqueous solutions. An initial example of this approach used phospholipids to encapsulate QDs in the hydrophobic core of a micelle [*18*]. In this experiment, a mixture of n-polyethylene glycol phosphatidylethanolamine (PEG-PE) and phosphatidylcholine (PC), micelle-forming polymer-grafted lipids, were allowed to assemble onto the surface of the QD forming a water soluble micelle, effectively trapping

a QD in the hydrophobic core. This resulted in a suspension of nanocrystals with improved colloidal stability and minimal nonspecific cellular interactions. A similar methodology utilizes ampiphilic polymers to encapsulate the hydrophobic QD in a hydrophilic polymeric shell [*19-21*]. As illustrated in Figure 1-1A, the alternating nature of the ampiphilic polymer allows the hydrophobic alkyl chains to intercalate with the TOPO ligands present on the QD surface, while the hydrophilic carboxylic acid functionality renders the nanocrystal water soluble. These carboxylic acids also permit further functionalization as a means to introduce biological specificity. Additionally, these QDs have been shown to display excellent stability in aqueous solutions and, since there is no chemical reaction directly at the QD surface, the inherent photophysical properties are retained. This type of hydrophobic/hydrophilic assembly has emerged as the preferred methodology for biological imaging applications, as is evident by the extensive commercial development of these probes. Notably, Evident Technologies® has adopted the phospholipids micelle approach for their water soluble product line; while Invitrogen® (which acquired Quantum Dot Corp.) utilizes ampiphilic poly(acrylic) acid (AMP) coated QD as the basis of all their commercially available QD-congujates. Although detractors may claim improved specificity and decreased hydrodynamic diameter of alternate approaches, the improved colloid stability and optical properties outweigh these disadvantages for most applications.

Reduction of Nonspecific Cellular Interactions

Having addressed the initial challenge of rendering QDs water soluble, methodologies for eliminating nonspecific cellular interactions to generate optimized

fluorescence detection will be discussed. Given the widespread utilization of the AMP-QD platform, the remaining discussion will focus on surface modifications of this particular platform for optimized incorporation in biological applications. It has been reported that the carboxylic acid functionality on the surface of AMP-QDs lead to nonspecific interactions with oligonucleotides [*22*], and passivation of this surface with PEG derivatives reduces these nonspecific interactions in mouse animal models [*23*]. Consequently, nonspecific binding (NSB) of AMP-QDs to a cell's surface is presumably the result of a combination of both hydrophobic/hydrophilic and electrostatic interactions of the reactive carboxylic acid surface with the cell's plasma membrane and surface proteins. This interaction has also been demonstrated to be highly dependent upon the different cell lines employed in various studies [*24*]. As illustrated in Figure 1-2, differing cell types clearly yield a differential amount of NSB ranging from extremely high backgrounds in HEK cells, moderate labeling in HEp-2 and CHO cell lines, to minimal interactions with LLC cells. In all cases, however, modification of the AMP-QD surface with PEG reduces the amount of NSB present, regardless of cell line. PEG modification, consequently, allows a generalized approach for the reduction of the NSB of QDs to both live and fixed cells.

Standard immunohistochemical blocking strategies, such as bovine serum albumin or fetal bovine serum blocking solutions, can also be used in conjunction with these surface modifications to further reduce NSB. Care must be taken, however, to optimize blocking conditions for the particular system of interest as demonstrated by Pathak *et al.* [*25*]. Additionally, Hanaki *et al.* have demonstrated the capability of QD-albumin complexes to associate in the endosomes of living cells [*14*]. As a consequence, one must carefully

ensure that albumin, present in standard blocking solutions, is not complexing to the QDs and interfering with the observed biological interaction. This seemingly subtle association introduces the possibility of numerous false positives and other interferences associated with QD-based live cell imaging applications. Complete passivation of the QD surface with PEG ensures minimal albumin-QD association and can be verified by standard chromatographic techniques, as demonstrated by Zimmer *et al.* for extremely small InAs/ZnSe core/shell QDs [*26*].

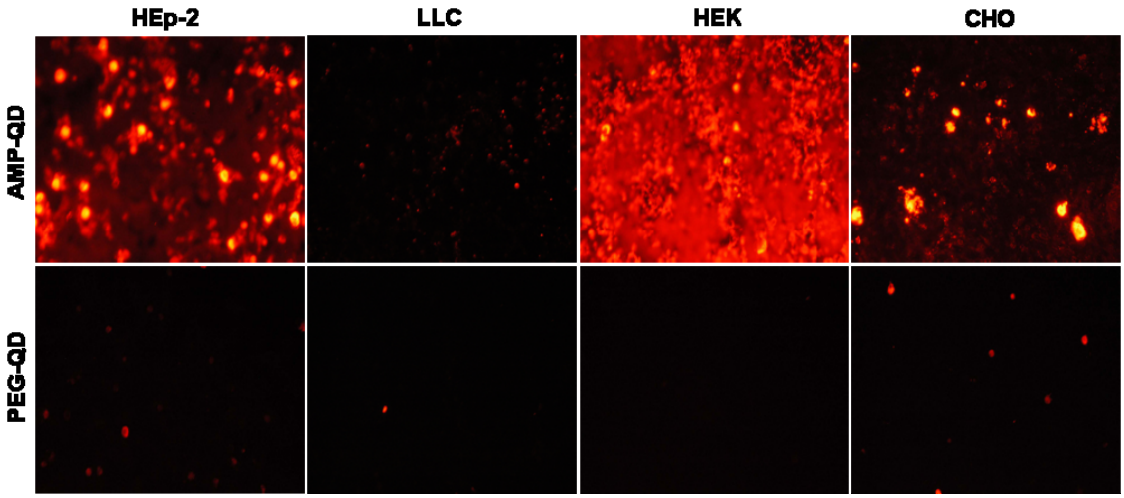

Figure 1-2. Comparison of the non-specific interactions of 30 nM AMP-QDs (top images) to 30 nM PEG-QD conjugates (bottom images). Non-specific binding of AMP-QDs varies in intensity for different cell lines, as illustrated for (from left to right) HEp-2, LLC, HEK, and CHO cells. In all cases, however, PEG surface modifications reduce these non-specific interactions, allowing for improved specificity and sensitivity of detection. Adapted from [*24*].

Covalent Conjugation Methodologies

Taking into account the modifications required to eliminate, or at least reduce, nonspecific cellular interactions, this section will detail attachment strategies available for further modifications to the QD surface in order to introduce biological specificity of QD probes to a given cellular target. Numerous attachment strategies are available given the reactive carboxylic acid functionality of the AMP-QD surface. Covalent attachment

by means of a 1-ethyl-3-(3-dimethylaminopropyl) carboiimide (EDC) coupling has been reported extensively. This EDC coupling strategy is widely employed in general peptide synthetic chemistry as it covalently attaches a carboxylic acid to a terminal amine [*27*]. As terminal amines are prevalent in antibodies and peptides, and can be introduced into small molecule derivatives, this methodology permits covalent attachment of a wide variety of biomolecules directly to the QD surface. In the rare case where no terminal amine is available, or in order to avoid crosslinking compounds with multiple terminal amines present, an alternate covalent attachment of a free thiol can be carried out via a malemide coupling. This attachment methodology involves first coupling a bifunctional linker arm with both amine and sulfhydryl reactivity (i.e. SMCC, Sigma Aldrich Cat. # M5525) via EDC coupling to introduce a malemide to the surface of amine terminated QDs. This malemide can then be allowed to form a covalent bond with a free thiol, often providing a more selective attachment of biomolecules. These two covalent attachment mechanisms, EDC and malemide, have been the predominant methodologies employed to modify the AMP-QD surface to facilitate a specific interaction with a cellular target.

Streptavidin-Biotin Assembly

One alternate attachment methodology incorporates the extremely high affinity streptavidin-biotin interaction to specifically target cellular processes. This approach was initially proposed in the first reported application of QDs for biological imaging [*2*], and has since found wide scale use due to commercially available products from both Invitrogen® and Evident Technologies. While this interaction is not intrinsically covalent in nature, it is one of the tightest non-covalent interactions known, with a sub-*pico*molar

dissociation constant and off rates on the order of days [*28*]. Additionally, streptavidin conjugates yield very little endogenous labeling and are stable for several months in solution. Several noteworthy applications have employed streptavidin-conjugated QDs for attachment to a specific biotinylated biomolecule. Lidke *et al.* conjugated a biotinylated epidermal growth factor (EGF) to streptavidin-QDs and were able to dynamically observe retrograde transport of individual conjugates and monitor their subsequent endosomal trafficking [*29*]. The QDs' inherent photostability permits these dynamic cellular processes to be imaged on time scales previously unattainable with organic dyes. Additionally, this experiment provides verification that the seemingly bulky size of the QD-streptavidin conjugate does not sterically interfere with the binding and function of the EGF ligand. Streptavidin conjugated QDs have also been employed, following attachment of biotinylated kinesins, to elucidate the intracellular dynamics of these single molecular motors [*30*]. Similarly, biotinylated Annexin V conjugated to streptavidin QDs has been shown to specifically target apoptotic cells via recognition of phosphatidylserine, an inner-leaflet phospholipid present in the outer-leaflet of the cell membrane during programmed cell death [*31*]. While these three examples all utilize biotinylated versions of receptor-specific proteins, there is an extensive literature precedent showing that biotinylation of any biomolecule (i.e. antibody, peptide, DNA, or small molecule) is a suitable mechanism for QD conjugation.

Recently, Howarth *et al.* have proposed an alternate and extremely versatile method for the attachment of QDs to a variety of surface proteins *in vitro* [*32*]. This approach, as illustrated in Figure 1-3A, uses the *Escherichia coli* enzyme biotin ligase (BirA) to covalently attach biotin to a fifteen amino acid sequence called the acceptor peptide (AP).

Specificity is introduced by genetically encoding the AP sequence at the C or N terminus of the target protein. Since specificity is not dependant upon antibody-antigen or ligand-receptor type interactions, which have varying degrees of instability, the resulting labeling is extremely robust and essentially covalent in nature, given the extremely high affinity of streptavidin for biotin. Additionally, the overall size of the QD probe is reduced since no further biomolecule attachment is necessary to facilitate a specific interaction. In this initial paper, the authors genetically introduce the acceptor peptide sequence into both the platelet-derived growth factor receptor and glutamate receptor subunit 2 (GluR2, Figure 1-3B) and observe QD labeling for both, demonstrating the versatility of this approach. Furthermore, a point mutation in the AP sequence, or experiments performed in the absence of either BirA or biotin, result in no observable QD labeling, illustrating exquisite specificity. Receptor trafficking experiments were subsequently performed and seem to indicate decreased accessibility of QD-labeled GluR2 receptors to neural synapses compared to organic dye labeled receptors, presumably as a result of the QD's relatively bulkier size (Figure 1-3B). Similar receptor trafficking experiments have since been performed by an alternate group which utilize this enzymatic biotinylation as a means of targeting streptavidin QDs to Kv2.1 potassium channels [*33*]. It is apparent that enzymatic modification of cell surface proteins can now be considered a specific, sensitive and versatile approach for *in vitro* QD labeling applications.

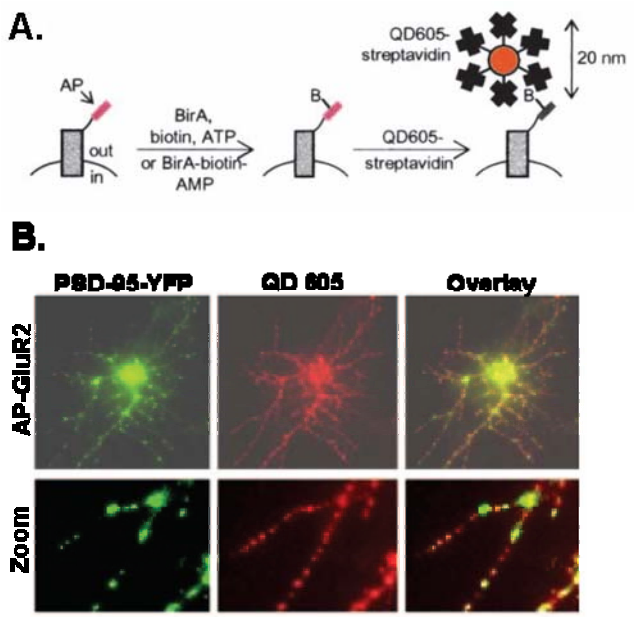

Figure 1-3. Enzymatic modification of target protein and subsequent QD labeling proposed by Howarth et al. (A) An acceptor peptide (AP) sequence, GLNDIFEAQKIEWHE, is first genetically encoded at the C or N terminus of the protein of interest. Biotin ligase (BirA) then enzymatically attaches biotin, in the presence of ATP, to this AP. Finally, streptavidin-conjugated QDs are allowed to bind the biotin, resulting in a specific and extremely stable interaction. (B) Detection of QD labeling in hippocampal neurons expressing an AP-tagged glutamate receptor (AP-GluR2) and the synaptic marker PSD-95-YFP. Exposure to BirA for 10 min at 37 °C, and subsequent staining with streptavidin-QD605, results in the specific QD labeling of AP-GluR2 (*top*). A zoomed in view (*bottom*) illustrates that some synaptic AP-GluR2 molecules, indicated by PSD-95-YFP, are not accessible to the streptavidin QDs, presumably due to the QD size. Reproduced with permission from [*32*].

Conjugates to Introduce Biological Specificity

Directing QDs to specifically interact with a particular cellular target has traditionally been accomplished by biomolecule conjugation. Broadly categorized, this biological specificity has been introduced by attachment of either antibody [*16, 19, 34-42*], peptide [*13, 42-56*], DNA [*18, 22, 57-60*], or small molecule [*61, 62*] biomolecules. Consequently, these resulting QD-conjugates function as a nano-scaffold, incorporating biological functionality to facilitate a specific interaction while retaining the improved spectroscopic properties of the QD. In this section, advantages and disadvantages of

differing approaches which have been used to introduce biological specificity will be discussed.

Antibodies have been used extensively in QD imaging applications due to both the specificity introduced by the antibody-antigen interaction, as well as the plethora of antigen targets obtainable by established antibody production techniques. Additionally, standard immunohistochemical labeling protocols, initially developed for conventional fluorophores, are easily applied to QD-based systems. As a general method, a primary antibody is initially used to target the specific cellular target of interest, and a secondary antibody attached to a QD, either covalently or through a streptavidin-biotin bridge, is then used to detect the primary antibody. While this two step scaffolding approach may seem somewhat redundant, it is often employed to conserve supplies of the expensive primary antibody, and also allow one type of QD conjugate to label a wide variety of cellular targets. Alternately, primary antibodies can be covalently attached directly to the QD via standard, commercially available coupling techniques circumventing the necessity of this two-step approach. Regardless of the protocol employed, QD immunofluorescent labeling has been demonstrated for targets ranging from membrane bound cancer markers [*19, 21, 37*], to glycoproteins [*16*], neurotransmitter receptors [*34*], viral fusion proteins [*35*], and immunological cytokine receptors [*40*]. Despite the diversity of targets available to this approach there are, however, associated disadvantages with these antibody conjugates. Of primary concern, antibodies are generally expensive; often times costing several hundred dollars for a few precious micrograms, assuming of course that a commercially available antibody even exists. Secondly, while the antibody-antigen interaction is generally strong, it is variable from

antibody to antibody which introduces added experimental complexity. Finally, the relatively large size of the antibody (~150 kDa) adds increased steric bulk to the already sizeable QD probe. Despite these noteworthy disadvantages, antibody conjugates continue to provide a versatile targeting approach for QD-based fluorescent assays.

Peptide conjugates have also been employed as a means of introducing biological specificity for QD targeting applications. Peptides, the building blocks of proteins, are biologically relevant amino acid sequences that interact with proteins through sequence-specific peptide-protein interactions. Once again, as in the case of antibody recognition, the strength of these peptide-protein interactions are highly variable, but peptides have the added advantage of being considerably smaller in size and have significantly less expense associated with synthesis. Signaling peptides involved in post translational transport of proteins, such as the nuclear localization signal (NLS) peptide, have been attached to QDs and demonstrate effective delivery to assigned cellular organelle [*44, 52*]. Cationic cell-penetrating peptides, such as TAT, Pep-1 and poly-arginine sequences, have been employed to facilitate intracellular delivery of QD probes [*51, 53, 54*], while arginine-glycine-aspartic acid (RGD) peptides have proven to efficiently direct QDs to integrin $\alpha_v\beta_3$, a cell surface receptor overexpressed in several tumor vasculatures, both *in vitro* and *in vivo* [*42, 45, 55*]. Additionally, angiotensin, a circulating peptide involved in signaling cascades for the cardiovascular, renal and central nervous systems, has been used with QDs to interrogate angiotensin receptor expression *in vitro* [*48, 56*]. A significant drawback with peptide mediated QD targeting approaches is that they cannot be universally applied to any given cellular target, as these techniques are only effective in systems where a known peptide functions as a natural substrate. As a result, peptide

conjugation lacks the diversity of an antibody-based approach, but still continues to facilitate numerous imaging applications.

Biological recognition can also be incorporated in the QD nanoarchitecture through the use of biologically active small molecule conjugates. These small molecule nanoconjugates rely on ligand-receptor interactions to provide specificity. While the nature of these interactions is variable in strength, they can be systematically optimized through improved ligand design. Additionally, this small molecule targeting approach can design conjugates that elicit either an agonistic or antagonistic response, which is to say they can either cause or inhibit a physiological response subsequent to binding, providing an additional degree of experimental control for imaging experiments. The cost associated with synthesis is reduced compared to either antibody or peptide conjugates, and the size of the biomolecule is obviously not as significant a concern as in the antibody conjugate. Also, an extremely wide variety of cellular targets are available either through rational ligand design based on a receptor's known substrate or derivatives of drug candidates from the known pharmocopia. The feasibility of this approach was initially demonstrated with the specific labeling of serotonin transporter (SERT) proteins using serotonin derivatized QDs [*61*], and has since been applied to gamma-aminobutyric acid (GABA) neurotransmitter receptors with muscimol-conjugated QDs [*62*]. As with previous methodologies, there are associated limitations of this approach including a time-consuming, iterative ligand optimization process, which will be described in greater detail in a subsequent section of this chapter. Additionally, ligand presentation (i.e. surface coverage of the nanocrystal, linker arm composition, linker length, etc.) has to be optimized for each small molecule to insure a suitably robust interaction with a cellular

target. Continued development, however, should alleviate some of the technical difficulties associated with small molecule design and presentation, ultimately allowing for an increasingly versatile QD targeting methodology.

Alternate approaches also exist for incorporation of QDs into biologically relevant assays, although they are currently limited in number compared to these conventional biomolecule attachment methodologies. Utilizing specific DNA interactions, QDs have been shown to be effective fluorescence in situ hybridization (FISH) probes following surface derivatization with oligionucleotides [*57-60*]. Additionally, non-targeted QDs can also be incorporated into biological assays without any additional biomolecule attachment. An assay to measure metastatic potential by imaging phagokinetic tracks utilizes QDs without any specific biological recognition functionality [*63*], and passive endocytosis of non-targeted QDs proved sufficient to demonstrate the improved sensitivities of these probes via time-gated fluorescence imaging [*64*]. Recent applications have even demonstrated QD self-assembled encapsulation in viral capsids yielding a particle similar in many respects to a native virus [*65*]. Undoubtedly, alternate and novel surface modifications, which may ultimately incorporate improved biological recognition elements, will continue to emerge given the continued expansion of research in this field. In the meantime, however, sufficient targeting options are currently available which have allowed for numerous QD-based fluorescent imaging applications.

Previously Reported Quantum Dot Imaging Applications

Having addressed the current scaffolding techniques for incorporation of QDs into biological assays, several reported applications utilizing these biologically compatible

QDs which allow for improved fluorescent imaging experiments will now be highlighted. While the superior spectral characteristics of QD fluorophores continues to allow for further improvement beyond existing fluorescence imaging limitations, this section will hopefully provide a snapshot of what is currently considered to be state-of-the-art in QD imaging methodology.

Multicolor Fluorescent Imaging

The narrow fluorescent emission spectra of QDs have always been associated with an added promise of increased multiplexing capabilities. While multicolor detection is certainly not out of the realm of possibility for conventional organic fluorophores, the presence of added fluorophores always results in increasing spectral overlap of their comparatively broad fluorescent emissions. As such, multiplexed experiments with more than three fluorophores, while certainly possible, has generally required specialized spectral deconvolution algorithms and added experimental complexity. Multiplexed QD detection, on the other hand, can be routinely performed with at least six spectrally isolated fluorescent probes, all commercially available, without the necessity of added image processing. Certainly, the application of QD probes to both western blot analyses [*66*] and FISH techniques [*57*] has reportedly improved the detection capabilities of these methodologies. Recently, an exquisite demonstration of the multicolor fluorescent imaging capabilities of commercially available QD fluorophores has been reported by Fountaine *et al*. [*67*]. This report has utilized a sequential immunohistochemical QD labeling technique to simultaneously detect five cell line-specific antigens in tonsil and lymphoid tissue. As such, antibodies specific to CD20 and IgD, both B cell markers,

CD3, a T cell indicator, CD68, a macrophage marker, and MIB-1, indicating the proliferative areas of a germinal center, allowed for the specific and simultaneous detection of differentially expressed surface, cytoplasmic and nuclear antigens. Obviously, the continued application of QDs to these types of multiplexed experiments will facilitate clinically relevant investigations of multidimensional cellular interactions.

Perhaps the most striking demonstration to date of the superior multiplexing capabilities of QD fluorophores is the recent application of QDs to polychromatic flow cytometry analyses. Recently, Chattopadhyay *et al*. have reported the resolution of **seventeen** fluorescent emissions through the incorporation of QD fluorophores [*68*]. This seventeen color analysis, consisting of eight colors of QDs in conjugation with nine other conventional fluorophores, was used in immunophenotyping experiments on various T cell populations. The ability to independently quantify at least 17 fluorophores on a cell-by-cell basis vastly extends the capability of flow cytometry technology and allows for the design of considerably more complex experiments. The promise of truly multiplexed experimental design through the incorporation of QD fluorophores is increasingly being realized for a variety of applications. Continued improvement, through improved synthetic methodologies resulting in even narrower fluorescent emissions, may well extend these capabilities even further in the years to come.

Dynamic Receptor Trafficking

QDs' inherent photostability and brightness have recently allowed an increasing number of applications which monitor the trafficking dynamics of cellular receptors at the single molecule level. Dahan *et al*. initially demonstrated single molecule tracking

experiments investigating the cellular trafficking of individual glycine receptors (GlyR) in the neuronal membrane [*34*]. Individual QDs, presumably interacting with individual receptors, were identified by the fluorescent intermittency, or blinking, characteristic of single nanocrystals. This intermittency, a result of a combination of both radiative and nonradiative relaxation pathways present in the nanocrystal, is a useful signature for identification of individual QDs and has been reviewed elsewhere [*8, 69, 70*]. In this study, the QD's added photostability routinely permitted visualization of individual GlyRs for time frames exceeding 20 minutes, compared to imaging durations of only five seconds for conventional Cy3 coupled antibodies. Additionally, the signal-to-noise ratio for the QDs was almost a full order of magnitude larger than those obtained with standard fluorophores as a result of improved brightness. Antibody-QD conjugates specifically targeted to GlyRs (Figure 1-4), were found to be located at the synapse (synaptic), alongside the synapse (perisynaptic), or away from the synapse along the dendrite (extrasynaptic). Notably, the diffusion coefficients of these receptors were found to be dependant upon this membrane localization, illustrated in Figure 1-4C, generally showing decreased diffusion for synaptically associated receptors and increased rates of diffusion for extrasynaptic receptors. This report serves as an excellent illustration that the optical properties of QDs enable dynamic monitoring of individual molecules within a cellular environment.

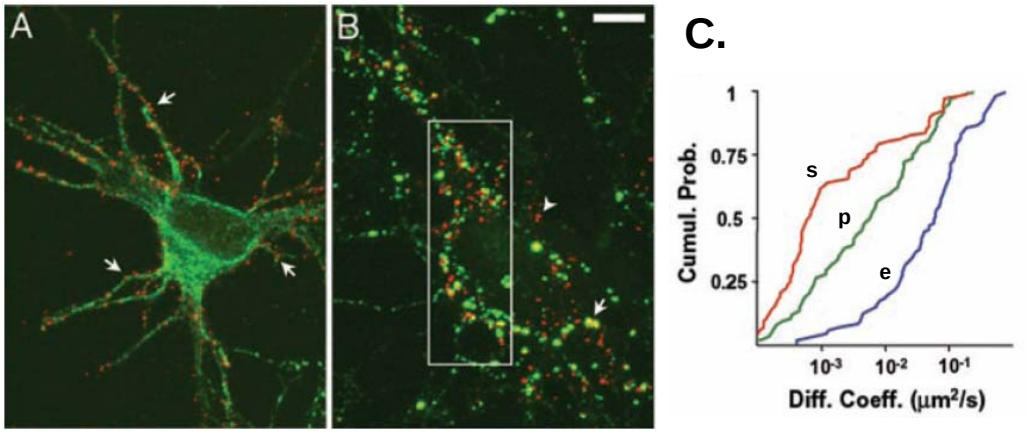

Figure 1-4. Glycine receptor trafficking with single-QD detection. (A) Localization of QD-GlyRs (red) in neuronal cultures identified by microtubule-associated protein-2 (green). Arrows indicate clusters of QD-GlyRs on dendrites. (B) Relation of QD-GlyRs with inhibitory synaptic boutons labeled for vesicular inhibitory amino acid transporter (green). (C) Localization was observed to be either stable at synapses (s), perisnyaptic (p), or extrasynaptic (e). The observed cumulative probability of diffusion coefficients differed as a function of their membrane location. From [Dahan, M.; Levi, S.; Luccardini, C.; Rostaing, P.; Riveau, B.; Triller, A. *Science*, **2003**, *302*, 442-445]. Reprinted with permission from AAAS.

Since this first reported application, an increasing amount of research has been devoted to QD-based molecular tracking experiments. Dynamic imaging of QD probes has allowed for the elucidation of a novel retrograde transport mechanism in filopodia [*29*], and has been applied to glutamate receptors [*32*], as well as intracellular molecular kinesin motors [*30, 50*]. More recently, dynamic QD imaging has been employed to monitor tyrosine kinase A (TrkA) receptor dynamics in neuronal cell cultures. Vu *et al*. initially demonstrated the ability of the βNGF peptide, the beta subunit of nerve growth factor, to specifically direct QDs to surface bound NGF-TrkA receptors in PC12 cell cultures. Additionally, they report that βNGF-QD conjugates are effective at activating these neuronal receptors, initiating downstream signaling and neurite growth, albeit with a diminished activity compared to free βNGF [*46*]. A subsequent study utilized these βNGF-QD conjugates as well as antibody conjugates to visualize the endocytosis, redistribution, and shuttling of NGF-TrkA receptors to PC12 neuronal processes and

growth cone tips [*47*]. Transport and concentration of βNGF-QD-TrkAs at the growth cone tips was observed, consistent with normal trafficking of fluorescent protein-tagged TrkA and myc-tagged NGF. This is further illustration that QDs do not act to hinder receptor activity or diffusion, and can serve as effective probes to visualize receptor trafficking.

In Vivo Imaging

Another area which has recently seen a dramatic increase in the amount of research devoted to the incorporation of QDs is *in vivo* imaging applications. Once again, the unique optical properties of QDs offer several advantages over existing fluorophores. Of particular interest for *in vivo* applications is the QDs' tunable fluorescent emission, which can span into the near-infrared (NIR) regime. This region, known as the 'water-window,' provides reduced autofluorescent background from the tissue and an improved tissue penetration. Additionally, initial *in vivo* studies have demonstrated enormous two-photon action cross sections for QD probes, a direct measure for brightness with two-photon imaging, allowing for further improvements in tissue imaging depths [*71*]. Other studies have also shown that PEG surface modifications reduce clearance by the reticuloendothelial system enabling longer circulation times *in vivo* [*13, 23*]. To date, QD-based *in vivo* imaging applications have been predominantly applied towards cancer research with a great deal of work directed towards tumor targeting. In one application, non-targeted QDs with a polydentate phosphine coating have been shown to accumulate in the sentinel lymph node facilitating fluorescent contrast for major cancer surgery [*72*]. Alternate approaches, where cells were initially labeled with QDs *ex vivo* and then

tracked following *in vivo* administration, have been employed to monitor metastatic tumor cell extravasation [*73*] and differentiate tumor vessels from perivascular cells and matrix [*43*]. Targeted, intravenous delivery of QDs to tumor tissues has been demonstrated with peptide-QD conjugates designed to preferentially recognize elements of the tumor vasculature [*13*], as well as antibody recognition for directed tumor targeting to prostate-specific membrane antigen [*21*]. In a recent *in vivo* application, RGD peptide conjugated QDs have been utilized for the directed targeting and imaging of tumor vasculature [*45*]. Furthermore, experiments have been performed to analyze the trafficking of single QD conjugates within the tumors of living mice by means of a skinfold chamber and confocal microscope [*74*]. Development of improved QD probes for NIR *in vivo* imaging applications continues to have great potential for cancer diagnosis and treatment, as well fluorescent imaging-guided surgery and therapy.

Further Biological Applications

QDs are also uniquely suited to facilitate a number of multimodal imaging applications. While fluorophores are routinely employed in conventional light microscopy techniques, these applications are fundamentally limited with regards to spatial resolution as a result of the diffraction limit described by Rayleigh's criterion. QDs, however, have the added benefit of being both fluorescent and electron dense, allowing for the incorporation of the additional resolution of the electron microscope for certain biological imaging applications. Recently, QDs were employed in a correlated microscopy application, which allows the mapping of proteins with fluorescent microscopy and the higher resolution localization at the ultrastructural level with electron

microscopy [*36*]. This technique, however, is critically dependant upon sample preparation and utilizes a novel sample holder which permits imaging on both microscopes. In one protocol described in this study, two colors of antibody-QD conjugates were used to stain connexin43 (Cx43), a gap junction indicator, and microtubles in fixed RFL6 fibroblasts which were subsequently embedded on an epoxy resin and mounted on an acrylic support. Initial low magnification fluorescent microscopy (20x) of the entire sample area allowed for navigation through the specimen at higher magnification to obtain coincidental fluorescent (63x oil immersion) and electron micrographs of the same field of view. The overlaid fluorescent and electron micrographs presented in this report are illustrative of the unprecedented spatial resolution obtainable in cellular colocalization imaging applications through the use of QDs with correlated light and electron microscopy.

An alternate bimodal imaging application has been demonstrated through the incorporation of paramagnetic gadolinium into the QD architecture to provide contrast for magnetic resonance imaging (MRI) [*75-77*]. Gadolinium has been effectively introduced though lipid coatings on the QD surface, allowing the QD to retain its fluorescent properties, resulting in a versatile probe for noninvasive imaging with both MRI and fluorescent techniques. Additionally, QDs have shown promise for photodynamic therapy applications [*78*], as well as targeted drug delivery [*79*]. The multivalent nature of the QD surface can, conceivably, be modified to incorporate both targeting and drug compounds, ultimately providing an improved platform for a targeted delivery of therapeutic payloads. Sophisticated attachment strategies have also been suggested to include an enzymatically cleavable region which provides an additional

level of control for selective drug delivery [*80*]. All of these applications, in order to meet their therapeutic potential, require that the QDs themselves have no deleterious effect on cell physiology. Differing reports throughout the scientific literature have tried to asses the level of cellular toxicity associated with QD exposure. An excellent review has illustrated that QD cytotoxicity is critically dependent upon numerous physiochemical and environmental factors [*81*]. Regardless, continued research will undoubtedly provide a more definitive determination of the cytotoxic effects of QDs, ultimately allowing for a comprehensive understanding regarding the nature of these cellular interactions.

Small Molecule Synthetic Strategies

The remaining discussion will detail the design and synthesis of high-affinity ligands for the dopamine transporter (DAT) as an illustration of a small molecule-QD targeting approach currently in development by the Rosenthal research group. DAT, an 80 kDa integral membrane protein [*82*], acts to remove excess dopamine from the synaptic cleft via a sodium chloride coupled transport mechanism. It has a primary amino acid sequence of 620 residues consisting of twelve transmembrane hydrophobic stretches with both the C and N termini located intracellularly [*83, 84*]. DAT is located on the presynaptic membranes of mesotelencephalic dopaminergic neurons which are located in the substantia nigra and ventral tegmentum in the midbrain and converge in the basal ganglia of the forebrain [*85*]. Changes in both dopamine receptor distribution and the dopamine transporter system have been shown to be important factors in a number of different disease states including Parkinson's disease, Huntington's chorea and

schizophrenia [*85*]. Additionally, the dopamine transporter system has been shown to be responsible for the locomotor and reinforcing effects of cocaine [*86*]. The development of high-affinity ligands specific to DAT and their subsequent attachment to QDs will result in highly fluorescent conjugates, enabling the imaging of localization and distribution of DAT in neuronal cell cultures. Ultimately, the ability to dynamically interrogate DAT's distribution and localization in response to applied stimuli will provide a better understanding of these disease states as well as the dopaminergic role in cocaine addiction.

The initial step in the development of these fluorescent QD-conjugates involves the identification of a suitable ligand which will interact with DAT selectively. Many different classes of compounds have been demonstrated to bind to DAT, some of which include phenyl tropanes, 1,4-dialkyl piperazines, hybrid tropane 1,4-piperazine derivatives, phencyclidines and Mazindol derivatives [*82, 87-90*]. The DAT antagonists GBR 12909 and GBR 12935 are 1,4-dialkyl piperazine derivatives, illustrated in Figure 1-5, have been studied extensively [*91-93*]. Microdialysis experiments have shown that GBR 12909 attenuates the extracellular dopamine levels enhanced by cocaine in rat striatum, and there is also evidence that this ligand dissociates from the transporter slowly, resulting in a long duration of action [*92, 94-100*]. Additionally, structure activity studies reported for GBR 12935 indicate that derivatives with a substituent on the phenyl ring via a propyl piperazine attachment retain their biological activity. Furthermore, competitive inhibition assays indicate effective binding of both GBR 12909 and GBR 12935 to DAT, with IC_{50} values in the nanomolar range. The biological properties and ease of synthesis of these GBR compounds make them ideal candidates for

the development of small molecule-QD conjugates which will aid in the development of highly selective and sensitive fluorescence-based assays. In this section, we report the synthesis of analogues of GBR 12909 and 12935 that retain a high affinity for DAT while also allowing for covalent attachment to the surface of fluorescent nanocrystals.

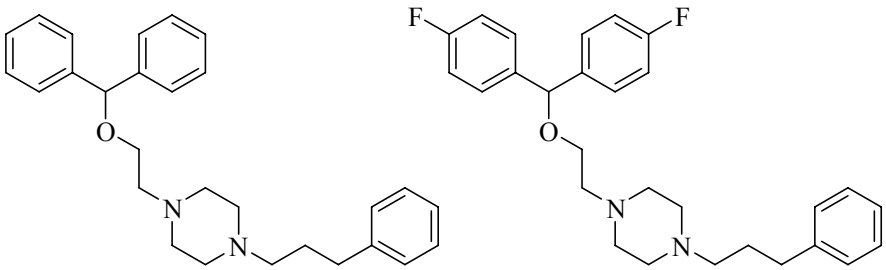

GBR 12395 GBR 12309

Figure 1-5. Structure of GBR 12935 and GBR 12309, 1,4-dialkyl piperazine derivatives which are extremely potent and selective inhibitors of the dopamine transporter.

Initial drug derivatives were based upon the parent compounds GBR 12935 and GBR 12909 (shown in Figure 1-5). Two noteworthy derivatives, previously reported, with modifications to the phenyl ring that do not interfere with biological activity are illustrated in Figure 1-6. An azido derivative (I), with a bulky iodo substituent on the phenyl ring, has been utilized for photo-affinity labeling studies of DAT [*101*]. Also, a biotinylated derivative (II) has been synthesized [*102*] and is routinely used in the purification of DAT expressing cells following attachment to avidin coated magnetic beads (Kaspar Zimmermann, private communication). Given this structure activity information, it was assumed that attachment of a linker arm to the para position of the phenyl ring on the propyl chain would not interfere with the ligand's high affinity for DAT. Selective substitution at this para position can be carried out using an amino modified analogue which has been reported in an earlier publication [*103*]. As indicated

in Scheme 1, the synthesis of this parent compound can be carried out utilizing relatively inexpensive starting materials (the detailed synthetic strategy is outlined in [*103*]). Linker arms can subsequently be attached selectively to this para-amine modification via an acid chloride, resulting in the formation of the appropriate amide bond. Thus, this parent analog ultimately allows for the attachment of a variety of linker arms selectively at the para position of the phenyl ring. Compounds (III), (IV), (V) and (VI), all illustrated in Figure 1-7, were synthesized by means of this method in order to examine the linker arm's effect on the ligand's affinity for DAT.

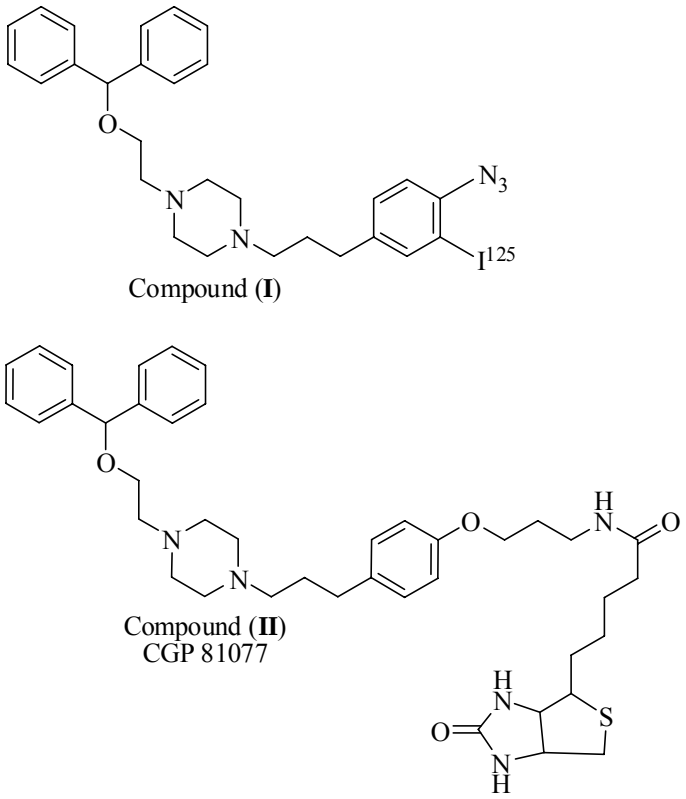

Figure 1-6. Previously reported GBR 12935 derivatives that retain biological activities. (I) An azido derivative, with a bulky iodo substituent on the phenyl ring, applied to photo-affinity labeling of DAT [*101*]. (II) A biotinylated derivative used in the purification of DAT expressing cells [*102*].

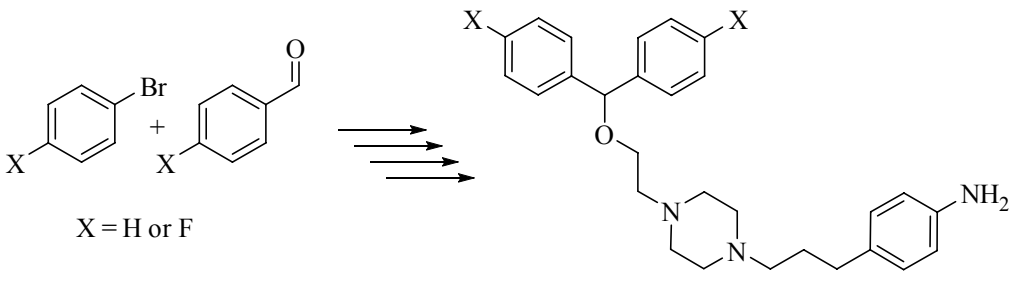

Scheme 1. Synthesis of parent para-amino GBR 12935 derivative.

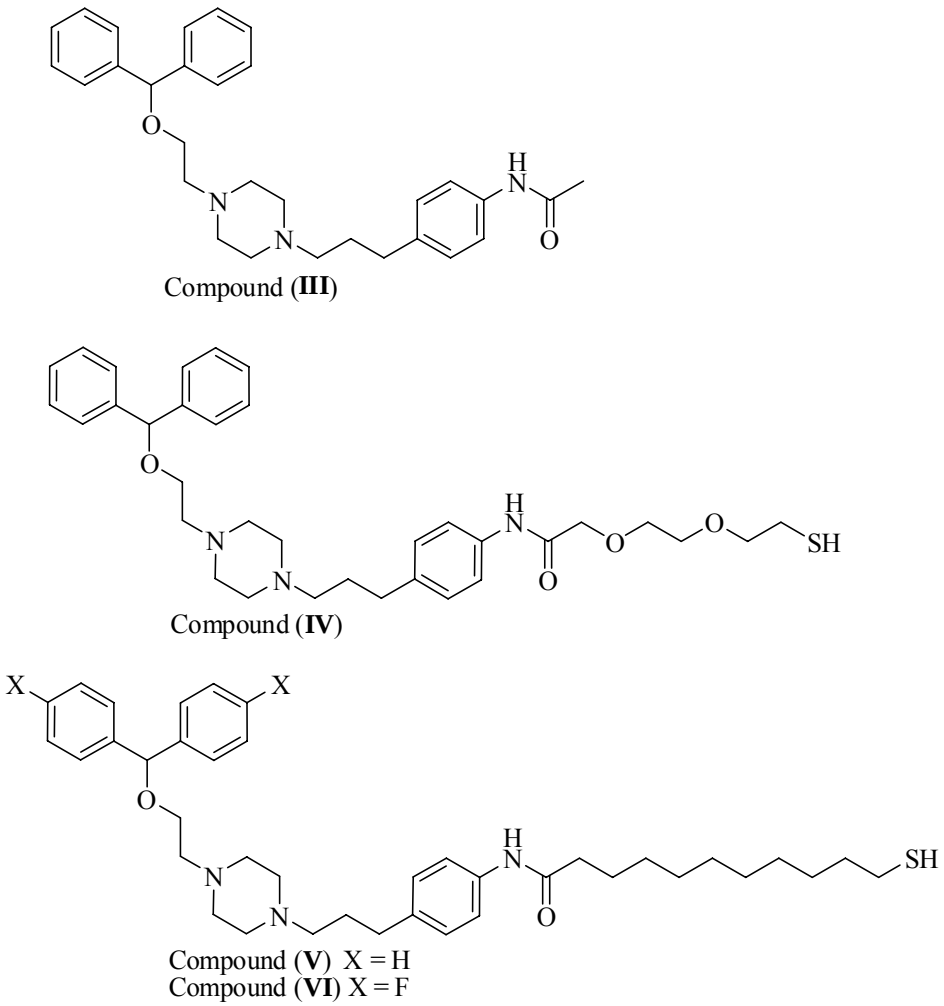

Figure 1-7. Initial GBR derivatives incorporating a linker arm functionality. EDC coupling chemistry was used to attach either acetic acid functionality (III), polyethylene glycol linker (IV), or and alkyl spacer (V) to the parent para-amino GBR 12935 derivative. In a similar fashion, a GBR 12909 derivative was also synthesized with an alkyl linker arm at the para position (VI).

Optimization of the composition and length of this linker arm must be performed in order to ensure that this chemical modification does not interfere significantly with the biological interaction of the ligand. Determining the biological activity of each intermediate can be performed using a competitive uptake assay. This assay measures the ability of either a ligand or a ligand-QD conjugate to inhibit substrate uptake, and is quantified radiologically for DAT using tritiated-dopamine as the substrate. Experimentally, treating the cells with increasing amounts of ligand in the presence of tritiated-dopamine allows for the determination of an IC_{50} value, the concentration of ligand which causes 50% inhibition of the transporter's activity. Consequently, these IC_{50} values represent a measure of the biological activity of these conjugates. A low IC_{50} value implies a stronger interaction with the transporter and a reduced uptake of [^{3}H]dopamine; while a larger IC_{50} value is indicative of a weaker interaction with the transporter allowing for increased uptake.

The biological activities of compounds (III), (IV), (V) and (VI) were measured by means of this competitive uptake assay, and the IC_{50} values are presented in Table 1. Of particular interest is the significant reduction in activity due to polyethylene glycol substitution at the para position of the phenyl ring for compound (IV). Previous structure activity studies have indicated that GBR 12935 binds to a hydrophobic cleft or pocket within the DAT transporter, which is consistent with this observed loss of activity due to addition of the hydrophilic polyethylene glycol functionality. Additionally, this loss of activity is not observed for compounds (V) and (VI), both of which have alkyl substitutions at the same para position, presumably due to the hydrophobic nature of this linker arm allowing for a stronger interaction with the hydrophobic binding site.

Compounds (IV) and (V) were synthesized with a terminal thiol functionality to allow for attachment directly to the surface of the QD via a Lewis acid-base interaction, and the IC_{50} values for these QD-conjugates are also presented in Table 1. While the measured IC_{50} values indicate that these conjugates are indeed biologically active, this type of surface modification has several drawbacks including increased non-specific interactions with cellular membranes in fluorescent imaging assays. Additionally, as these ligands were not conjugated irreversibly, over the course of several months the ligand had a tendency to dissociate from the surface of the QD causing them to aggregate and precipitate from solution. In order to improve the long-term stability of the QD conjugates and reduce the associated non-specific interactions, the conjugation methodology was modified to utilize alternate quantum dots which have been encapsulated in an ampiphilic polymer (ITK-Qdots™, Invitrogen; formerly AMP-Qdots™, Quantum Dot Corporation), supplied as a gift from Quantum Dot Corporation.

Table 1. IC_{50} values of initial GBR derivatives both as free ligands or QD-conjugates.

Compound #	IC_{50} (nM) Free Ligand	IC_{50} (nM) Bound Ligand
(III)	30	N/A
(IV)	6000	N/A
(V)	18	32
(VI)	10	140

Incorporation of these modified QDs into our conjugation strategy required a modification of the aforementioned Lewis acid-base coupling method. The ampiphilic polymer used to encapsulate ITK-Qdots™ is terminated with poly-carboxylic acid residues; consequently ligands with a terminal amine can be covalently attached to the

QD surface via standard EDC coupling methodology. Scheme 2 summarizes the synthetic approach by which a terminal amine was introduced on the alkyl linker arm of compound (VI). A phthalimide protection scheme previously described by Wada et al. [*104*] allows for selective attachment of an alkyl chain to the parent para-amino GBR compound (from Scheme 1). Subsequent removal of the phthalimide protecting group by treatment with hydrazine yielded compound (VII), an amine terminated derivative of compound (VI). EDC coupling of compound (VII) to AMP-QDs, however, resulted in a reduced solubility of the QDs in buffer due to the increased hydrophobicity of the ligand. QD-conjugates of compound (VII) only remained water soluble in cases where the coupling reaction was performed to ensure minimal ligand coverage on the QD surface. A competitive uptake assay was then used to measure the relative activity of this compound and the IC_{50} for the free ligand (VII) was determined to be 5.7 nM. Upon conjugation to the AMP-QDs, despite the solubility difficulties encountered, the IC_{50} was measured and found to be 1 nM relative to the QD concentration. While this activity was an indication of improvement relative to previous conjugates, further modifications were still required to improve the overall stability of these probes and optimize the nature of their interactions with cellular targets.

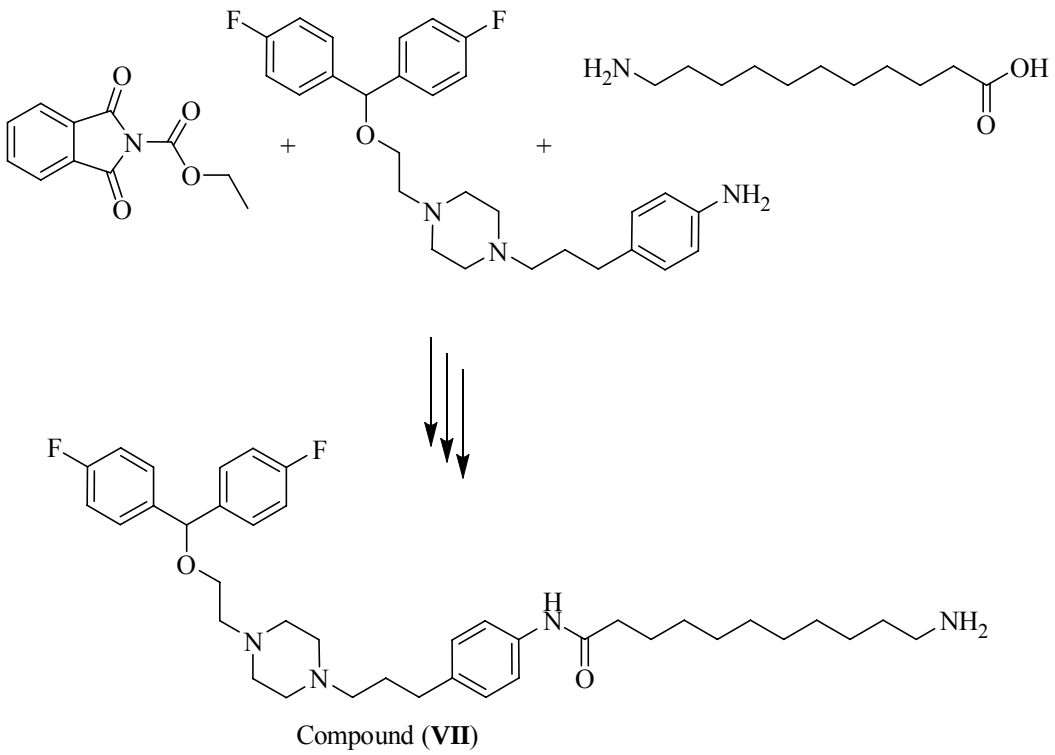

Compound (**VII**)

Scheme 2. Synthetic approach to obtain modified GBR derivatives with a terminal amino functionality to allow selective ligand attachment to AMP-QDs.

In order to address concerns regarding a diminished water solubility of these QD conjugates, compound (VII) was modified to include a poly ethylene glycol chain at the end of the alkyl chain. This modification acts to increases the water solubility of these conjugates as well as limit non specific interactions with cell surfaces due to a passivation of the AMP-QDs reactive surface [*24*]. Outlined in Scheme 3, this approach utilized a PEG linker which was first synthesized by the reaction of polyethylene glycol with phthalimide using conditions described by Mitsunobu [*105*]. The terminal hydroxy group of this modified PEG was then converted to a carboxylic acid moiety via a Jones oxidation with chromium (VI) oxide. Attachment to the terminal amine of compound (VII) by means of an EDC coupling and subsequent removal of phthalimide with hydrazine yielded compound (VIII). The IC_{50} value determined from the competitive

uptake assay for this free ligand was determined to be 80 nM, significantly more active than compound (IV), where the polyethylene glycol was directly attached to the parent GBR compound. Continued experiments will eventually determine the biological activity of compound (VIII) conjugated to QDs.

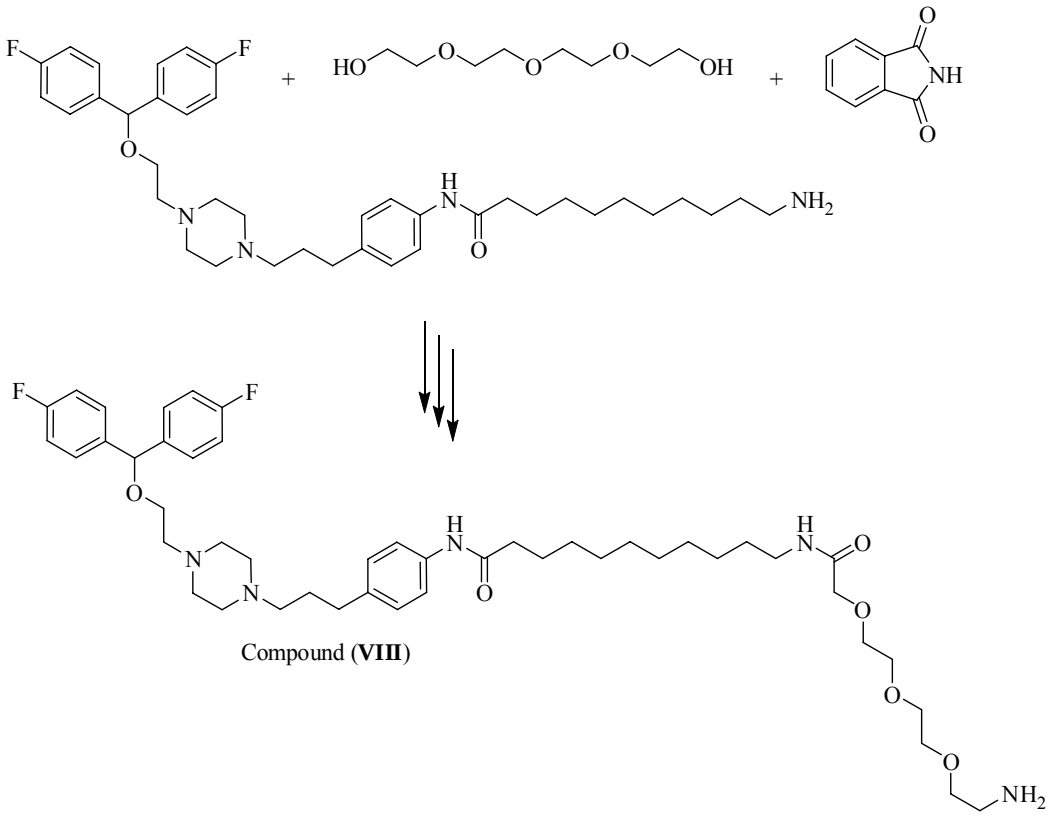

Compound (**VIII**)

Scheme 3. Synthetic modification of compound (VII) to incorporate a polyethylene glycol chain onto the alkyl linker facilitating improved QD water solubility while retaining biological activity.

Fluorescent imaging applications utilizing small molecule-QD conjugates have proven to be elusive, however, despite continued optimization of these conjugates' affinity for DAT. It is now apparent that the presentation of small molecules on the QD surface must first be optimized in order to facilitate specific binding of the QD to a cellular target. Incomplete surface modification, presumably caused by the steric bulk of large PEG derivatives or incomplete EDC coupling reactions, allows for albumin

adsorption to the reactive carboxylic acid functionality present on the QD surface. Albumin, a 66 kDa serum protein present in standard blocking solutions, has previously been shown to complex to reactive QD surfaces and facilitates QD endocytosis [*14*]. Consequently, incomplete passivation of the QD surface with small molecule conjugates results in an endosomally associated fluorescent staining pattern consistent with QD-albumin complexes (discussed in greater detail in Chapter 4). This albumin adsorption presumably prevents the small molecules on the QD surface from interacting with DAT due to its added size and steric bulk. Additionally, literature precedent seems to indicate that albumin absorption is less problematic in the case of bulkier antibody (~150 kDa) or streptavidin (~50 kDa) QD conjugates. Continuing research will determine an optimized conjugation methodology for these small molecule QD conjugates, completely passivating the reactive QD surface, and incorporating a suitable linker to facilitate specific, high affinity interactions of these small molecules with DAT. Despite the associated experimental difficulties of this approach, an optimized small molecule conjugation methodology will ultimately allow for a relatively low cost means of interrogating a wide variety of membrane bound cellular targets. In addition to the dynamic, multiplexed, and single-molecule fluorescent imaging applications obtainable with QD fluorophores, this small molecule architecture would facilitate additional biological assays for drug discovery applications.

While the focus of this section has been surface modification to specifically target DAT, a similar generalized approach can ultimately be used to develop QD-nanoconjugates specific to any membrane bound cellular target. The use of a functional assay to interrogate the relative activity of each intermediate allows for an improved

design of the molecular architecture required for an optimized interaction. This approach has provided convincing evidence that an alkyl spacer is required to retain biological activity before attachment of PEGylated GBR derivative to the surface of a QD. This seemingly subtle difference in ligands results in one full order of magnitude difference in biological activities. Future studies will continue to use this approach to determine the optimal polyethylene glycol chain length and examine differences in ligand coverage for optimized small molecule-QD conjugates.

Summary

It is apparent that QDs have emerged as improved fluorophores for several biological imaging applications, and continued research will certainly provide further improvement of their scaffold-like architecture providing for sustained advances in fluorescence-based assays. While it would be foolish to think they will ever completely replace traditional organic dyes and fluorescent proteins, they certainly can be utilized in conjunction with these existing technologies to access a more detailed understanding of cellular processes. Obviously, QDs provide an additional tool biologists can employ in certain applications to take advantage of their unique spectral properties. Progress in truly multiplexed fluorescent assays utilizing QD probes will continue to provide an increasing amount of information regarding protein-protein interactions and cell signaling events. Advances in temporal and spatial resolution, which has already been realized for dynamic imaging applications, will undoubtedly see additional development and continue to provide detailed information on receptor trafficking events at the single molecule level. Additionally, QDs possess a great deal of promise for numerous *in vivo* applications,

perhaps even the eventual design of combined diagnostic and therapeutic agents, allowing for targeted drug delivery in cancer treatment. This chapter has presented several unique applications which clearly illustrate the remarkable promise QDs provide through their incorporation in biological imaging assays. Hopefully, ongoing research and continued development will allow for an increased association of QDs in biological applications, and ultimately provide a more detailed understanding of numerous cellular processes.

The remainder of this dissertation will detail my efforts to expand the utilization of QDs in a variety of biological imaging applications, with a particular emphasis on the development of small molecule QD conjugates to fluorescently label SERT expressed in mammalian cell cultures. Chapter II details the pertinent experimental methods, materials and protocols which were developed and utilized throughout the course of this research. Chapter III discusses initial imaging efforts which utilized antibody conjugated QDs to fluorescently label interleukin-2 receptor (IL-2R) expression in activated populations of Jurkat T cells. This fluorescent assay utilized QD conjugates to verify the time-course associated with IL-2R translation and expression as well as investigate the trafficking of IL-2R subsequent to surface expression. Chapter IV highlights several significant interferences which were unknowingly affecting the continued development of a small molecule targeting strategy based on an AMP-QD scaffold. One such interferences involving the self-assembly of hydrophobic PEG derivatives to the AMP-QD surface, initially demonstrated via electrophoresis and subsequently confirmed with ^{1}H-NMR spectroscopy, raises concerns regarding effective ligand presentation at the QD surface. Additionally, it was further demonstrated that incomplete surface passivation

can lead to unwanted protein adsorption at the QD surface in the presence of serum blocking conditions, ultimately leading to an artifactual fluorescent staining in cellular assays. Building upon this improved appreciation for potential interferences, the optimal labeling conditions for the fluorescent labeling of SERT expressed in mammalian cell cultures are then described in Chapter V. This represents the first reported method to fluorescently assess SERT expression in mammalian cell cultures, either by fluorescence microscopy or flow cytometry, which takes advantage of the improved photophysical properties of the AMP-QD platform. Furthermore, the importance of the length of the alkyl chain length which attaches the drug derivative to the PEG backbone has been highlighted, and an eleven carbon chain has proven to be suitable for labeling SERT. Finally, Chapter VI wraps up with a conclusion and summary of the research performed, while Appendix A details fluorescent imaging experiments performed to determine the localization of IDT307, a small molecule selectively transported by monoamine transporters.

CHAPTER II

EXPERIMENTAL METHODS

Surface Modifications to Introduce Biological Specificity

Surface modifications are initially required in order to introduce specificity for any biological fluorescent application utilizing these QD conjugates. Numerous biomolecules have been utilized to generate biologically compatible QDs, and several approaches are available for QD conjugation and surface modification. Commercially available QDs from Invitrogen (formerly Quantum Dot Corporation) were used for the research reported herein, and surface modification generally involved antibody conjugation, biotinylated ligands, or covalent ligand attachment. Antibody conjugation (Chapter III) was performed using a commercially available QD antibody conjugation kit (Invitrogen) with IL-2Rα antibodies (R&D Systems). Covalent attachment of the antibody occurs through a maleimide coupling of a free thiol on the antibody to an amine functionality on the dot's surface. Following antibody modification, QDs were separated from any unconjugated antibody by means of size exclusion chromatography and characterized by electrophoretic mobility and UV-Vis spectroscopy prior to their subsequent use in cellular assays.

Small molecule attachment to the QD surface relied on either covalent modification of the QD surface or site specific ligand biotinylation for targeting streptavidin-conjugated QDs. Reactive ITK-Qdots™ (Invitrogen, formerly AMP-QDs from Quantum Dot Corporation) were utilized for the covalent attachment of specially synthesized amine-terminated poly(ethylene glycol) (PEG) ligands. Covalent attachment was

performed through the use of a 1-(3-Dimethylaminopropyl)-3-ethylcarbodiimide hydrochloride (EDC) coupling reaction. Optimized coupling conditions which result in PEG ligand attachment while retaining optimal fluorescent QD emission have been previously reported [*24*]. These optimized conditions were generally retained for QD conjugate preparation; however, in some instances the conjugation reaction was performed with a higher ratio of ligands in order to ensure complete QD surface coverage. Consequently, EDC couplings were performed in borate buffer by the reaction of 2000-8000 molar equivalents of amine terminated ligand and 1500-6000 molar equivalents of both EDC and NHS for each molar equivalent of quantum dots. The reaction was allowed to proceed for one hour with stirring at room temperature. Conjugates were purified from unconjugated ligand by size-exclusion chromatography (Sephadex G-50) and/or 100K molecular weight centrifugal filters (Millipore), and characterized by electrophoresis, UV-Vis spectroscopy and fluorescence spectroscopy.

While the EDC coupling reaction is intended to result in a covalent attachment of the ligand's terminal amine to a carboxylic acid on the polymeric QD coating, surface modification in the absence of added coupling reagents have also been demonstrated (Chapter IV). For these self-assembly reactions, 8000 molar equivalents of ligand for each molar equivalent of quantum dot were stirred together in borate buffer for one hour at room temperature. Surface modifications resulting from this approach cannot be due to covalent attachment, due to a lack of added coupling reagents. Through the testing of a variety of PEG derivatives, each with differing terminal functionalities, it is apparent that this self assembly results from hydrophobic interactions with the QD surface.

Specific targeting utilizing biotinylated ligands to specifically target streptavidin-QD conjugates will also be discussed (Chapter V). Direct conjugation of these ligands to the QD surface by means of the aforementioned EDC coupling reaction proved to be ineffective due to an apparent self-assembly of ligands to the QD surface, driven by the added hydrophobicity of the targeting terminus. For these instances where direct surface modification proves unsuccessful, a two-step labeling approach taking advantage of the high affinity streptavidin-biotin interaction can be employed. Biotin terminated PEG derivatives can first be incubated with cells expressing a desired cellular target, which allows the targeting terminus to initially seek out its intended target in the absence of QDs. Streptavidin-conjugated QDs can then be employed to specifically seek out the biotin, effectively resulting in specific QD labeling without the need for ligand attachment to the QD surface. This two-step labeling eliminates any interference due to the hydrophobic targeting functionality interacting with the QD surface. Preconjugated QDs can also be prepared simply by mixing biotinylated PEG derivatives with streptavidin-QDs, with a subsequent purification from any unbound ligand, but generally resulted in diminished cellular labeling as compared to two-step labeling.

Quantum Dot Conjugate Characterization Techniques

Spectrophotometric Concentration Determination

A determination of QD concentration was required for all QD-conjugates prior to their incorporation into cellular assays. QD concentrations were therefore determined by UV-Vis spectroscopy using a NanoDrop® ND-1000 spectrophotometer (Nanodrop

Technologies, Wilmington, DE). This NanoDrop spectrophotometer requires only 2 μL of sample and does not use a cuvette for spectroscopic determinations, significantly reducing any potential loss of sample due to transfer to and from a cuvette. Concentrations were calculated from absorbance readings at 350 nm, 405 nm, 488 nm and 532 nm, each with a reported extinction coefficients [*106*], which were then averaged to yield a final concentration.

Fluorescent Quantum Yield Determination

Quantum yields were measured by comparing integrated fluorescence intensity of absorbance matched solutions using either a Carey Eclipse Fluorescence Spectrophotometer (Wright Lab) or an ISS PCI photon counting spectrofluoremeter (Chemistry Department Instrumental Lab). In general, the Carey Eclipse instrument is rapid but less sensitive, while the ISS instrument is more cumbersome but provides increased sensitivity. QD solutions as well as reference standard solutions were initially diluted to an identical optical density at a given excitation wavelength (~0.05 AU), ensuring that each solution has an identical absorbing power at the excitation wavelength. Generally, Rhodamine 101 in methanol (QY=0.95) with excitation 530 nm was employed as a reference standard for red emitting QDs, but alternate reference standards are certainly available. The integrated fluorescent intensities were subsequently measured for both the sample and the standard, and the ratio of these values multiplied by the reported reference quantum yield gives the absolute sample quantum yield. The added effect resulting from differences in refractive index can also be accounted for using equation (1).

$$\Phi_x = \Phi_{st}\left(\frac{Int_x}{Int_{st}}\right)\left(\frac{\eta_x^2}{\eta_{st}^2}\right) \quad \textbf{(1)}$$

Where Φ is the quantum yield, *Int* is the integrated fluorescent intensity, η is the solvent's refractive index, *st* indicates the reference standard while *x* represents the sample being measured. Quantum yield determinations provided a measure to assess any potential fluorescence quenching subsequent to surface modifications, a critical parameter to consider in developing fluorescent probes.

Electrophoretic Characterization Techniques

It is important to have methodologies to verify conjugation of biomolecules to the surface of the quantum dot, especially to confirm the presence of the biomolecule in the case that an initial cell labeling experiment fails. Further, in designing optimized probes, it is important to have a measure of biomolecule coverage. Too many biomolecules on the surface of the nanocrystal can lead to steric hindrance, while too few could reduce activity. Therefore, any surface modification to the QD surface was initially confirmed using agarose gel electrophoresis. All agarose gels were prepared at a concentration of 1% agarose (Ultrapure™, Invitrogen) in Tris-acetate-EDTA (TAE) buffer, and run for 80 minutes at a constant 80 volts in TAE running buffer. Fluorescent images of all gels were acquired on an AlphaImager 2000 imaging station (Alpha Innotech Corp.). Since surface modification acts both to passivate charged residues on the QD surface and increase the overall probe size, successful ligand attachment results in an overall reduction of the observed electrophoretic mobility. Consequently, PEG-QD conjugates exhibit a significantly reduced electrophoretic mobility in agarose gels, providing a clear demonstration of successful surface modification.

A non-denaturing polyacrylamide gel electrophoresis (PAGE) approach was developed to verify protein adsorption to the QD surface. Since PEG-QDs already have a diminished electrophoretic mobility in agarose gels, any subsequent protein adsorption or antibody conjugation does not result in any appreciable difference to assess surface modifications. PAGE, however, provides the capability to initially separate QDs from any unadsorbed protein and subsequently stain to determine protein distribution. Native, non-denaturing polyacrylamide gels were therefore prepared according to established protocols [*107*] utilizing a 2.5% polyacrylamide stacking gel with a 10% polyacrylamide resolving gel. QD conjugates, with and without added albumin, were run at a constant 25 mAmp for 2.5 hours. A fluorescent image was then recorded using the AlphaImager 2000 imaging station to verify location of QD bands present in the gel. The gel was subsequently removed from it's glass cassette and stained for protein distribution using a Commassie Blue staining solution overnight as per manufacturer's instructions (Note: fluorescent images of the gel must be acquired prior to protein staining since the Commassie solution quenches the QD fluorescence). A brightfield image following gel destaining provides a colorimetric determination of protein content throughout the gel. Protein adsorption to the QD surface is clearly resolved using this approach as it results in protein bands which co-localize with the previously observed QD bands.

Fluorescamine Assay for Approximation of Ligand Loading

Another way to determine the efficiency of biomolecule coupling to the nanocrystal is the fluorescamine assay [*23, 24*]. This assay is particularly useful if the functional group of the biomolecule being attached to the nanocrystal is an amine, which is often the case

when coupling biomolecules to carboxylic acid terminated dots. The general strategy of the assay is to determine the number of free amines both before and after the conjugation, with the difference being the conjugation yield and the number of biomolecules on the surface. After performing the coupling reaction, the unconjugated amine terminated ligand can be easily separated from the conjugated nanocrystals by means of a molecular weight cut-off filter. Quantification of this free ligand can then be performed by addition of an excess amount of fluorescamine (3 mg/mL in acetone), which forms a blue fluorescent species when reacted with an amine. Comparison of this fluorescent intensity (at 480 nm) to the fluorescent signal produced by the same number of ligands in the absence of coupling reagents allows the determination of the number of unreacted amines present, which is equivalent to the number of unconjugated ligands. The difference between the number of ligands added initially, and the number present after conjugation is therefore assumed to be the number of ligands that have been conjugated to the nanocrystals.

Verification of Ligand Conjugation Using NMR Spectroscopy

^{1}H NMR experiments were performed to provide spectroscopic proof of QD-ligand complexes. For these reactions, QD conjugation was carried out as before, with and without EDC coupling reagents, for two PEG derivatives (IDT319 and IDT320, described in greater detail in Chapter IV). Following conjugation, the reaction mixtures were run through Sephadex G-50 columns to help eliminate any unconjugated PEG ligands, and only the fluorescent QD fraction was collected. These QD solutions were then concentrated by means of 100K molecular weight centrifugal filters (Millipore),

with one added rinse to ensure complete removal of any unbound ligand, to a final volume of ~20 μL. This concentrated QD solution was then diluted in deuterium oxide to a final concentration of 200 nM, and UV-vis absorption measurements were then made to ensure identical QD concentrations for each NMR sample. All ^{1}H spectra were then recorded on a Bruker 501 spectrometer at ambient temperature in D_2O. A small portion of the residual H_2O signal was suppressed. The resulting spectra were analyzed using TopSpin 2.0 software.

Control ^{1}H NMR experiments for both free PEG derivatives and unconjugated AMP-QDs demonstrated a lack of any spectral overlap (Figure 2-1). The spectra of PEG ligands, as illustrated for IDT319 and IDT320 in Figure 2-1A, are dominated by a single peak at 3.64 ppm due to large number of chemically equivalent protons in their long PEG chains. Unconjugated AMP-QDs (Figure 2-1B), on the other hand, presented no spectral feature at this chemical shift but instead had characteristic spectral features due to the protons present in their polymeric coating. Consequently, this strong PEG signal at 3.64 ppm served as a useful feature in providing spectroscopic characterization of ligand interactions with the QD. Furthermore, the additional AMP-QD features provided an internal standard to normalize the integral area of this ligand peak to the amount of QDs in solution.

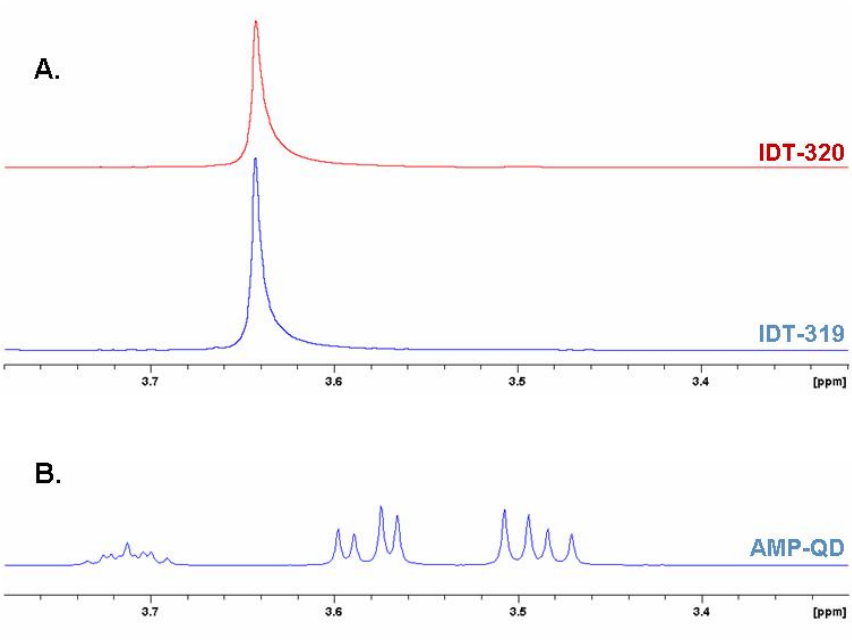

Figure 2-1. Control ^{1}H NMR spectra of free PEG ligands (A.) and unconjugated AMP-QDs (B) which demonstrate a lack of spectral overlap. PEG derivatives consist predominately of a single peak at 3.64 ppm, while no interfering peak is present in AMP-QD samples at this chemical shift.

Cell Culture Protocols

General Cell Line Maintenance and Subculture

All cell cultures were maintained in accordance with recommended culture conditions and reagents as established by ATCC. As such, all cell lines were maintained in a sterile environment at 37 ^{o}C with 5% CO_2, and standard aseptic techniques were followed for all cell maintenance protocols. Jurkat T cells (clone E6-1) were obtained from ATCC (ATCC #: TIB-152) and cultured in RPMI 1640 media supplemented with 10% fetal bovine serum (FBS) and either 10 mg/ml Ciproflaxin (Cellgro) or 100 U/mL penicillin with 100 U/mL streptomycin (Gibco). Jurkat T cells reportedly have a doubling time of 48 hours [*108*], and these cells should be subculture two to three times a week to maintain and optimal cell density between 1×10^5 and 1×10^6 viable cells/mL. Cultures

were maintained either by the addition of fresh medium or the complete replacement of medium to prevent the cell density from exceeding 3×10^6 cells/mL. Ideally, subculture should always be performed by centrifugation with subsequent resuspension at an initial seeding concentration of 1×10^5 viable cells/mL. Half of the time, however, subculture simply involved transferring an aliquot of cells to fresh media based on approximated cell counts (assuming a 48 hours doubling time). Cell counts and centrifugation were employed at every other subculture interval to initially verify cell density and further to prevent accumulation of waste products present when transferring aliquots of old media.

LLC-PK1 (ATCC#: CL-101) were obtained as a gift from the laboratory of Dr. Randy Blakely (Vanderbilt University) and cultured in Dulbecco's Modified Eagle's Medium (DMEM) containing 4.5 g/L glucose, 1.0 mM sodium pyruvate and 2 mM L-glutamine, supplemented with 10% FBS, 100 U/mL penicillin, and 100 U/mL streptomycin. This epithelial cell line was initially isolated from a the kidney of a Hampshire pig [*109*] and has subsequently been employed in generating cells stably expressing the serotonin transporter (SERT) [*110*]. Both parent LLC-PK1 (untransfected) and stably transfected SERT-LLC-PK1 cells were maintained under identical conditions. Subculture of this adherent cell line was performed once cells reached 95-100% confluence, generally occurring two to three times per week depending on initial seeding density. Once cells reached 100% confluence, the media was aspirated from the culture flask to a waste container, and the cells were rinsed with either Ca/Mg free PBS or a trypsin/EDTA solution (since these cells tend to be quite adherent, a trypsin/EDTA rinse is preferred). Additional trypsin/EDTA solution was then added (3 mL for a T75 culture flask) and the culture vessel was transferred to the 37 °C incubator until the cells

completely detached from the plate (~ 5 minutes). Complete media was then added to in a three-fold excess as compared to initial trypsin/EDTA volume, to ensure complete neutralization of trypsin activity (i.e. 9 mL complete media for 3 mL trypsin/EDTA). An aliquot of this cell suspension could then be deposited into a culture flask and diluted in an appropriate volume of fresh media. A subcultivation ratio of 1:3 to 1:8 is recommended by ATCC, while a 1:6 split was generally sufficient for routine maintenance.

HEK-293T cells (ATCC #: CRL-11268) were also supplied as a gift from the laboratory of Dr. Randy Blakely and were cultured in Modified Eagle's Medium (MEM) containing 4.5 g/L glucose, 1.0 mM sodium pyruvate and 2 mM L-glutamine supplemented with 10% FBS, 0.1 mM MEM nonessential amino acids (Gibco), 100 U/mL penicillin, and 100 U/mL streptomycin (Gibco). The 293T (293tsA1609neo) cell line is a highly transfectable derivative of the 293 cell line into which the temperature sensitive gene for SV40 T-antigen has been inserted [*111*]. Subculture of these cells was generally performed two to three times per week, at 90-95% confluence. Once the cells were reached the desired confluence, the media was aspirated off and a trypsin/EDTA solution was added (3 mL for T75 culture flask) to induce cell dissolution at 37 °C. (Note: no rinsing step after media aspiration was required as these cells are much less adherent than the previously described LLC-PK1 cultures.) After the cells have lifted off the plate, a three fold excess of complete media was then added to neutralize and residual trypsin activity, and an appropriate aliquot of cells were then transferred to a new culture flask and diluted with fresh media. ATCC recommends a subcultivation ratio of 1:4 to 1:8, and a 1:6 split was generally employed for these studies.

Inducing IL-2R Expression in Jurkat T Cells

An initial research effort was focused on the development of QD-conjugates capable of specifically labeling activation products in populations of T cells (Chapter III). One common membrane-associated receptor associated with T cell activation, interleukin-2 receptor (IL-2R), was chosen as a cellular target for initial experiments to demonstrate specific QD labeling. Unactivated T cells, which do not express IL-2R, consequently provide a suitable negative control to verify specificity of QD labeling. IL-2R expression was chemically induced by exposing populations of Jurkat T cells to the activating agents phorbol myrastoyl acetate (PMA) and ionomycin. Consequently, unactivated Jurkat T cells were initially seeded in 8 separate flasks at an initial density of 1×10^5 cells/mL in complete media. Every 12 hours following seeding, a single flask of cells was activated by addition of 10 nM PMA and 4 μM ionomycin such that after 84 hours there was a set of eight flasks of cells each exposed to 0 (control), 12, 24, 36, 48, 60, 72, and 84 hours of the activating agents, respectively. After 84 hours, the cells were counted, centrifuged, and supernatants collected (immediately frozen at –20 ^{o}C for later ELISA analysis). Cells from each time point were then used immediately for all subsequent QD labeling experiments. It is important to note that freshly prepared solutions of PMA and ionomycin are critical to induce successful activation. PMA degrades rapidly in aqueous environments, but aliquots stored at -80 ^{o}C will not undergo degradation as rapidly. Consequently, 1000×stock solutions of both PMA and ionomycin were freshly prepared, aliquoted out into individual bullet tubes, and stored at -80 ^{o}C prior to their use. At each activation time point, individual bullet tubes of PMA and ionomycin stock solutions were thawed and used immediately, while any excess reagent was subsequently disposed of.

This procedure routinely resulted in successful demonstrations of controllable Jurkat T cell activation.

ELISA Approach for Measuring Secretion of IL-2

Successful T cell activation initiates a cascade of cellular processes which eventually result in the expression of cellular activation products. IL-2R expression is accompanied by secretion of IL-2, which acts in an autocrine fashion to promote proliferation and clonal expansion of antigen-specific T cells [*112*]. Therefore, the presence of IL-2 in the supernatants T cell populations, following exposure to PMA and ionomycin, would provide an indicator of successful activation, and verify controlled expression of cellular activation products. Consequently, supernatants from each time point were analyzed using a Quantikine® ELISA (R&D Systems) specific for IL-2 in order to quantify the amount of IL-2 secreted following activation. This assay employed a microplate which was pre-coated with monoclonal antibodies specific for IL-2. Standards and samples were incubated in these wells, and any IL-2 present was bound by the immobilized antibody. An enzyme-linked polyclonal antibody specific for IL-2 was subsequently added to each well after washing away all unbound substances. After additional washing to remove any unbound antibody-enzyme reagent, a substrate solution was added to each well and color develops in proportion to the amount of IL-2 bound in the initial step. This development was stopped, and the absorbance at 450 nm was measured by UV-Vis spectroscopy using a Bio-Tek Synergy-HT plate reader (Wright Lab). Calibration of optical densities to standard samples of known concentrations consequently permits a straightforward quantification of IL-2 present in cellular supernatants.

Plasmid DNA Expansion and Purification

Transfection is the process by which foreign DNA is introduced intracellularly as a means to induce desired protein expression [*113*]. Plasmid DNA encoding for both SERT and DAT in a pcDNA3.1 vector (as previously described [*110*]), were initially supplied as a gift from the laboratory of Dr. Randy Blakely. Expansion of these initial stocks was eventually performed as a means of generating an independent supply of plasmid DNA for all subsequent transfections. As such, competent DH5α *E. coli* cells (Molecular Cell Biology Resource Core, Vanderbilt) were initially incubated with 1 μL of plasmid DNA, and then placed at 42 ^{o}C for 30 seconds to induce the transformation bacteria, inducing them to take up exogenous plasmid. These heat shocked cultures were subsequently streaked onto ampicillin-selective agar plates and stored overnight at 37 ^{o}C. As the pcDNA3.1 vector incorporates an ampicillin resistance region, only those *E. coli* cells which have taken up plasmid will be able to survive under the selective pressure of ampicillin. Bacterial cultures for plasmid preparation were then grown from a single colony picked from this selective agar plate, and deposited directly into 125 mL of LB medium containing ampicillin (Gibco). These cultures were then expanded overnight at 37 ^{o}C with vigorous shaking, owing to a logarithmic-phase bacterial growth. Following this expansion, purification of plasmid DNA was then performed using a plasmid midi kit (Qiagen), which employs alkaline lysis to initially extract plasmid from bacterial cultures and an anion-exchange column for subsequent purification. Spectroscopic determination of plasmid concentration was then performed using a NanoDrop spectrophotometer. All plasmid DNA was subsequently stored in Tris-EDTA (TE) buffer at 4 ^{o}C prior to use.

Transient Transfection to Induce Protein Expression

Initial research efforts in developing QD conjugates to specifically interact with biogenic amine transporters generally employed stably transfected cell lines expressing a protein of interest. Uncertainty with regards to transporter expression levels in these stable lines after routine subcultivation, however, led to the use of transient transfection as a means of generating cells with substantially increased transporter expression. While stable transfections generally involve a chromosomal DNA integration event, protein translation from transient plasmid DNA transfection occurs independent of host cell chromosomal influences, which can ultimately provide higher expression levels. While numerous transfection reagents and conditions are commercially available, four such reagents were initially tested in an effort to elucidate optimal transfection conditions to induce either SERT or DAT expression. HEK-293T cells were therefore transfected with SERT plasmid DNA according to manufacturer's recommended conditions for Lipofectamine 2000, Lipofectamine LTX with Plus reagent, Lipofectamine LTX without Plus reagent (all from Invitrogen), and Fugene HD (Roche). These cells were then assayed for SERT expression 48 hours after transfection using IDT307, a small molecule which is intracellularly fluorescent and selectively transported by monoamine transporters (discussed in greater detail in Appendix A). Consequently, successful expression of SERT results in an observable intracellular green fluorescence upon exposure to IDT307, while no such fluorescence is present in the absence of SERT expression. Fluorescent imaging results for each transfection reagent are illustrated in Figure 2-2. These data indicate that the Lipofectamine 2000 transfection resulted in the

highest expression of SERT, while transfection efficiencies for each of the alternate reagents are greatly diminished.

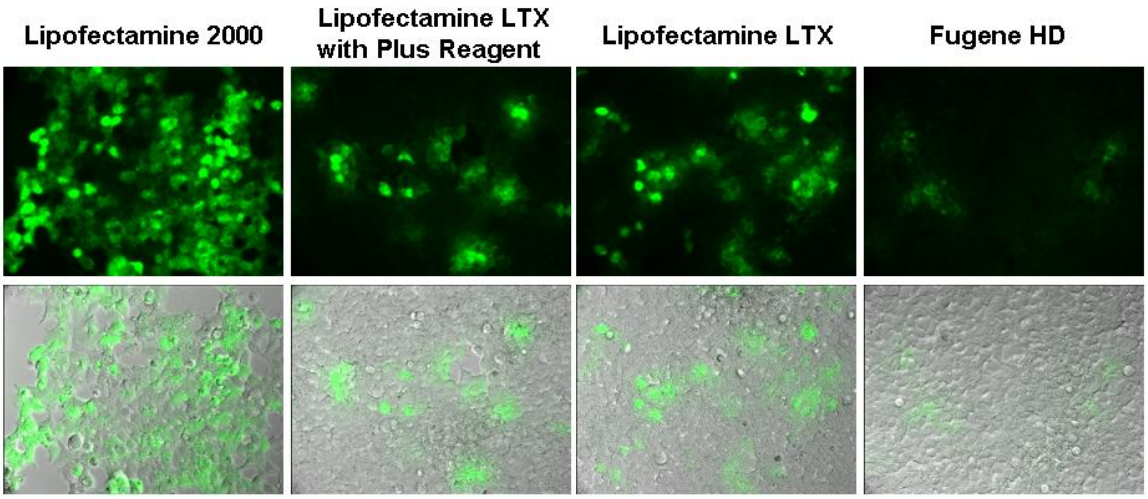

Figure 2-2. Identifying an optimal transfection reagent to induce expression of SERT. IDT307 fluorescent images (top row) and bright field composite overlay images (bottom row) to assess SERT expression following transfection with four commercially available transfection reagents (as indicated on top). As IDT307 is selectively transported intracellularly by monoamine transporters; its characteristic green fluorescence is indicative of SERT expression. Lipofectamine 2000 results in the highest transfection efficiencies for the expression of SERT in HEK-293T cells.

Lipofectamine 2000 was therefore utilized in all subsequent transfections as a means of inducing the highest possible expression of SERT. Transfections were performed in a 24 well plate format and utilized 0.8 μg plasmid DNA and 2 μL Lipofectamine 2000 per well, as per manufacturer recommendations. Control populations of cells lacking monoamine transporter expression were generated by transfection of empty pcDNA3.1 vector. These 'sham-transfected' cells provided an improved negative control for cellular assays as compared to non-transfected cells, and eliminated any potential experimental interference resulting from exposure to transfection reagents. Transfections were performed at a confluence of ~90% and transporter expression was assayed 48 hours following transfection to ensure sufficient time for successful translation and expression.

Assessing Monoamine Transporter Expression with IDT307

Cellular assays dependent upon monoamine transporter expression have undoubtedly benefited from the discovery of IDT307, a small molecule first synthesized in the Rosenthal research group which is selectively transported by monoamine transporters. IDT307 provides a non-isotopic means of assessing transporter expression owing to its unique intracellular fluorescent characteristics (discussed in greater detail in Appendix A). IDT307 was therefore utilized prior to any fluorescent imaging experiments as a means of verifying successful monoamine transporter expression, saving time and reagents as well as eliminating any associated uncertainty in experimental design. A straightforward assay to verify successful transporter expression simply involved the addition of IDT307 directly to the culture media at a final concentration of 5 μM, and incubating at 37 ^{o}C for five to ten minutes. Fluorescent images using a standard GFP filter set were then acquired immediately, and successful transporter expression was evident by an observable increase in intracellular fluorescence. No additional rinsing was required since IDT307 is only fluorescent in an intracellular environment, and any excess IDT307 in solution did not result in any observable fluorescent background.

Quantum Dot Labeling Protocols

Initial QD labeling experiments utilized IL-2Rα antibody-conjugated QDs as a means of specifically interrogating IL-2R expression in activated Jurkat T cells. This labeling protocol utilized centrifugation as a means of transferring these suspension cells from cell culture to various labeling and rinse solutions. Consequently, at selected time points following activation, a population of cells was initially centrifuged using a table top

microcentrifuge for 5 min at 1500 rpm to pellet the cells and permit removal of the cell culture media. This cell pellet was then resuspended in 100 μL of 10 nM anti-IL2Rα-conjugated QD in PBS for 30 minutes on ice. Unbound QDs were subsequently removed by centrifugation, with one additional rinse in cold PBS, and labeled cells from each time point were then divided into two populations: 5×10^5 cells were resuspended in media containing 10% FBS and 1 nM Yopro-1 (Cell viability indicator, Molecular Probes) for fluorescent imaging analysis and the remaining cells were resuspended in PBS with 2% FBS and 1 nM Yopro-1 for flow cytometry analysis. This labeling protocol resulted in sensitive detection of IL-2R expression due to a diminished fluorescent background from unbound QDs and minimal nonspecific cellular interactions.

Demonstrating specific labeling of SERT with small molecule-conjugated QD probes was the primary aim of this research project, and numerous labeling protocols were tested in an effort to specifically interrogate this target. All labeling protocols therefore employed two negative control populations to demonstrate specificity: (1) a parental cell line lacking receptor expression, and (2) a receptor-expressing population pre-blocked with an inhibitor specific to the intended target. These negative controls would ultimately permit an assessment of whether any observed QD labeling was the result of nonspecific cellular interactions, or the result of specific interactions with an intended target. While specific labeling parameters such as QD concentration, incubation time and temperature have to be optimized for each particular protocol, some general conclusions can be made to expedite the development of future QD labeling protocols. Firstly, QD concentrations of 1-10 nM have proven to be sufficient for numerous fluorescent imaging applications, and should provide a useful starting point for subsequent labeling protocols. Secondly, it

is important to determine the effect of incubation temperature for the development of an optimized labeling protocol. Generally, incubation at 37 °C permits membrane cycling and receptor trafficking, while these processes are significantly slowed by incubation on ice at 4 °C. Subsequent labeling efforts could therefore be initially performed at 4 °C to slow any receptor internalization processes and maintain receptor expression at the cell surface. Additionally, all efforts should first be made to verify successful receptor expression before blame is placed on the QD probe for ineffective labeling. Finally, while the inclusion of blocking agents such as BSA or serum could dramatically reduce any observed fluorescent background labeling, care should be taken to avoid any potential artifactual labeling due to unintended protein interactions with the QD surface.

Cellular labeling studies were eventually performed to verify the artifactual fluorescent response caused by protein adsorption to the QD surface (Chapter IV). These studies examined the different responses two chemically similar PEG derivatives had on cellular assays. For these experiments, LLC-PK1 cells (both parental and SERT-expressing) were initially plated in MatTek 35 mm culture dishes with a cover-glass bottom (to permit high magnification imaging with oil immersion optics). QD labeling was performed once the cells reached ~95% confluence, following an initial incubation in a blocking solution of 2% BSA and 10% horse serum in KRH buffer for 30 min. This high serum blocking solution was utilized as an effort to completely block nonspecific binding sites and eliminate any background QD fluorescence. Cells were then exposed to 5 nM QD solutions, either IDT319 conjugated QDs or IDT320 conjugated QDs diluted in the same 2% BSA and 10% horse serum in KRH buffer, for 30 min at 37 °C. The cells were rinsed three times with cold KRH buffer and immediately imaged on a widefield

fluorescent microscope at 100× magnification. This protocol resulted in a non-uniform cellular labeling for the IDT319 conjugates, while no significant QD labeling was observable for the IDT320 conjugates. Several different labeling conditions were then investigated in an attempt to elucidate the underlying cause of IDT319 QD conjugate labeling. Labeling at 4 °C eliminated any intracellular fluorescent labeling, indicative of an active transport mechanism following QD labeling. Cells which had been serum deprived prior to QD labeling had a much higher and uniform fluorescence, indicative of a cell cycle dependence. Attempts to block fluorescence labeling with excess free IDT319 seemed to indicate that the labeling was not receptor-mediated, and changing the blocking solution to 5% BSA without horse serum did not cause in any difference. A similar labeling pattern was also observed with HEK-293 cells, demonstrating that this phenomenon was not unique to LLC-PK1 cells. Eventually, QD labeling attempts with unmodified AMP-QDs reproduced the same fluorescent labeling result, ultimately leading to the conclusion that protein interactions at the QD surface were in fact the cause of the observed cellular interactions.

A principle observation from this protein adsorption investigation was that the added hydrophobicity of the SERT-selective region of IDT320 was in fact causing this ligand to self-assemble to the QD surface. This immediately raised concern over the effectiveness of ligand presentation at the AMP-QD surface; if the targeting region was interacting with the QD surface then it would not be able to specifically interact with an intended biological target. A two-step labeling approach using biotinylated PEG derivatives, altogether eliminating the necessity of ligand presentation at the AMP-QD surface, eventually proved to be effective. Nevertheless, care must be taken in subsequent labeling

protocols to optimize ligand presentation at the QD surface, especially for increasingly hydrophobic targeting functionalities on PEG derivatives. Another observation from repeated cellular imaging studies was that background QD fluorescence predominately occurs on the culture vessel surface, and no amount of rinsing was effective at eliminating this background. Furthermore, minimal QD nonspecific interactions were observed when labeling cells in suspension, even without serum protein blocking. The added background fluorescence due to QD interactions with the surfaces of the culture vessel was eventually eliminated by labeling the cells in suspension.

These observations eventually culminated in the development of a specialized two-step labeling protocol for the specific targeting of SERT with small molecule QD conjugates. In this assay, HEK-293T cells, transiently transfected to express SERT, were incubated with 1 μM biotinylated ligand (IDT318) in PBS for one hour at 37 °C. Cells were subsequently labeled in suspension, following dissolution from the plate with 0.05% trypsin-EDTA (Gibco), in order to minimize any background QD fluorescence due to nonspecific QD interactions with the plate. The cells were pelleted after dissolution from the plate by centrifugation to eliminate any free ligand and then resuspended in 2.5 nM streptavidin-QDs in PBS for 5 minutes at 4 °C. Labeled cells were then rinsed three times by centrifugation and resuspension in cold PBS and assayed for QD fluorescence immediately. While these parameters were initially derived from successful imaging in an oocyte model, subsequent analyses were performed to determine optimal ligand concentration and incubation time (Chapter V).

Widefield Fluorescent Microscopy

Widefield fluorescent images were obtained using a custom-built Zeiss Axiovert 200M inverted fluorescence microscope equipped with a Cool-SnapHQ^2 (Photometrics Corp.) electrically cooled CCD camera. Initially, this microscope was equipped with a Zeiss Axiocam color digital camera which was eventually replaced due to inadequate sensitivity and resolution. The Cool-SnapHQ^2 is a monochrome alternative which provides superior detection sensitivity, routinely capable of detecting single QD blinking events. The microscope currently has 5×, 10×, 20×, 40×, and 100× objectives, each with the necessary optics to permit differential interference contract (DIC) imaging. The 100× objective is an oil-immersion lens with a working distance of 0.17 mm, limiting its use solely to samples prepared on glass coverslips; all other objectives *should not come in contact with immersion oil*, therefore transitioning from 100× to lower magnification without first cleaning any oil from the sample is **strictly prohibited**. A HBO 103 mercury short-arc lamp provides broad-spectrum excitation illumination for fluorescent imaging, and a five position reflector turret facilitates multi-channel fluorescent detection. Consequently, as many as four different fluorescent images can be acquired in rapid succession, with the fifth turret position devoted to DIC (brightfield) detection. The entire system is interfaced with a Pentium 4 workstation running Metamorph image acquisition and analysis software (Molecular Devices) which is capable of automating basic functions for efficient operation of both the microscope and the camera.

Zeiss Axiovert 200M Inverted Fluorescent Microscope Operation

This section is meant to provide a general procedure for image acquisition using the Axiovert 200M inverted fluorescent microscope, while more detailed instructions can be found in the operating manual (kept in the lab with the microscope). The HBO-103 power source should always be the first component turned on and the last component turned off, to avoid any potentially destructive interference which could affect workstation operation. The remaining system components (except the camera) can be turned on once the lamp indicator light switches on. If this lamp indicator light remains off, the HBO-103 W/2 bulb has burnt out and needs to be replaced. Specific instructions for replacement of this bulb are described in the operating manual, but one bulb should provide ~300 hours of operation. The camera should then be turned on only after the computer has completed its startup operations. Once all system components are powered up, double-click the Metamorph desktop icon to open the image acquisition software. A common error reported upon starting Metamorph indicates that no cameras are available. If this message is displayed, exit out of Metamorph, turn the camera off and then back on, and restart Metamorph. This should allow the computer to recognize the camera, but this message can generally be avoided by only turning the camera on after the computer has completely booted up.

Once Metamorph has initialized, critical parameters for image acquisition can be controlled through the 'Acquire' dialogue box. The 'show live' button initializes a live video stream from the camera useful for focusing and identifying regions of interest. If no signal is observable for the live stream, it is probable that the light path has not been directed to the camera. The Left/Right button on the (middle button on the lower left side

of the microscope) directs the light path to one of three orientations: 100% to binoculars, 100% to camera, or 50/50 binoculars/camera. The default setting is 100% to binoculars upon startup, and depressing the button twice will direct 100% of the light to the camera. With the light now directed to the camera, and a live video of your sample displayed on the monitor, settings such as exposure time and binning can be set in the 'Acquire' dialogue box. It is also possible to switch between illumination settings by selecting the appropriate fluorophore from the 'Settings' drop-down menu in the 'Acquire' dialogue box. Selecting a fluorophore from the 'Settings' menu causes the reflector turret to rotate placing a fluorescent filter set in the light path. *It is important for the user to verify that the appropriate filter cube is in place.* Since multiple users utilize this system, filter cubes are frequently swapped out, so care must be taken to ensure the correct placement of the appropriate filter cube. To maintain some order regarding filter placement, the following placement scheme has generally been utilized: Position 1, DIC; Position 2, DAPI or white light; Position 3, QD605 or TRITC; Position 4, QD655; and Position 5, GFP. Therefore, a user attempting to acquire a TRITC fluorescent image will first have to verify that the appropriate TRITC filter set is in position 3 to ensure accurate image acquisition. Once the appropriate filter set is in place and all settings have been established, simply click the 'Acquire' button to collect the appropriate image.

The Metamorph software package also provides numerous useful image analysis tools in addition to image acquisition capabilities. The 'scale image' and 'overlay images' commands in the 'Display' toolbar are likely the most widely used commands. Generally, fluorescence microscopy is utilized to demonstrate differences in fluorescent intensity of one sample as compared to a control sample. The 'Scale image' command allows the user

to establish uniform scales to permit straightforward sample-to-sample comparisons, assuming of course that identical acquisition conditions were used to obtain each image. The 'overlay images' command is useful for overlaying a fluorescent image onto a corresponding brightfield image or for demonstrating colocalization of two fluorescent images. Additionally, a calibration bar can be superimposed onto an image by selecting 'Calibration Bar' from the graphics menu in the display toolbar. One final problem frequently encountered has to do with opening these image files with programs other than Metamorph. Metamorph image files have a large bit-depth and are encoded so that they can only be opened in Metamorph. The 'Duplicate as displayed' command under the 'Edit' toolbar can be used to create a lower resolution 8-bit image which can be opened by all other image editor programs (or cut and paste directly into MS Office applications). It is still important, however, to retain the original Metamorph file for any subsequent analysis, because a significant amount of information (bit-depth) is lost upon this conversion to an 8-bit image.

Confocal Fluorescent Microscopy

All confocal image analyses were performed on a Zeiss LSM 510 Meta imaging system available through the Vanderbilt Cell Imaging Shared Resource (CISR). While all users of this microscope facility must first complete a short training course, it is available to researchers at Vanderbilt University for a nominal hourly charge. The system is equipped with an argon ion laser and two HeNe lasers capable of excitation at 458 nm, 477 nm, 488 nm, 514 nm, 543 nm, and 633 nm. Single color QD analysis generally utilized excitation at 488 nm, with an appropriate band pass filter for fluorescent

detection using a photomultiplier tube (PMT). Dual color fluorescent images incorporated either single or dual channel excitation with appropriate dichroic mirrors, band pass filters, and long pass filters in place to ensure negligible fluorescent bleed-through between channels. Appropriate single color control samples were always examined as a means to assess and eliminate any cross-talk between fluorescent channels. Generally, routine day-to-day fluorescent imaging analyses were performed using the widefield fluorescent microscope, while the confocal microscope was used more sparingly as a means of verifying intracellular localization or generating higher quality images.

Flow Cytometry

Flow cytometry analysis provides a convenient means to rapidly assess individual cellular fluorescence and demonstrate specific QD labeling for populations of cells in suspension. These analyses were initially performed to verify specific labeling of activated Jurkat T cells (a suspension cell line) using fluorescence activated cell sorting (FACS) analysis, then performed on a Becton Dickinson FACStar+ cell-sorter. This approach successfully corroborated the fluctuations in fluorescence intensity throughout the time course of activation, initially observed using microscopy. Eventually, successful labeling of SERT was demonstrated for suspensions of transiently transfected HEK-293T cells, and flow cytometry was once again employed to corroborate fluorescent imaging data, this time using a BD LSRII flow cytometer. All flow cytometry analyses were conducted with the equipment and assistance of the VMC Flow Cytometry Shared Resource. All analyses employed discrimination gates based on scatter parameters to

ensure interrogation of only viable, single cells. A typical gating approach is presented in Figure 2-3, and illustrates how scatter parameters can be utilized to identify specific populations of individual viable cells. Histograms displaying the number of cells at a given QD fluorescence intensity were then generated using BD FACSDiVa^{TM} software. This approach has proven to be faster and more efficient than fluorescent microscopy at determining fluorescent intensity for populations of cells in suspension. Microscopy, however, is still preferable for analysis of adherent cell cultures and for visualizing dynamic cellular processes.

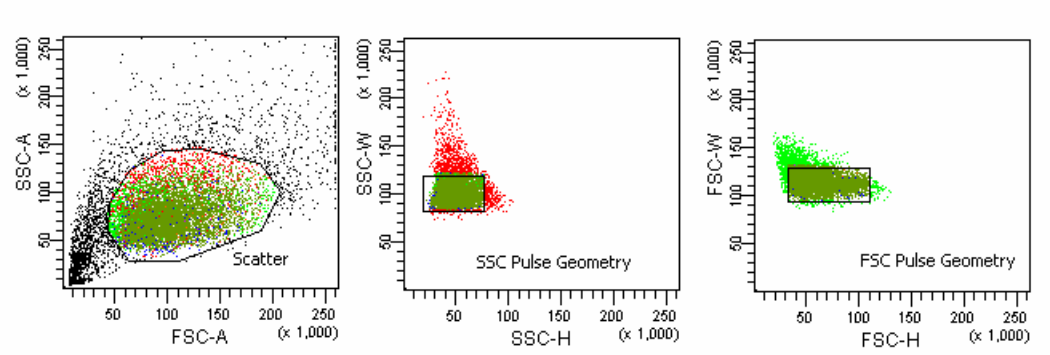

Figure 2-3. Gating individual, viable cells using scatter parameters from flow cytometry data. An initial population of viable cells is initially identified from a plot of front scatter area versus side scatter area (left). This population is then displayed with regards to side scatter width versus height (middle) and an additional gate is established to discriminate single cell events from multiple events. Finally, this population is plotted as a function of front scatter height versus width (right) and a final gate further discriminates individual cellular events.

CHAPTER III

QUANTUM DOT ANTIBODY CONJUGATES FOR MONITORING THE DYNAMICS OF IL-2R EXPRESSION [*114*]

Introduction

In this chapter the feasibility of using QDs as nanoprobes for Thymocyte (T cell) signaling events is examined, with the intention of demonstrating the benefits of incorporating QDs as a major read-out component of a proposed T cell based cell-signaling platform. To date, there have been a limited number of imaging applications which interrogate a dynamic cellular response utilizing QDs despite their improved photostability. An initial dynamic imaging application employed non-targeted, endocytic loading of QDs into both mammalian and *D. discoideum* cell lines and confirmed no deleterious effects on cellular physiology [*16*]. Single quantum dot tracking methods have since been used to elucidate diffusion dynamics of glycine receptors in the neuronal membrane over time frames ranging from seconds to minutes [*34*]. More recently, QDs were used to demonstrate retrograde transport of epidermal growth factor receptors and track their subsequent endosomal trafficking [*29*]. Peptide-conjugated QDs have also been used intracellularly, following transfection, for imaging nuclear targets allowing visualization of the transport of the QDs from the cytoplasm to the nucleus [*44*]. It is apparent that QDs, given their unique optical properties, may ultimately allow for unprecedented temporal resolution for imaging dynamic cellular processes. The research described in this chapter utilizes antibody conjugated QDs to interrogate the signaling dynamics of T cell activation, providing a clear demonstration of their improved dynamic imaging capability.

T cell Activation and the Adaptive Immune Response

The immune system of mammalian organisms responds to antigenic challenges utilizing both innate and adaptive immune responses. Innate immunity provides immediate defense against infection either by preventing microbial entry or by recognizing conserved antigens expressed on microbes, such as lipopolysaccharide (LPS). This innate immunity initially relies on epithelial barriers to prevent microbial entry, but also employs circulating effector cells (i.e. neutrophils, macrophages and NK cells), circulating effector proteins (complement, mannose-binding lectin, C-reactive protein) and cytokines to illicit an immediate immune response. The adaptive immune response, however, results from cellular recognition of a pathogen with subsequent clonal expansion and proliferation to produce an antigen specific response. Consequently, the adaptive immune response is much slower as compared to the innate response, but the additional specificity and diversity ensures an overall improved immune function. T cells are the major signal transducers of the adaptive immune response in mammalian systems. Acting in concert with antigen presenting cells, T cells are capable of recognizing an incredibly wide variety of distinct antigens and provide enhanced responses to repeated exposures to the same antigen. T cells coordinate the adaptive immune response through cytokine signaling to promote the destruction of microbes residing in phagocytes, stimulate B cells to secrete antibodies, or even direct the killing of infected cells in order to eliminate potential reservoirs of infection. This is not to say, however, that the innate and adaptive immune responses act independent of one another, but, rather, are both components of an integrated cooperative system of host defense [*112*].

Signaling Pathway of T cell Activation

In the presence of a perceived threat, T cells undergo a process of activation and proliferation to coordinate an antigen specific immune response. Cell surface expression of the cytokine receptor interleukin-2 receptor-α (IL-2Rα) in T cells, as well as secretion of the cytokine interleukin-2 (IL-2), is widely used as an indicator of T cell activation [*112*]. Figure 3.1 illustrates the major signaling pathways leading to IL-2 and IL-2Rα production. Successful engagement of the T-cell receptor (TCR) by antigen presenting cells (APCs) results in a cascade of intracellular events including the DAG (diacylglycerol), IP_3 (inositol 1,4,5-triphosphate), and MAPK (mitogen-activated protein kinase) pathways. Activation of phospholipase C (PLCγ1) by adaptor proteins and ZAP-70 results in the cleavage of phosphatidylinositol 4,5-bisphosphate (PIP_2) to produce IP_3 and DAG. IP_3 binds to the endoplasmic reticulum and releases calcium stores, activating transcription factor NFAT (nuclear factor of activation in T cells), which then moves to the nucleus. The recruitment and activation of protein kinase C (PKC) by DAG [*112*] has been shown to be integral to the activation of both NFκB (nuclear factor kappa beta) [*115*] and AP-1 [*116, 117*]. Alternatively, T cell activation can be chemically induced *in vitro* by treatment with phorbol myrastoyl acetate (phorbol ester or PMA) and ionomycin, which act together to upregulate NFAT, NFkB, and AP-1 [*118*]. Once in the nucleus, the transcription factors NFAT, NFκB, and AP-1 act in concert to coordinate the activation of several genes involved in host defense and inflammatory responses, including production of IL-2 and expression of IL-2Rα.

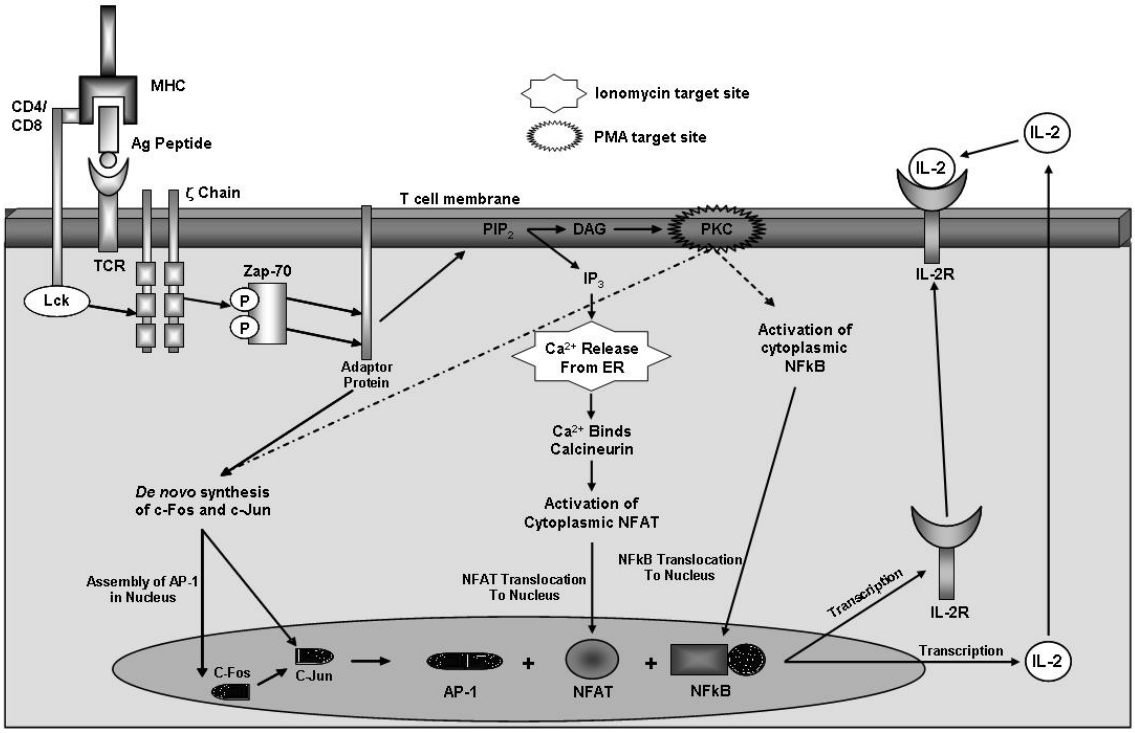

Figure 3.1 Signaling pathway associated with T cell activation. Engagement of the TCR and coreceptors by an APC results in a signaling cascade producing transcription factors NFAT, NFκB, and AP-1 required for successful activation of the T cell and expression of IL-2 and IL-2Rα. As indicated, chemical stimulation can occur by treatment with PMA and ionomycin. PMA activates PKC initiating the signaling cascades responsible for the transcription of AP-1 and NFκB, while ionomycin causes a release of intracellular calcium stores resulting in transcription of NFAT. Thus, treatment with both PMA and ionomycin upregulates all three transcription factors required for successful activation and expression of IL-2Rα and IL-2.

Interrogating Protein Expression as a Means of Elucidating Toxin Exposure

This high level of complexity and discriminatory ability within the signaling pathways of T cells not only allows these cells to be highly effective for mediating immune responses against novel pathogens, but may also permit the cells to be utilized as biosensors to gain insight into methods of detection, prevention and treatment for biological warfare agents. Construction of a detection system with the ability to sense novel pathogens of both known and unknown pathogenesis could be accomplished by utilizing T cells as biosensors and taking advantage of the discriminatory power of their diverse intracellular signaling pathways. Previous studies support the feasibility of this

premise as both anthrax toxin [*119*] and immunomodulatory agents [*120*] have been shown to suppress T cell activation with a significantly varied response on cytokine production levels. Platforms to study signaling dynamics of single T cells and other cells by utilizing technology that allows the simultaneous detection of multiple signals in live cells are currently in development [*121*]. Additionally, it would be desirable to detect signaling on an individual cell basis to avoid averaging out either rare but important signaling events or spatial and relational correlations of signaling events with regard to the overall signaling cascade. Incorporation of QDs in this platform will ultimately allow for the interrogation of multiple pathways given their narrow fluorescent emission spectra, while the inherent brightness of QD probes provides an improved chance of detecting the limited amounts of cytokine production at the level of a single cell. Finally, their intrinsic photostability permits further investigation into the temporal dynamics of receptor expression and subsequent localization following expression.

Results and Discussion

Time-Course of IL-2R Expression

Initial research efforts were necessarily focused on demonstrating specific labeling of IL-2R using QDs conjugated to an antibody specific to IL-2Rα (see complete experimental details in Chapter 2). For these fluorescent imaging assays, Jurkat T cells were initially activated by treatment with both PMA and ionomycin to induce expression of IL-2R. These activated cells were subsequently incubated with antibody-conjugated QDs to assess IL-2R expression at various time points following activation. A green

fluorescent cellular viability indicator, YOPRO-1 (Invitrogen Corp., Carlsbad CA), was included in the final rinse solution to eliminate any potential fluorescent artifact labeling resulting from nonspecific QD interactions with dead cells. Representative fluorescent images obtained at 0, 12, 18, 32, 48, 60, 72, and 84 hours following activation are illustrated in Figure 3.2. Minimal QD fluorescence is observed in unactivated cell populations (0 hour time point) due to a lack of basal IL-2R expression, therefore this population of cells provides a suitable negative control to demonstrate specific labeling. The QD fluorescence observed at later time points is indicative of maximal IL-2R expression following 32-48 hours of activation, consistent with previous reports of IL-2R transcription and translation [*112*]. Consequently, these antibody-conjugated QDs provide a useful tool to specifically interrogate the dynamics of receptor expression.

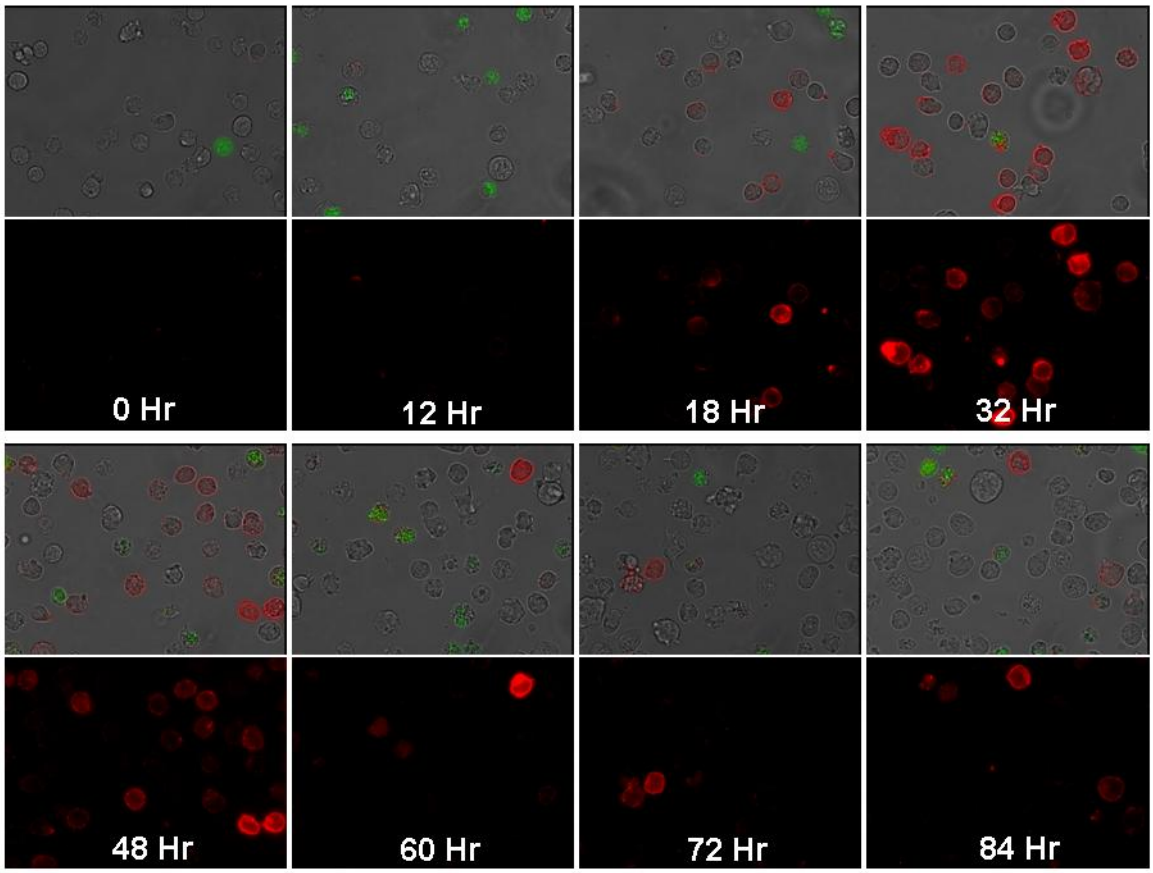

Figure 3.2 Fluorescent microscopy experiments demonstrating T cell activation. Fluorescent images (bottom) and bright-field composite overlay images (top) of QD-labeled Jurkat T cells at specified time points following activation with both PMA and ionomycin. Green fluorescence from YOPRO-1 indicates non-viable cells.

Verification of IL-2R Labeling Using Flow Cytometry

Flow cytometry analysis was then performed to corroborate these fluorescent imaging results, which suggest maximal IL-2R expression at approximately 48 hours following activation and a subsequent decrease in fluorescent intensity at longer activation times. Flow cytometry provides a convenient readout of cellular fluorescence in this assay, especially given the non-adherent nature of Jurkat T cell cultures. Correspondingly, cells were activated as before (with both PMA and ionomycin) and subsequently labeled for IL-2R expression at various time points using antibody-conjugated QDs. Representative flow cytometry histograms displaying differential IL-2R expression at 0, 48 and 84 hours

following activation are displayed in Figure 3.3. As in the fluorescent imaging experiments, minimal fluorescence is observed for unactivated cells (0 hr) owing to a lack of IL-2R expression in unactivated T cells. Fluorescent intensity has correspondingly increased for the entire cellular population following 48 hours of activation, indicating an overall increase in IL-2R production in this activated cell population. At longer activation times (84 Hr), the fluorescence due to IL-2R expression drops off dramatically for a significant fraction of this cell population, while a small number of cells remain fluorescent. This decrease in fluorescent intensity is consistent with the expected wax and wane of IL-2R expression as the receptor is internalized upon engagement of secreted IL-2 for lysosomal degradation [*112*]. Additionally, this internalization of the IL-2•IL-2R complex acts in an autoregulatory manner to down-regulate further transcription of IL-2R, further decreasing receptor expression, and attenuating the T cell's IL-2 responsiveness [*122*].

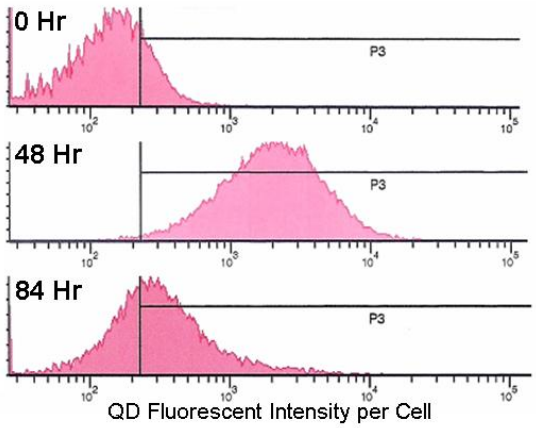

Figure 3.3 Flow cytometry analysis verifying selective QD labeling of IL-2R. Minimal background fluorescent intensity is observed for unactivated cells (top) compared to those cells activated for 48 hours (middle). The large increase in fluorescent intensity per cell is due to IL-2R expression. This fluorescence drops off by 84 hours (bottom) with a small population still exhibiting increased IL-2R expression.

Quantitative Determination of Cellular Activation Products

Having demonstrated the specificity of these antibody-conjugated QDs for labeling IL-2R, quantification of specific cellular products was then performed to further evaluate the time course of T cell activation. Quantification of IL-2R expression was carried out utilizing fluorescence measurements on individual cells specifically labeled for IL-2R with QDs. Intensity measurements were made from fluorescent images using Metamorph® image analysis software. Briefly, circular regions containing individual cells were first identified in the bright field image as illustrated in Figure 3.4. These regions were then superimposed on the fluorescent image allowing readout of the integrated fluorescent intensity for each cell. Subsequent background subtraction and averaging over the entire population of cells for a given time point yielded the average fluorescent intensity per cell. The population of cells per time point varied between 50 and 200, due to differences in the number of viable cells in each image. Consequently, this fluorescence image analysis protocol provides a facile approach to rapidly assess IL-2R expression in activated populations of Jurkat T cells.

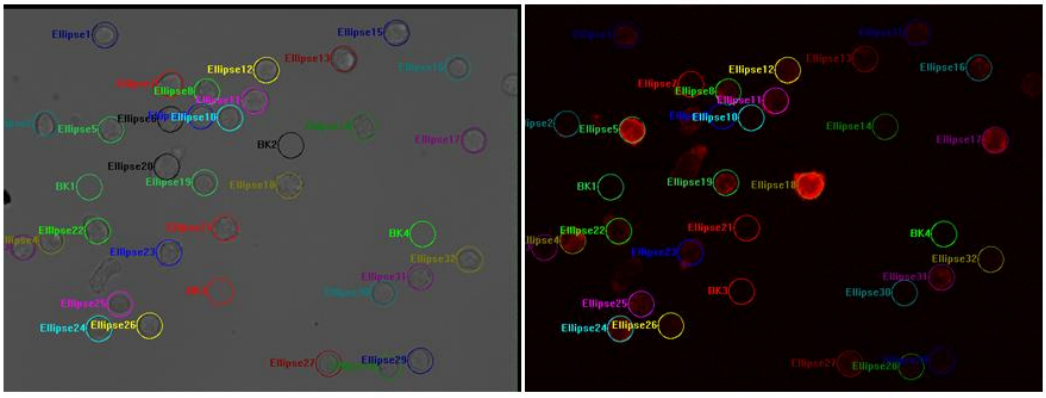

Figure 3.4 Quantification of fluorescent intensity from microscopic images. Metamorph® image analysis software was used to create circular regions containing individual, viable cells from a bright field image (left). This region mask was then superimposed onto the corresponding fluorescence image (right) to read out integrated fluorescent intensity per cell.

A graphical representation of IL-2R expression throughout the time course of T cell activation, as determined utilizing fluorescent image analysis, is presented in Figure 3.5 (top panel). As anticipated, IL-2R expression peaks roughly 48 hours after activation, and is significantly diminished at longer activation times (but still above basal expression levels). Error bars at each time point in this graph represent one standard deviation of the mean. Additionally, since T cell activation is accompanied by the translation and secretion of IL-2, analysis of the supernatants at each time point utilizing an IL-2 ELISA provided verification of successful activation (Figure 3.5, bottom panel). Initial examination of the IL-2 ELISA data seemed to indicate a delayed response, as IL-2 secretion is expected to coincide with IL-2R expression. However, since IL-2R acts to clear secreted IL-2 from the supernatant, accumulation of IL-2 in the supernatant is only observed after a significant portion of the expressed IL-2R has been internalized resulting in a sharp spike following the 48 hour time point. Thus, the IL-2 ELISA results confirm activation of the T cell populations by PMA and ionomycin.

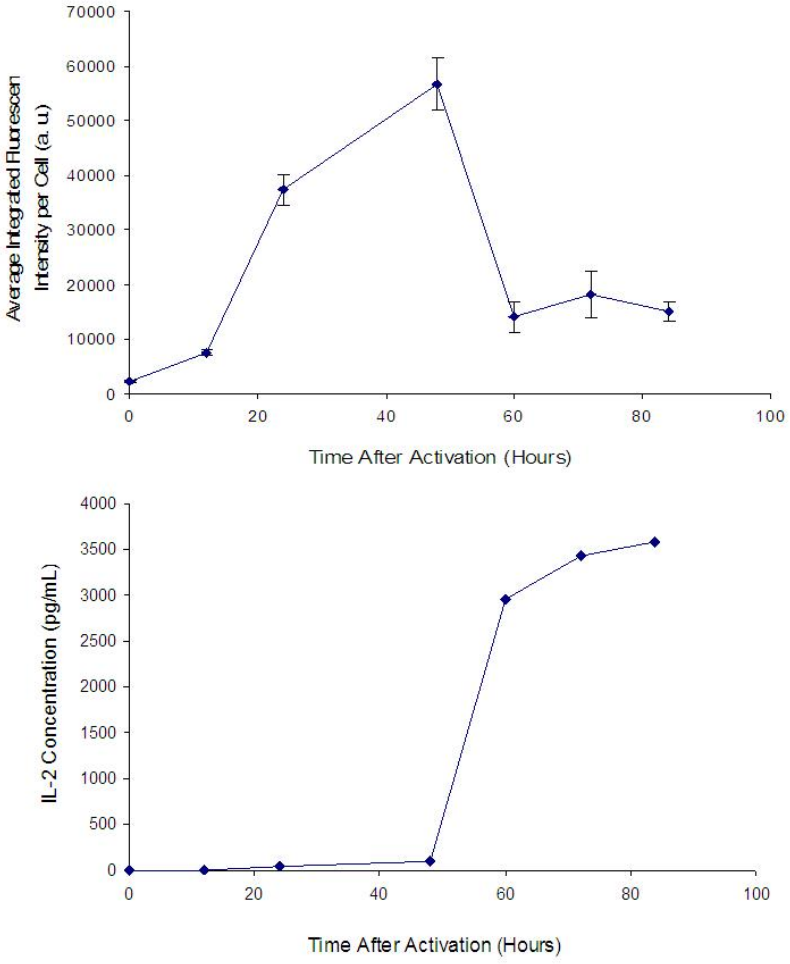

Figure 3.5 Quantification of cellular activation products by fluorescence image analysis and ELISA. (*Top*) Specific labeling and QD fluorescence permits quantification of IL-2R expression at various time points following activation. Average fluorescent intensity per cell was determined using Metamorph software and error bars represent one standard deviation of the mean. (*Bottom*) Quantification of IL-2 production by ELISA also provides verification of activation. Initially, IL-2R acts to clear secreted IL-2 from the supernatant, but a subsequent decreased expression of IL-2R allows for an eventual accumulation of IL-2 at later time points.

Receptor Localization Subsequent to Quantum Dot Binding

Confocal microscopy provided direct evidence of receptor internalization subsequent to expression and anti-IL2Rα-QD labeling (Figure 3.4). Cells that had been activated for 72 hours were labeled as before with 10 nM anti-IL2Rα-conjugated QDs for 30 minutes. Following centrifugation, the labeled cells were resuspended in fresh media from which a

small population of cells were immediately fixed with 4% paraformaldehyde on poly-L-lysine coated glass slides and mounted with Aqua PolyMount (Polysciences Inc.) for confocal microscopy. The remaining cells were allowed to remain in culture for an additional 24 hours before fixation and mounting. Confocal images of cells fixed immediately after labeling (Figure 3.4 A-B) show membrane associated extracellular labeling, while cells that have been allowed to remain in culture subsequent to labeling (Figure 3.4 B-C) demonstrate internalization of the QDs (Panels A and C are the center-slices from the z-stack of confocal images, while panels B and D provide orthogonal views of the XZ and YZ planes). This indicates that the QD-receptor interaction is sufficiently strong as to undergo internalization, and that the relatively bulky QD probe does not prevent this internalization.

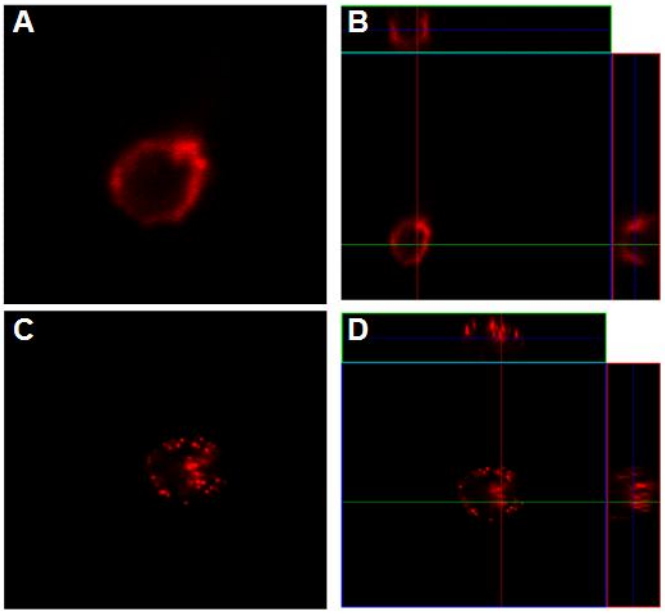

Figure 3.6 Receptor localization subsequent to QD labeling. Jurkat cells activated with PMA and ionomycin for 72 hours were labeled with anti-IL2Rα conjugated 655 QDs. Cells were fixed immediately following QD labeling (A&B) and 24 hours after labeling (C&D). Confocal images (A&C: center slice views; B&D: orthogonal views of the z-stack) indicate only membrane associated QDs for the cells fixed immediately following labeling. Cells fixed 24 hours later, however, have clearly internalized at least a portion of the QD conjugates.

Summary and Future Directions

Antibody-conjugated quantum dots (QDs) have been used to map the expression dynamics of the cytokine receptor IL-2Rα following Jurkat T cell activation. Controlled activation of populations of Jurkat T cells has been demonstrated and it is apparent that the dynamics of receptor expression can be monitored using antibody conjugated fluorescent QD probes. Maximal receptor expression was observed 48 hours after activation, followed by a sharp decrease consistent with IL-2R internalization subsequent to IL-2 engagement. Verification of T cell activation and specificity of QD labeling were demonstrated using fluorescence microscopy, ELISA and FACS analyses. These antibody conjugates provide a versatile means to rapidly determine cell state and interrogate membrane associated proteins involved in cell signaling pathways.

Ultimately, incorporation with a microfluidic platform capable of simultaneously monitoring several cell signaling pathways will aid in toxin detection and discrimination. This microfluidic platform capable of isolating and maintaining non-adherent cells, currently in development, will allow these time course studies to be performed in real time on thousands of individual cells in a massively parallel format. Additionally, other signaling pathways can be simultaneously monitored in a similar manner by varying the emission wavelength of the QD probes and targeting these probes to other relevant membrane associated receptors. Future experiments will address simultaneous detection of multiple cell surface targets in order to more accurately portray the signaling state of the cell. In addition, it may prove to be beneficial to compare the brightness of these QD conjugates to fluorophores traditionally used for low expression applications, although the improved sensitivity of QD probes has been demonstrated extensively. Furthermore,

methods to use QDs intracellularly are being developed to obtain functional information of earlier events occurring within the signaling pathways that may be used in discrimination or prediction of cellular response to toxins. The effect of toxin exposure on expression dynamics will provide insights not only to the identity of the chemical or biological agent in question, but also provide valuable information on the method of pathogenesis as well as treatment.

CHAPTER IV

SMALL MOLECULE APPROACH TO ELIMINATE SERUM PROTEIN ADSORPTION AT THE QUANTUM DOT SURFACE [*123*]

Introduction

Modifications of the quantum dot (QD) surface are routinely performed via covalent biomolecule attachment, and poly(ethylene glycol) (PEG) derivatization has previously been shown to limit nonspecific cellular interactions of QD probes. Attempts to functionalize ampiphilic QDs (AMP-QDs) with custom PEG derivatives having a hydrophobic terminus resulted in self-assembly of these PEG ligands to the AMP-QD surface in the absence of covalent coupling reagents. These self-assembled PEG-QDs exhibit improved passivation in biological environments, as demonstrated by electrophoretic characterization techniques, and are less susceptible to unwanted protein adsorption to the QD surface. Additionally, the artifactual fluorescent response protein adsorption can cause in biological assays is highlighted, and considerations for improved small molecule presentation to facilitate specific QD interactions are discussed.

Background and Significance

Quantum dots (QDs) were first reported as improved fluorophores for biological imaging applications in 1998 [*2, 3*], and have since seen increasing incorporation into numerous biological assays ranging from multiplexed fluorescent detection [*67, 68*] to tumor targeting *in vivo [13, 72]*. Their remarkable photostability has permitted biological processes to be observed on time scales unattainable with conventional organic fluorophores [*29*]. Their inorganic composition, which gives rise to these robust, size-

dependent optical properties, is not conducive, however, to direct integration into biological assays. Surface modifications are initially required to permit dispersion in aqueous environments, and further functionalization is necessary to facilitate specific biological interactions. Initial attempts at water solubilization generally involved the displacement of organic capping ligands present on the quantum dot surface [*2, 3, 61*], but these approaches generally had a deleterious effect on the QD optical properties as well as reduced colloid stability. Retention of these organic capping ligands seemingly results in improved fluorophores; as such, encapsulation in phospholipids [*18*] or ampiphilic polymers [*19, 20*] has been widely used to confer water solubility. Biological specificity can subsequently be introduced through biomolecule attachment (refer to Chapter 1 for a comprehensive review). Consequently, the surface of a biologically active QD probe is surprisingly complex, with alternating regions of hydrophobicity and hydrophilicity, the possibility of a net positive or negative surface charge depending on functionalization, as well as the presence of numerous reactive chemical functionalities. A better understanding of this potentially reactive surface is required and will ultimately result in improved surface passivation and the elimination of undesirable biological interferences.

Small Molecule Strategy for Labeling Membrane Associated Receptors

A majority of fluorescent imaging applications involving QD probes utilize antibody conjugation to introduce biological specificity. The utility of biologically active small molecule QD conjugates for targeting membrane-associated receptors has been previously demonstrated [*61, 62*], and these small molecule conjugates have the potential

to provide several advantages over antibody recognition. Notably, the large size of antibodies (~150 kDa) adds significant steric bulk to an already sizable QD probe, whereas small molecule attachment provides minimal additional bulk. Despite the fact that antibodies can be designed to recognize virtually any biological target, the antibody-antigen interaction varies dramatically from antibody to antibody, and the associated cost of antibody production significantly limits their utility. Small molecules, on the other hand, can have significantly reduced costs associated with synthesis, and the strength of the ligand-receptor interaction can be optimized through iterative ligand development. Additionally, a wide variety of cellular targets are available based on drug candidates from the known pharmocopia, and these improved probes would be of immediate benefit for various drug discovery applications. A small molecule QD targeting approach is schematically illustrated in Figure 4-1a. This ligand design incorporates a biologically active drug derivative (pink) on one end of a poly(ethylene glycol) (PEG) chain (blue). The PEG chain acts to reduce nonspecific interactions [*23, 24, 124*] as well as provide additional degrees of freedom for the drug derivative to interact with its cellular target. The terminus of the PEG chain is designed with a chemical functionality to facilitate attachment to the QD surface. Generally, a terminal amine is utilized in conjunction with standard carbodiimide coupling chemistry to covalently modify carboxylic acid derivatized AMP-QDs (ITK Qdots, Invitrogen Corp., formerly Quantum Dot Corp.). Alternately, a biotin can be introduced at this terminus to assemble ligands on commercially available streptavidin QDs, utilizing the extremely high affinity streptavidin-biotin interaction. Fluorescent imaging applications utilizing this small

molecule architecture have remained elusive, however, due to technical difficulties involving ligand design and associated ligand presentation on the QD surface.

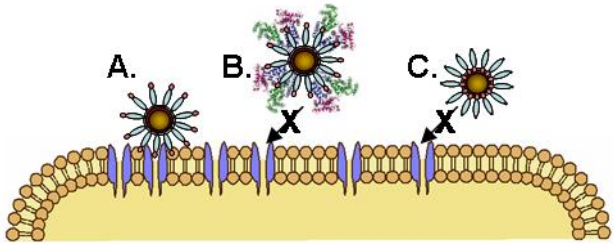

Figure 4-1: Cartoon schematic illustrating (a) small molecule QD targeting approach, (b) potential interferences due to protein adsorption and (c) ineffective ligand presentation as a result of ligand interaction with the QD surface.

It is apparent that ligand presentation on the QD surface must be optimized to facilitate specific binding of the small molecule-QD conjugate to a cellular target. Furthermore, nonspecific protein adsorption to the QD surface, specifically adsorption of the serum protein albumin, significantly inhibits the ability of a ligand to interact with a cellular target. Albumin, a 66 kDa serum protein present in standard blocking solutions and widely used in biological protocols, has previously been shown to complex to reactive QD surfaces and facilitate QD endocytosis [*14*]. This protein adsorption, or "biofouling" as it has been called, to the QD surface is less problematic in the case of the larger antibody (~150 kDa) or streptavidin (~50 kDa) QD conjugates, but it has a dramatic effect for the ligand-QD conjugates due to the added size and steric bulk of adsorbed protein (illustrated schematically in Figure 4-1b). PEG modification reportedly prevents serum protein adsorption [*26*], but in this chapter, continued protein adsorption despite PEG surface modification is demonstrated. Additionally, it is apparent that PEG derivatives with increasingly hydrophobic targeting functionalities have the ability to self-assemble to the surface of ampiphilic QDs in the absence of any added coupling

reagents (Figure 4-1c). This hydrophobic ligand self-assembly results in a passivated, nontargeted QD surface better suited to prevent nonspecific protein adsorption. In this chapter, electrophoretic characterization techniques useful for the identification of adsorbed proteins on the QD surface are discussed and the improved surface passivation resulting from the hydrophobic self-assembly of PEGylated ligands is demonstrated. Fluorescence microscopy further demonstrates the utility of these improved probes in reducing the QD background signal *in* v*itro*, and illustrates the artifact endosomal fluorescence staining which results from albumin adsorption.

Results and Discussion

Self-Assembly of Hydrophobic PEG derivatives to the Quantum Dot Surface

Initial efforts were focused on the development of small molecule QD conjugates which would specifically interact with the serotonin transporter (SERT) membrane bound receptor. As such, custom ligands were synthesized to include a SERT selective terminus as well as a reactive amine terminus on either side of a PEG spacer. The amine functionality permitted covalent attachment to the carboxylic acid functionality on the surface of commercially available water-soluble ITK QDs, while the SERT selective small molecule would presumably be able to interact with its biological target. Agarose gel electrophoresis was used as verification of successful QD surface modification subsequent to covalent attachment of PEG ligands. As illustrated in Figure 4-2, the addition of PEG ligands acts both to decrease QD surface potential, by derivatizing negatively charged carboxylic acid residues, as well as increase the overall probe volume,

cumulatively resulting in a decreased electrophoretic mobility. Consequently, unconjugated QDs (lane 1) have an increased electrophoretic mobility in a 1% agarose gel as compared to IDT319 (lane 2) or IDT320 (lane 3) QD-conjugates. Unexpectedly, however, there was an observable difference between the relative mobility of IDT319 and IDT320 QD-conjugates. The only difference between these two ligands is a nine carbon alkyl linker between the PEG and the SERT-selective terminus, a seemingly negligible difference which should not result in any sizable disparity in electrophoretic mobilities, especially given the large overall molecular weight (~3400 Da) of the PEG ligand. This electrophoretic difference could therefore be attributed to differential ligand loading at the QD surface for these two similar ligands, perhaps mediated by added hydrophobicity at the IDT320 terminus.

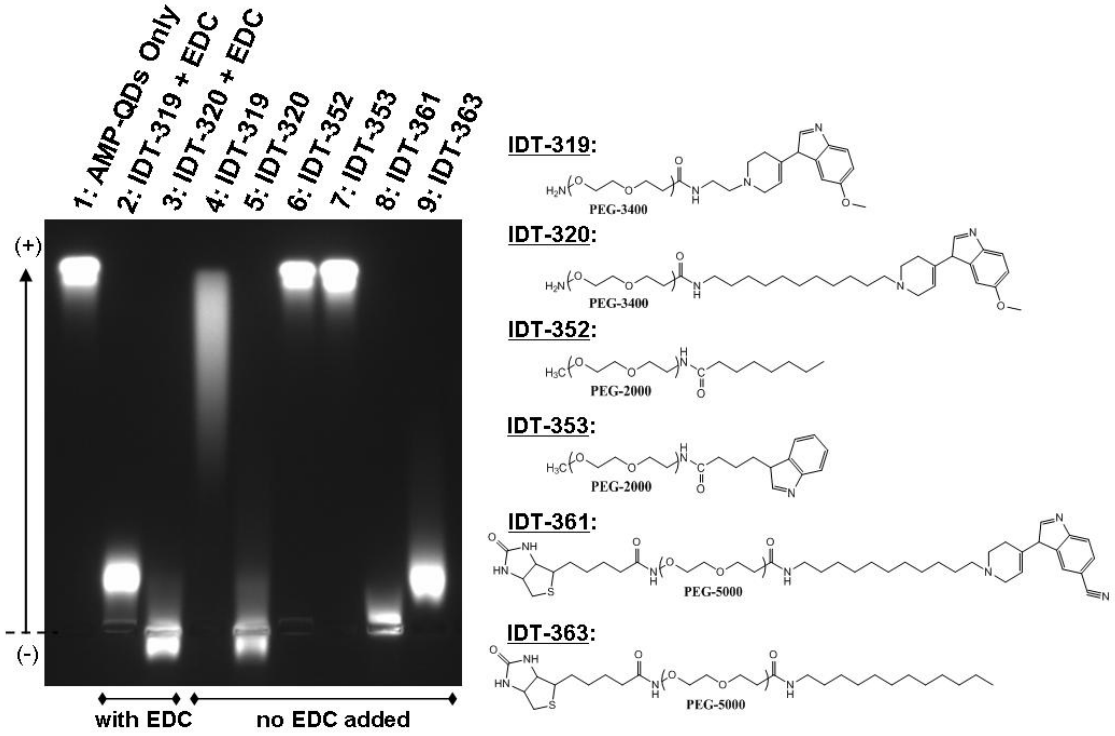

Figure 4-2. Agarose gel electrophoresis demonstrating assembly of PEG derivatives to QD surface. QD conjugates were run on a 1% agarose gel in TAE buffer for 80 min with a constant applied potential of 80 V. Unconjugated AMP-QDs (Lane 1) have a characteristic electrophoretic mobility due to the deprotonated carboxylic acid residues on their surface. Ligand conjugation to the QD surface retards the observed electrophoretic mobility, as seen for both IDT319 conjugates (Lane 2) and IDT320 conjugates (Lane 3). A diminished electrophoretic mobility is also observed for these ligands without added EDC coupling reagent, indicative of self assembly to the QD surface. Simply mixing IDT319 with QDs (Lane 4) results in conjugates which streak on the gel, indicating differential ligand loading; while IDT320 completely passivates the QD surface without covalent attachment (Lane 5). Other ligands were assayed in an attempt to understand the chemical functionality required to drive surface modification. PEG derivatives with either a short alkyl chain (IDT352, Lane 6) or an indole terminus (IDT353, Lane 7) both failed to drive surface modification in the absence of added coupling reagent. Self assembly is driven by added hydrophobicity at the PEG terminus, as illustrated for both IDT361 (Lane 8) and IDT363 (Lane 9). Structures of various IDT compounds are illustrated on the right.

To verify the possibility that a hydrophobic terminus could interact with the QD surface and cause self-assembly, the conjugation reaction was carried out without added EDC or NHS. EDC is a reagent that enables the formation of an amide bond between the terminal amine of the PEG ligand and carboxylic acid functionalities at the QD surface. Consequently, any observed surface modification in the absence of these coupling reagents would have to result from interactions with the ligand's more hydrophobic

SERT-selective region. The absence of added coupling reagents, presumably resulting in no ligand attachment, should result in products with the same electrophoretic mobility of unconjugated AMP-QDs. However, it is apparent that QD surface modifications do occur in the absence of added coupling reagents, most notably for increasingly hydrophobic PEG ligands (lanes 4-9, Figure 4-2). QDs mixed with IDT319 only resulted in partial surface modification (lane 4), suggesting that ligand attachment is at least partially dependent upon amide bond formation. The streaking observed in the IDT319 QD product in the absence of EDC and NHS is indicative of differential ligand loading at the QD surface. The IDT320 QD product (lane 5), however, results in complete surface modification and faithfully reproduces the electrophoretic mobility observed when the conjugation was carried out in the presence of EDC and NHS (lane 3). This indicates that IDT320 assembles independent of covalent ligand attachment and acts to passivate the reactive AMP-QD surface.

Additionally, alternate PEG ligands were synthesized to further elucidate the chemical functionality required to drive the self-assembly of PEG ligands to the AMP-QD surface in the absence of coupling reagents. PEG ligands terminated with either a seven-carbon alkyl chain (IDT352, lane 6) or an indole ring (IDT353, lane 7) did not result in appreciable QD surface modification. A PEG derivative with a longer twelve-carbon alkyl chain (IDT363, lane 9), however, did result in ligand assembly to the QD surface, as illustrated by a characteristic retardation of electrophoretic mobility. Taken together, these data indicate that this self-assembly of PEG ligands to the QD surface is driven by hydrophobic/hydrophilic interactions, and not a result of a specific chemical functionality present in the SERT-selective termini. Additionally, an alternate SERT-

selective cyano derivative (IDT361, lane 8), with a chemical functionality similar to IDT320 but synthesized via different intermediates, results in self-assembly to the QD surface; this further corroborates the importance of added hydrophobicity for driving assembly of PEG ligands to the QD surface.

Verification of Ligand Assembly by ^{1}H NMR

While agarose gel electrophoresis characterization qualitatively indicate the self-assembly of hydrophobic PEG derivatives to the QD surface, additional spectroscopic proof of this interaction is certainly necessary for verification of any such claims. As a result, a NMR experiment was devised to provide spectroscopic characterization of these QD-ligand structures and help quantify ligand coverage to verify any conclusions drawn from electrophoretic mobility measurements. Given the large number of structurally equivalent hydrogen atoms in their long PEG chains, the 1H NMR spectra of IDT319 and IDT320 predominately consist of a single large peak around 3.64 ppm (Experimental Methods, Chapter 2). The ^{1}H spectrum of unconjugated AMP-QDs (also Chapter 2) has no such feature present at that chemical shift, indicating the utility of this spectral feature in assessing ligand conjugation to the QD surface. NMR samples were diluted into deuterium oxide following QD conjugation to either IDT319 or IDT320, carried out as before both with and without added EDC coupling reagents, and special care was taken to eliminate any unbound ligand following conjugation (see Chapter 2). The ^{1}H NMR spectra of IDT319 and IDT320 conjugates, presented in Figure 4-3, illustrate IDT320 conjugation to the QD regardless of any coupling reagents, an indication that the observed differences in electrophoretic mobilities result directly from PEG surface

modifications. A large PEG peak is apparent for both the IDT319 and IDT320 QD-conjugates synthesized in the presence of EDC coupling reagents (Figure 4-3A). While this peak remains for IDT320 conjugates synthesized in the absence of any added coupling reagents, a demonstration that these hydrophobic PEG derivatives self-assemble to the QD surface, the IDT319 peak is significantly diminished in the absence of EDC (Figure 4-3B). The presence of additional peaks from the AMP-QD, presumably due to protons present in its ampiphilic polymer coating, permit normalization of integral areas with respect to QD concentration and facilitate straightforward sample-to-sample comparisons for determination of relative ligand loading. As expected, the integral areas for these QD-conjugates, each normalized to a doublet of doublets at 3.47 ppm from the AMP-QD, clearly indicate a similar ligand loading for IDT320 regardless of coupling reagents, while the IDT319 conjugates have approximately a 4-fold decrease in ligand loading without covalent attachment (Figure 4-3, inset). These results are obviously consistent with the results of the agarose electrophoresis experiment, in which any added ligand loading results in a diminished electrophoretic mobility. Taken together, these data provide an unambiguous demonstration of the attachment of PEG derivatives to the QD surface and provide an additional means to determine and compare ligand loading.

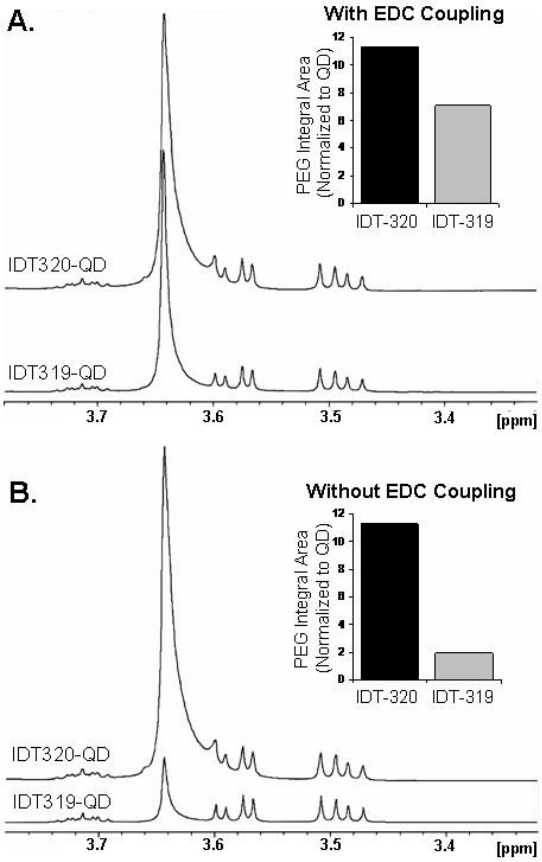

Figure 4-3. ^{1}H NMR characterization of QD-ligand conjugates. QD conjugation reactions to either IDT319 or IDT320 were carried out (A) with the addition of EDC coupling reagents or (B) in the absence of any coupling reagents; conjugates were then purified of any unbound ligand before analysis. Consequently, the presence of a peak at 3.64 ppm in the ^{1}H NMR spectra, due to the long PEG chain present in each ligand, is indicative of ligand attachment to the QD surface. (A) In the presence of EDC coupling reagents both IDT320 (upper spectrum) and IDT319 (lower spectrum) present a spectral feature indicating ligand attachment. (B) Without added coupling reagents, the feature is still clearly present for the IDT320 conjugates (upper spectrum), while this peak is greatly diminished for IDT319 conjugates (lower spectrum). The integral area of each PEG peak, which is directly proportional to amount of ligand present, is therefore indicative of ligand loading, but all areas must be first be normalized to a QD feature to permit any sample-to-sample comparison. (Inset) Quantification of integral areas, each normalized to the AMP-QD doublet of doublets at 3.5 ppm, clearly demonstrate equivalent ligand loading for IDT320 conjugates regardless of added coupling reagents, while the IDT319 conjugates demonstrate a roughly 4-fold decrease in ligand attachment in the absence of coupling reagents.

Artifact Fluorescent Staining in Cellular Assays Resulting from Albumin Adsorption

The utility of this surface modification approach, and the improved QD surface passivation, could be of great importance to biological imaging applications. Significant research efforts have been focused toward the development of small molecule conjugated QDs for biological imaging application, and these custom PEG ligands should ultimately

facilitate specific QD recognition of SERT. An initial attempt to demonstrate specific targeting of SERT in a cellular assay using these custom PEG derivatives, however, produced intriguing results. For this assay, SERT-expressing LLC-PK1 cells were incubated with either IDT319 or IDT320 ligand-conjugated QDs in a bovine serum albumin (BSA) blocking solution for 30 min at 37 °C, rinsed three times with cold PBS, and immediately imaged with a fluorescent microscope at 100× magnification. The observed fluorescent staining pattern for IDT319 QD conjugates (Figure 4-4A) was dramatically different from the negligible fluorescent staining observed for IDT320 conjugates (Figure 4-4B). This staining pattern observed for the IDT319 conjugates was not uniform across the field of view, but isolated to individual cells, an indication of specificity and apparently not the result of nonspecific QD interactions with the cellular membrane. This labeling, however, could not be blocked with the selective serotonin reuptake inhibitor paroxetine, and was apparent in parental cell lines which do not express SERT (data not shown), a clear demonstration that the custom PEG ligands were not mediating specific labeling of SERT. Additional imaging experiments indicated that the observed QD staining pattern involved active intracellular transport, demonstrated a cell cycle dependence, and could not be blocked with free ligand (Figure 4-5). It became apparent that albumin was mediating this effect when AMP-QDs, without any added surface modification, recapitulated the same fluorescent staining pattern following an initial incubation in a solution containing BSA (Figure 4-4C). Taken together, these data indicate that BSA adsorption (illustrated schematically in Figure 4-4) to AMP-QDs and IDT319 QD conjugates result in an endosomally associated fluorescent staining pattern,

while improved surface passivation of IDT320 QD conjugates prevent protein adsorption and any associated artifactual cellular labeling.

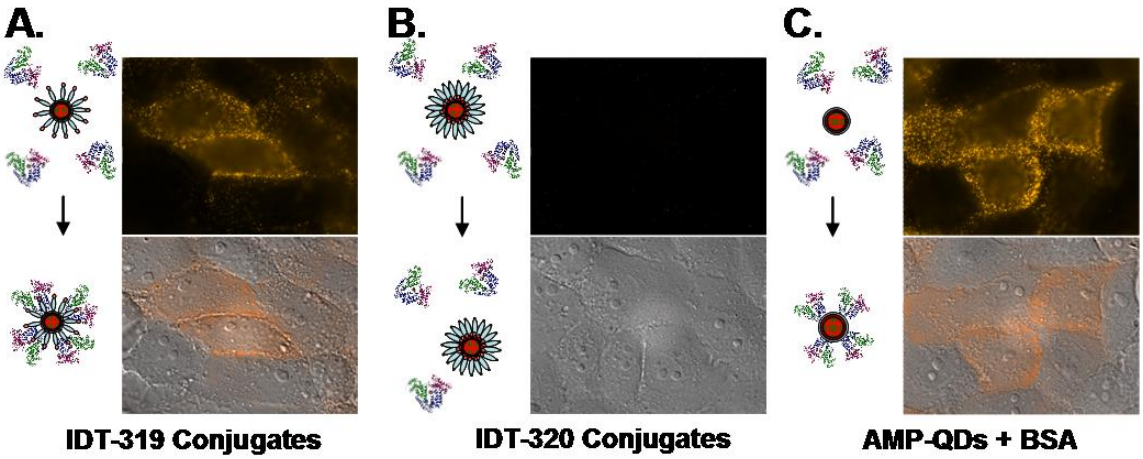

Figure 4-4. Cellular imaging with IDT319 and IDT320 QD conjugates. SERT-expressing LLC-PK1 cells were incubated with various QD conjugates in the presence of BSA, a standard blocking agent. QD fluorescence micrographs (top) and corresponding bright field composite overlay images (bottom) are shown for IDT319 QD-conjugates (A), IDT320 QD-conjugates (B), and unconjugated AMP-QDs (C). The fluorescent staining observed for the IDT319 conjugates is not ligand mediated, since the same pattern is observed with unconjugated AMP-QDs; rather this artifactual staining is apparently the result of albumin adsorption (illustrated schematically at left). No such albumin associated artifactual staining is observed for IDT320 QD conjugates, owing to the improved passivation of the IDT320 QD surface.

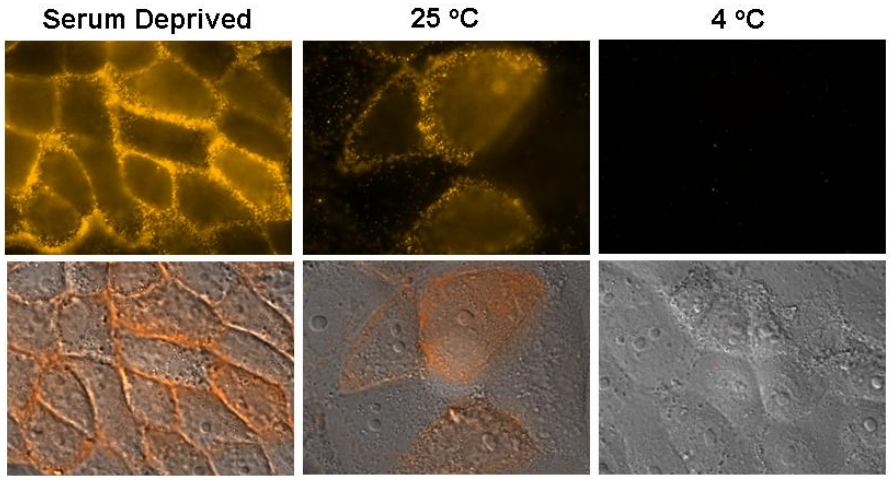

Figure 4-5. Characterizing the cellular response of IDT319 QD conjugates in the presence of serum proteins. Cellular labeling conditions were varied in order to better understand the nature of the observed artifactual labeling with IDT319 QD in a high serum protein blocking solution (2% BSA with 10% horse serum). Cells initially serum deprived overnight prior to QD labeling demonstrated a significant increase in QD fluorescence (Left, Serum Deprived)), an indication that this artifactual response is cell cycle dependent. This cell cycle dependence also explains the non-uniform nature of fluorescent staining for protein-QD conjugates in the absence of serum deprivation. Fluorescent staining caused by serum protein adsorption also exhibits a distinct temperature dependence. A non-uniform, endosomal fluorescent staining pattern is observed when the QD labeling is carried out at room temperature (Middle, 25 ^{o}C) while all fluorescent labeling is blocked upon QD incubation at 4 ^{o}C (Right). This temperature dependence suggests active cellular transport is involved in the observed fluorescent labeling, consistent with endosomal association.

Verification of Albumin Adsorption to Quantum Dot Surface

QD-BSA conjugates are reportedly photostable Endosomal markers [*14*], but it was assumed that PEG surface modification would passivate the reactive QD surface and eliminate any undesirable protein associations. A prior investigation has highlighted the utility of PEG to significantly reduce nonspecific interactions of AMP-QDs in live cell assays [*24*], but these previous results were collected in the absence of serum protein blocking conditions, and any potential protein interference was consequently not explored. It is now apparent that nontargeted PEG-QDs result in an endosomal fluorescent staining pattern for cellular assays where serum protein blocking conditions are employed (Figure 4-6). These cellular imaging results seem to indicate that BSA adsorption occurs despite PEG modification; yet, this protein adsorption to the QD

surface must first be verified in order to validate these assumptions. Gel-filtration chromatography has previously been employed as an analytical tool to assess serum protein interactions with QD surfaces [*26*], and has proven useful in identifying electrostatic interactions as the most likely cause of serum protein adsorption to QD surfaces [*125*]. An alternate approach using polyacrylamide gel electrophoresis (PAGE) to assess protein-QD interactions is described herein, without the added expense of gel-filtration chromatography instrumentation. Previous work has identified the utility of PAGE for characterization of QDs covalently modified with BSA [*126, 127*], but these studies focused on denaturing SDS-PAGE given the covalent nature of the QD surface modification. A nondenaturing, native gel was chosen for our assay in order to maintain the interaction which causes albumin adsorption to reactive QD surfaces. This approach initially facilitates electrophoretic separation of QDs from unconjugated protein, owing to a significant size difference; additionally, the resulting resolved gel can subsequently be stained to assess protein localization. Colocalization of a protein band, visualized via colorimetric detection, with the QD band, as determined by fluorescence, is therefore indicative of a protein-QD interaction; conversely, complete separation of protein from QDs occurs in the absence of any protein-QD interaction.

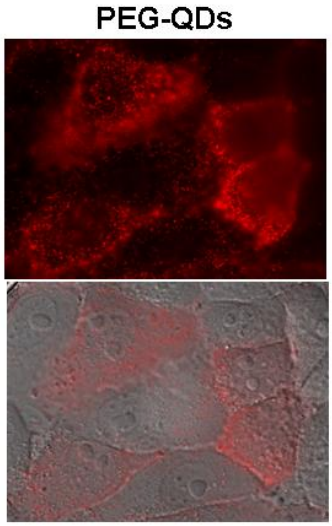

Figure 4-6. Demonstrating a similar artifactual response for other PEGylated QDs. Red emitting AMP-QDs (655 nm emission), covalently modified with PEG2000 as previously reported [*24*], result in the same non-uniform fluorescent staining pattern as IDT319 derivatized PEG conjugates upon cellular incubation in serum blocking conditions. This artifactual fluorescent staining is observed despite the improved passivation of PEGylated QD conjugates.

Protein analysis is routinely performed using PAGE and frequently incorporates both a lower percentage polyacrylamide stacking gel with a higher percentage resolving gel. The QD characterization technique developed in this study makes use of a 2.5% polyacrylamide stacking gel and a 10% resolving gel. As large particles experience a decreased electrophoretic mobility with increasing polyacrylamide concentration, the initial 2.5% gel facilitates QD migration and protein separation, while the 10% resolving gel acts a barrier to the QDs, concentrating them to an individual band (Figure 4-7, left). A Coomassie Blue stain after electrophoretic separation subsequently permits colorimetric determination of protein localization (Figure 4-7, right). Using this approach, free BSA separates into three distinct bands, characteristic of albumin monomers, dimers, and globulins (Figure 4-7, lane 1), but BSA adsorbed to the QD surface appear as an additional band coincidental with the QD fluorescence (highlighted with red box). Of particular notice, the dark band associated with AMP-QDs (lane 6)

indicates a large degree of albumin association. Additionally, IDT319 conjugates (lane 4) have an increased albumin adsorption as compared to their IDT320 counterparts (lane 2), consistent with the cellular imaging observations. The covalent PEG attachment for the IDT319 conjugates does act to reduce the amount of albumin adsorption as compared to AMP-QDs, but apparently this minimal amount of protein is still sufficient to cause the observed artifact in fluorescent imaging experiments. Control samples consisting of QD conjugates without added BSA (lanes 3, 5, and 7) provide verification that the observed staining is not due to QD interferences. While this PAGE characterization may lack the sensitivity of a comparable gel-filtration approach, it does serve as a facile tool to quickly assess potential protein interactions at the QD surface without any significant instrumentation expenditure.

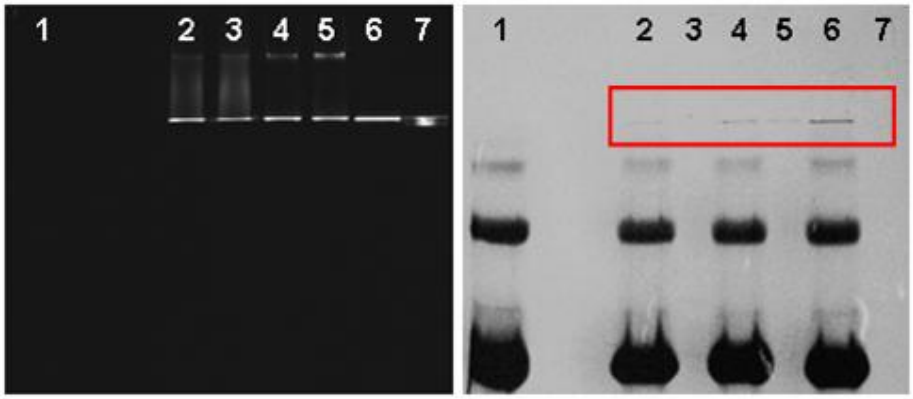

Figure 4-7. Polyacrylamide gel electrophoretic determination of albumin adsorption to reactive QD surfaces. A fluorescent image (left) illustrates QD accumulation at the interface between the 2.5% stacking gel and the 10% resolving gel. A bright field image following Commassie Blue staining (right) confirms protein localization. Unassociated BSA is evident in the resolving gel as three characteristic bands. Albumin adsorbed to the QD surface, however, colocalizes with the QD fluorescent bands (highlighted with a red box). Lane 1: BSA without any QDs. Lane 2: IDT320 QDs with BSA. Lane 3: IDT320 QDs, no BSA. Lane 4: IDT319 QDs with BSA. Lane 3: IDT319 QDs, no BSA. Lane 6: AMP-QDs with BSA. Lane 7: AMP-QDs, no BSA. The passivated IDT320 QD show minimal albumin adsorption (Lane 2) compared to IDT319 conjugates (Lane 4), while AMP-QDs show the highest degree of albumin association (Lane 6).

Summary and Future Directions

It is now apparent that increasingly hydrophobic ligands will self-assemble to the QD surface, presumably through an interaction with the hydrophobic organic capping ligands present on the QD surface. The development of a small molecule approach to specifically target membrane associated receptors with QDs is obviously dependent upon ligand presentation at the QD surface. Unfortunately, with regards to small molecule targeting, these hydrophobic termini are not able to interact with their intended targets due to this intimate association with the QD surface. An improved architecture for optimal ligand presentation on the surface of AMP-QDs must therefore incorporate a less hydrophobic targeting compound, limiting the potential interaction the drug derivative will have with the QD surface. Previous small molecule $GABA_c$ receptor specific muscimol-QD derivatives [*62*] incorporate a more hydrophilic targeting functionality which is deprotonated at physiological pH, thus permitting covalent attachment to the QD surface without adversely affecting ligand presentation. It is apparent, however, that certain biological targets will necessarily require hydrophobic compounds for effective labeling. In these instances, one possible QD targeting strategy would utilize a two step labeling approach incorporating biotinylated ligands to initially facilitate a specific interaction with an intended biological target and subsequently be recognized by a streptavidin conjugated QD. This method will allow the hydrophobic targeting terminus to seek out its intended target in the absence of QDs, altogether eliminating the necessity of ligand presentation at the QD surface [*128*]. Alternately, effective presentation of hydrophobic drug derivatives on the AMP-QD surface could be accomplished through the use of a rigid linker, such as an oligoproline for example, in the place of a PEG chain. This added

rigidity would conceivably prevent the ligand from being able to wrap back on itself and limit the potential interaction it might have with the QD surface. Furthermore, recent advances in developing water soluble QD conjugates via the displacement of organic capping ligands, thus eliminating significant regions of hydrophobicity, may ultimately provide a suitable platform for hydrophobic ligand presentation, but issues regarding diminished colloidal stability and fluorescence quenching are still of concern for these novel conjugates [*129, 130*]. In addition to these observations regarding ligand presentation, we have demonstrated the improved passivation resulting from self assembly of PEG derivatives, which have proven to be even less reactive than covalently modified PEG-QDs. These self assembled conjugates may ultimately provide a useful platform for biological applications owing to their ability to eliminate unwanted protein adsorption and other associated interferences.

Previous reports have focused on identifying appropriate blocking strategies and surface modifications which limit biological recognition of nanoparticles and reduce their nonspecific binding to cellular membranes. The data presented in this chapter, however, highlight a seemingly subtle difference; certain biological compounds can inadvertently alter the QD surface, resulting in an altogether different type of artifactual labeling. These data highlight the potential interference protein adsorption can cause in cellular assays which incorporate QD probes, despite efforts to limit QD reactivity through PEG surface modification, and it is immediately apparent that the observed endosomal staining could easily be mistaken for a specific interaction. These results could provide insight into several seemingly anomalous QD labeling patterns reported throughout the scientific literature. Serum protein adsorption, and in particular albumin adsorption, is likely to

occur in any *in vivo* analysis and is also likely to occur in numerous *in vitro* assays, where serum blocking is widely employed to limit unwanted fluorescent background staining. While the use of serum proteins is generally accepted in biological protocols, and furthermore necessary for maintaining long term cellular viability, their potential reactivity with QD probes is frequently neglected. At least one study has demonstrated the importance of selecting an appropriate blocking solution for effective and specific QD labeling [*25*], and these results provide further insight into the persistent nature of this problematic interference. Conversely, an alternate report has highlighted a potential application utilizing protein adsorption on gold nanoparticles to facilitate intracellular delivery and mediate materials transfection [*131*], consistent with the intracellular staining observed with our own albumin-modified QDs. Consequently, protein adsorption can be either desirable or an unwanted interference depending on the nature of the biological assay in question, which further highlights the importance of improved approaches to control the QD surface and mediate biomolecule attachment.

CHAPTER V

SPECIFIC LABELING OF THE SEROTONIN TRANSPORTER WITH SMALL MOLECULE QUANTUM DOT CONJUGATES

Introduction

A family of Na^+- and Cl^--coupled neurotransmitter transporter proteins has long been known to play a critical role in regulating extracellular monoamine concentrations and terminating synaptic transmission. These substrate-specific membrane transporters, including the transporters for serotonin (SERT), dopamine (DAT), norepinephrine (NET), γ-aminobutyric acid, glycine, and proline (among others) [*132*], all share a distinct structural homology, each consisting of 12 transmembrane domains with intracellular C- and N-termini [*133*]. These transporters represent established targets for numerous psychostimulants and antidepressants, which exert their psychotropic effect through the inhibition of transporter function to cause elevated extracellular monoamine concentrations. Furthermore, several neurotoxins have been identified which utilize transporters to gain intracellular delivery and induce a cytotoxic effect [*134*], and genetic mutations affecting transporter expression and activity have been implicated in various disease states [*135*]. Analytical approaches to investigate fundamental transporter processes such as their expression, function, and localization have largely relied on autoradiographic methodologies incorporating radiolabeled substrates. These techniques, however, are limited due to poor spatial and temporal resolution, and are additionally cumbersome due to specialized training and licensing required for the handling and disposal of radioactive compounds. The research presented in this chapter highlights

recent progress in the development of small molecule QD conjugates to specifically interrogate SERT expression in living cells.

Pharmacological Significance of the Serotonin Transporter

Cell surface receptors, ion channels, and transporters are critical components of signaling and excitability within the nervous system. As such, they represent the majority of drug targets currently being explored in the pharmaceutical industry. Serotonin, in particular, is a critical neurotransmitter in brain circuits subserving mood, emotion, appetite, social behavior and libido. Whereas serotonin levels in the presynaptic neuron are established by biosynthetic and degradative pathways, the synaptic actions of serotonin at serotonin receptors are principally constrained by rapid clearance sustained by the serotonin transporter (SERT). SERT is the principle site of action for selective serotonin reuptake inhibitor (SSRI) antidepressants and has been an established drug target for decades [*136, 137*] (e.g. Prozac, Paxil, Zoloft, Desiril and Elavil are all SSRIs). In fact, by the year 2000, annual U.S. sales of SSRI antidepressants totaled approximately seven billion dollars [*138*]. Only recently, however, has it been shown that transporter-mediated clearance of neurotransmitters is under tight regulation including polarized expression of transporter proteins [*139*], protein kinase-mediated alterations in cell surface expression [*140*], and activity-dependent phosphorylation and redistribution [*141*]. Consequently, many drugs appear to alter the responsiveness, distribution and/or surface abundance of their protein targets following chronic occupancy. Additionally, the SERT gene exhibits polymorphisms that alter expression and activity which have been correlated with disease states such as autism, obsessive compulsive disorder (OCD),

depression, and anxiety [*135, 142*]. Advances in understanding the basic mechanisms underlying these patterns of localization, ligand-dependent redistribution, and correlation with specific disease states require tools sufficient to localize transporter proteins *in situ* in living cells.

Small Molecule Quantum Dot Conjugates to Interrogate SERT

Small molecule QD conjugates capable of interacting with SERT were initially prepared to circumvent the numerous disadvantages associated with various isotopic approaches [*61*]. Prior to this proof-of-concept demonstration, fluorescent imaging of SERT has been limited to immunofluorescent (IF) staining on fixed and permeablized cell cultures, where selectivity was introduced with an antibody specific to the intracellular N- or C- terminal domains of SERT [*143, 144*]. While antibodies specific to an extracellular epitope of SERT have been developed [*145, 146*], no fluorescent imaging employing an extracellular antibody has been demonstrated to date for live cell cultures. These extracellular antibodies have instead proven useful for both western blot analyses and immunoprecipitation assays, but they apparently lack a sufficiently strong interaction to facilitate IF staining. The SERT-selective, small molecule QD conjugates have therefore provided the only demonstration of fluorescent labeling of SERT in a live cell assay [*61*]. These QD conjugates, however, had associated drawbacks which ultimately limited their utility in expanded biological applications. Most notably, the QDs employed in this study had a reduced colloidal stability as well as a diminished quantum yield, an unintended consequence of the ligand exchange reaction used to derivitize the QD surface. Improved fluorescence and solution stability was eventually afforded,

through a collaboration with the Quantum Dot Corporation, by encapsulating QDs in an ampiphilic polymer (AMP-QDs) [*19*], and all subsequent research efforts were then focused on modifying this AMP-QD scaffold to generate improved small molecule QD conjugates.

Despite their improved optical properties and enhanced solution stability of these AMP-QDs, numerous technical difficulties had to be overcome prior to their routine incorporation in biological assays using a small molecule targeting strategy. Notably, AMP-QDs exhibited a large degree of nonspecific interactions in cellular assays, and it was demonstrated that surface modifications with PEG could be employed to limit these undesirable interactions [*24*]. Having detailed an approach which greatly reduced the observed nonspecific cellular interactions without adversely affecting the QD's photophysical properties, significant research efforts were then directed at modifying the PEG chain to facilitate specific interactions with cellular membrane receptors. Consequently, the introduction of biological specificity has relied on a PEG backbone to both eliminate nonspecific cellular interactions and additionally provide a scaffold which extends a small molecule drug derivative away from the QD surface to facilitate small molecule recognition of a biological target. A universal approach was therefore developed to derivatize PEG linkers to include one receptor specific terminus and an opposing reactive amine terminus, permitting subsequent covalent attachment to AMP-QDs [*124*]. Consequently, high affinity ligands for both the dopamine transporter (DAT) and the serotonin transporter (SERT) have been developed and been shown to retain biological activity, via a competitive binding assay, even after conjugation to the QD surface [*147, 148*]. Despite the development of biologically active small molecule-QD

conjugates, specific cellular recognition and labeling was not immediately forthcoming as additional interferences further complicated fluorescent imaging applications.

Finally, two additional interferences became evident after continued attempts to demonstrate specific labeling of cellular targets with these biologically active QD conjugates, namely: (1) ineffective ligand presentation at the QD surface and (2) protein adsorption to the QD surface. As described in Chapter IV, small molecule drug derivatives which are employed to specifically interact with a biological target can self-assemble to the AMP-QD surface due to hydrophobic interactions [*149*]. Consequently, the hydrophobicity or hydrophilicity of the drug derivative targeting compounds is a key determinant in the efficacy of ligand presentation at the QD surface. While relatively hydrophilic ligands can be covalently attached to AMP-QDs surface and still be useful for fluorescent imaging applications, as is the case for effective small molecule-QD conjugate recognition of $GABA_c$ receptors [*62*], increasingly hydrophobic derivatives will have a strong interaction with the QD surface and not be available to interact with their intended biological target. Additionally, the presence of serum proteins in biological labeling protocols can result in another potential interference which can further complicate fluorescent imaging applications. While PEG modification undoubtedly reduces nonspecific interactions in cellular assays [*24*], we have demonstrated albumin adsorption to the QD surface will occur despite PEG attachment and result in artifactual fluorescent staining [*149*]. Care must therefore be taken to avoid or eliminate all potential interferences in designing an effective small molecule QD labeling protocol to specifically interrogate a biological target.

Successful Small Molecule Quantum Dot Labeling in Xenopus Laevis

Building on the successful demonstration of $GABA_c$ labeling with muscimol-conjugated QDs [*62*], the *Xenopus* oocyte model system was subsequently employed to demonstrate specific targeting of membrane bound SERT proteins. Isolated from the ovarian lobes of gravid adult female *Xenopus laevis* toads, *Xenopus* oocytes are easily transfected by means of cRNA microinjection, and have been widely used for studies involving membrane bound receptor expression. As such, these oocytes have evolved into a robust model system for QD labeling studies which provide intrinsically low nonspecific QD interactions. Initial investigations with SERT-expressing *Xenopus* oocytes identified IDT318 as a suitable ligand for specific labeling of SERT with QDs. IDT318 (Figure 5-1) consists of a SERT selective drug derivative attached to a biotinylated PEG-5000 via a long chain (11-carbon) alkyl spacer.

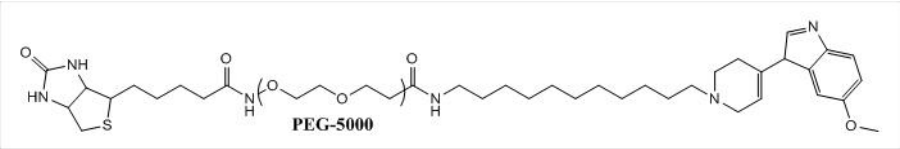

Figure 5-1. Structure of the SERT-selective ligand IDT318. This ligand incorporates a biotin terminus (left) to permit recognition by streptavidin-QDs, a long PEG chain with a long chain alkyl spacer (middle) and a SERT-selective drug derivative to facilitate specific recognition of SERT (right).

The added hydrophobicity of the long alkyl chain is apparently required for SERT recognition, which precludes its direct attachment to the QD surface due to ineffective ligand presentation as a result of hydrophobic interactions with the QD surface. The biotin terminus, however, permits a two step labeling protocol to be employed, taking advantage of the high affinity biotin/streptavidin interaction. In this protocol, IDT318 is first allowed to interact with SERT-expressing oocytes in the absence of QDs, eliminating any potential interaction the hydrophobic ligand may have with the QD

surface. Excess unbound ligand is then washed away and streptavidin-QDs (SA-QDs) can then be used to detect the biotin terminus of the ligand, ultimately facilitating specific QD labeling. While SERT expression in an oocyte model provides a useful platform for ligand screening, optimization in a mammalian cell model is ultimately required to realize the full potential of these unique QD conjugates in applications ranging from the elucidation of cellular signaling pathways, to high-throughput drug discovery and eventually to their administration *in vivo*.

Suspension Cells Result in Diminished Fluorescent Background

Having developed a better appreciation for the potential interferences that can adversely affect small molecule-QD conjugate recognition of biological targets, a modified protocol was subsequently developed in an attempt to demonstrate specific labeling of SERT expressed in a mammalian cell line using IDT318. As a control experiment for this two-step labeling method, adherent mammalian cells were incubated simply in a solution of SA-QDs in KRH buffer, without added serum proteins for blocking purposes, and an extremely high background fluorescence was observed with especially significant QD association to the glass slide (illustrated in Figure 1A). While a blocking solution would reduce this background, it would potentially interfere with small molecule recognition and QD labeling. Furthermore, extensive rinsing following QD labeling only marginally reduced the observed background and frequently caused the cells to lift from the plate altogether. Previous work, however, with Jurkat cells [*40*] as well as primary lymphocytes (Figure 1B), which are both suspension cell lines, indicated no significant QD background upon incubation with similar SA-QD solutions. This

reduced fluorescent background can be attributed to improved rinsing by centrifugation to rinse away unbound QDs and eliminating potential nonspecific QD interactions with the culture vessel. This exceedingly low background suggests that a suspension cell model would be an improved mammalian cell platform for QD detection.

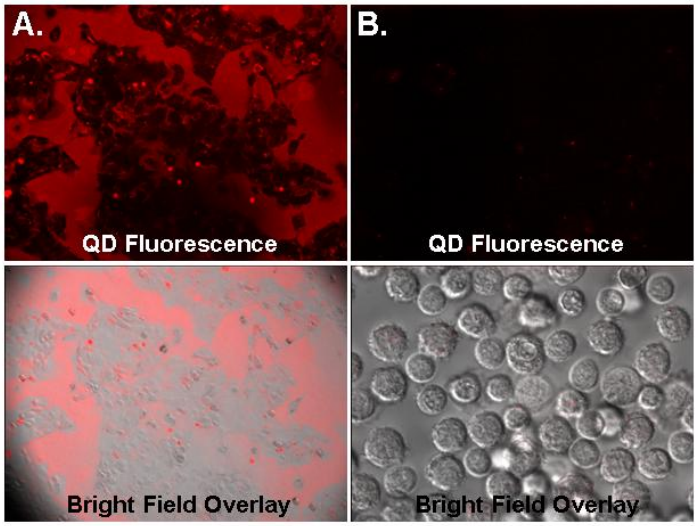

Figure 5-2. Nonspecific fluorescent background from 5 nM SA-QD exposure to adherent LLC-PK1 (A.) or primary lymphocyte suspension cells (B.) Fluorescent micrographs (top) with corresponding DIC overlay images (bottom) illustrate a high degree of nonspecific SA-QD interaction to the adherent cell culture, most notably to the regions where the glass slide is exposed. A significant reduction in fluorescent background is seen for suspension cells, causing a dramatic increase in the sensitivity of QD detection.

Results and Discussion

Identifying a Suitable Suspension Cell Line for SERT Expression

In order to take advantage of the extremely low fluorescent background afforded by suspension cells, it was initially necessary to identify a suitable non-adherent cell line to assay the expression of SERT. Previous reports have indicated that peripheral blood lymphocytes endogenously express functional SERT [*150*], but initial efforts to detect SERT in these cells were unsuccessful (apparently due to low expression levels).

Additional efforts to transiently transfect Jurkat cells to express SERT also failed; as suspension cell lines are notoriously difficult to transfect with cationic lipid or liposome transfection reagents [*151*]. A transient transfection approach was then employed to drive SERT expression in adherent HEK-293T cells, with the intention of generating a cellular model system with an elevated expression of SERT. These SERT expressing cells could then be lifted from the culture vessel, labeled with QDs in suspension, and subsequently assayed as suspension cells. While stable cell lines known to express SERT are available, this transient transfection of plasmid cDNA seemed to provide an added level of control over cellular expression levels. Stable lines gradually loose functional expression of transfected proteins with increasing cell passage number, while transient transfection can routinely provide a distinct population of cells with elevated SERT expression just 48 hours after transfection. Sham-transfected cells (Ø-293T) can also be generated by performing the transfection with empty pcDNA3.0 vector, resulting in a suitable negative control cell population which lack SERT expression.

Successful transfection, resulting in functional SERT expression, was subsequently verified with IDT307, a small molecule which is selectively transported by monoamine transporters and results in a distinct intracellular fluorescence [*152*]. This compound has therefore provided a rapid and facile approach to confirm the expression of SERT, altogether eliminating a great deal of uncertainty regarding receptor expression (cellular imaging with IDT307 is discussed in greater detail in Appendix A). Prior to the development of IDT307, verification of SERT expression could only be performed via isotopic uptake analyses, which were performed sparingly due to the experimental difficulty associated with this approach. IDT307, on the other hand, can be used to

demonstrate successful transfections by a simple fluorescent assay. Incubating cells with IDT307 results in a distinct intracellular green fluorescence for SERT-expressing populations (Figure 5-3A), while no such fluorescence staining is observed for cells lacking SERT expression (Figure 5-3B). IDT307 was therefore utilized in subsequent analyses as a means to initially confirm SERT expression, eliminating the expenditure of time and reagents in the instances where SERT is not functionally expressed.

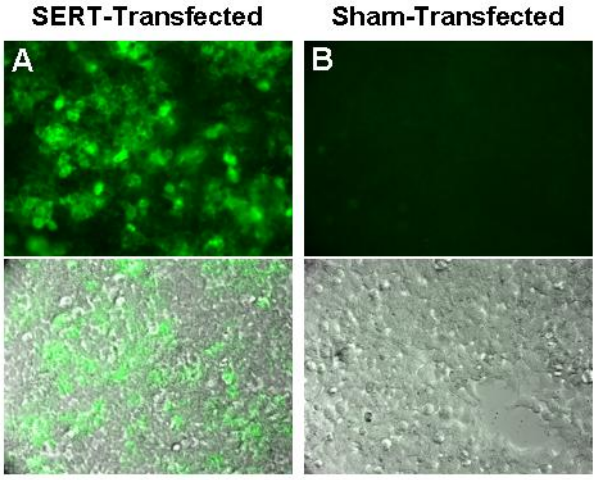

Figure 5-3. Demonstrating SERT expression with IDT307. Successful transfection was verified by incubating both SERT-transfected (A) and sham-transfected (B) cells with 5 μM IDT307. SERT expression is confirmed by a characteristic intracellular green fluorescence.

Successful Labeling of SERT in HEK-293T Cells with IDT318

This ability to verify SERT expression prior to QD labeling experiments, combined with the identification of previously mentioned interferences, ultimately allowed for the development of a protocol to successfully label SERT in mammalian cell cultures. This labeling protocol was derived from successful QD labeling experiments in an oocyte model system, and consequently utilized a two-step labeling with IDT318 and streptavidin-QDs to fluorescently interrogate SERT expression. Transiently transfected HEK-293T cells were therefore incubated with a 1 μM solution of IDT318 in PBS for

one hour, optimized parameters from experiments with oocytes, before dissolution from the plate using a trypsin-EDTA solution and subsequent QD labeling in suspension. The two-step labeling eliminated any ligand interactions with the QD surface, and interferences due to albumin adsorption were avoided by removing serum protein blocking. Specific labeling of SERT is evident for SERT-expressing HEK293T cells (Figure 5-4A), which can be blocked with the SSRI paroxetine (Figure 5-4B) and is not apparent in sham-transfected cells lacking SERT (Figure 5-4C).

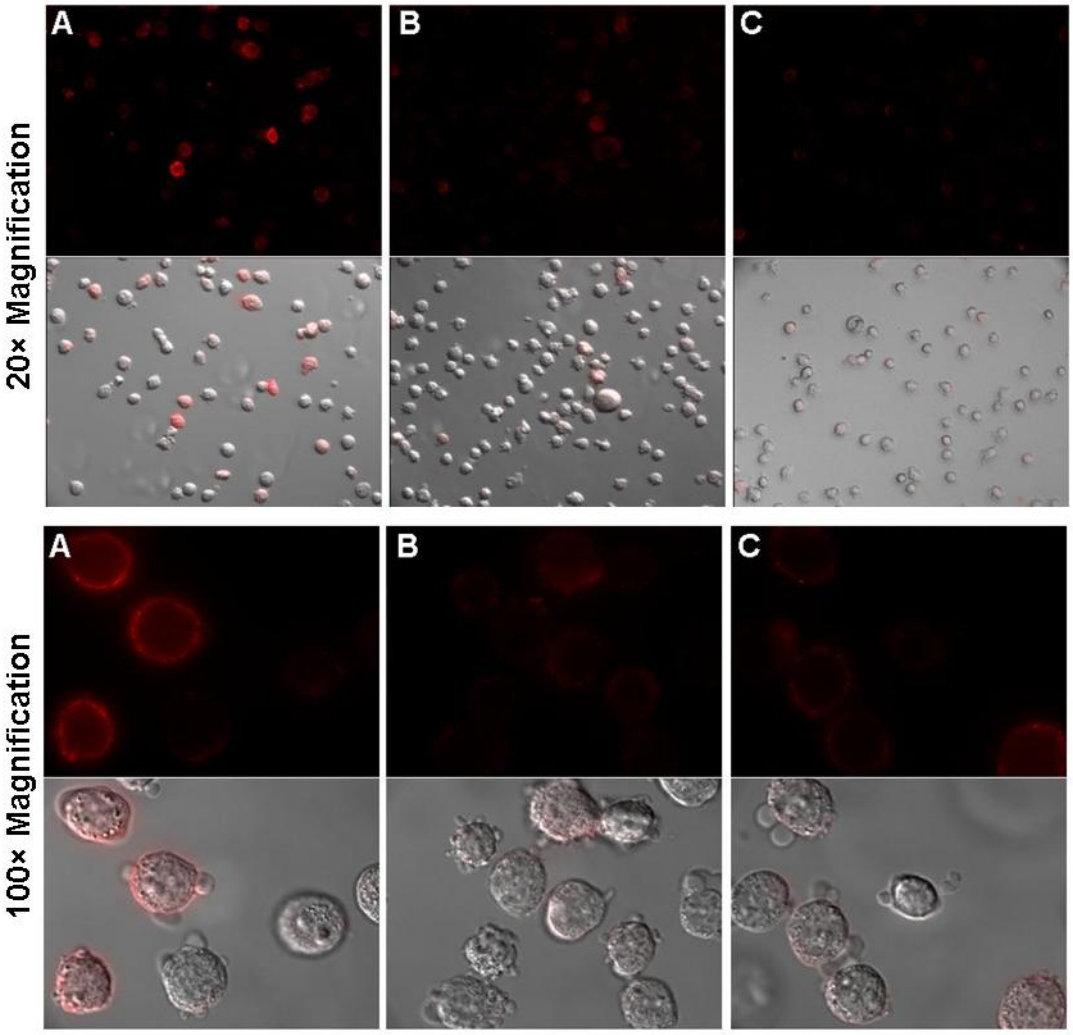

Figure 5-4. SERT specific labeling in mammalian cells with IDT318. Adherent HEK-293T cells were transiently transfected with plasmid DNA to drive SERT expression (A and B) or empty pcDNA3.0 vector (C, negative control). These cells were initially exposed to 1 μM IDT318 biotinylated ligand in PBS, then lifted from the plate and labeled in suspension with 2.5 nM streptavidin-QDs. Increased fluorescent intensity is apparent for SERT-expressing cells (A). Pre-incubation with 20 μM paroxetine (a SSRI) reduces the fluorescent labeling in SERT-expressing cells (B) to levels comparable to sham-transfected cells which lack SERT (C). Images were acquired at 20× (top) or 100× (bottom) magnification and have been thresholded equivalently for clear comparison.

Fluorescent microscopy experiments therefore demonstrated a SERT-specific IDT318 QD labeling for transiently transfected cultures which was not uniform across the entire cell population. This non-uniformity can be attributed to the transient transfection approach utilized to drive SERT expression, where only a fraction of the cells effectively

take up the plasmid and eventually express the encoded protein. This number of SERT positive cells in any given transfected cell population is therefore limited by transfection efficiency. However, the discriminate labeling of individual SERT positive cells within a mixed population does provide a further demonstration of SERT specificity.

Flow Cytometry to Verify Specific SERT Labeling

Fluorescent microscopy experiments were performed by simply depositing an aliquot of the cell suspension onto a glass slide and imaging once the cells had settled down to the focal plane. While this approach was effective at demonstrating specific labeling of SERT, the presence of cells outside the focal plane and large fluorescent aggregates frequently interfered with fluorescent imaging. The utilization of suspension cells, however, is perhaps more conducive to analysis by flow cytometry. Such an analysis provides the ability to rapidly assess the distribution of fluorescent intensities for an entire population of cells, and confers greater statistical certainty than photomicrographs of smaller numbers of cells. Flow cytometry analyses were subsequently performed on a BD LSRII flow cytometer available through the VMC Flow Cytometry Shared Resource. Population gates for all flow analyses were established from scatter parameters to ensure interrogation of only viable, single cells. Histograms displaying the number of cells at a given QD fluorescence intensity, as illustrated in Figure 5-5, were generated using BD FACSDiVa^{TM} software. SERT labeling is evident in these histograms as a shoulder at higher QD fluorescent intensity for SERT-expressing populations of cells (Figure 5-5, population indicated in orange). This population is diminished for both SERT-expressing cells pre-blocked with the SSRI paroxetine and sham-transfected cells lacking SERT,

indicating the specificity of IDT318 for SERT. Control experiments where SA-QDs were exposed to cells without IDT318 result in a dramatic decrease in fluorescence intensity across the entire population of cells (Figure 5-5, right). This finding indicates that the IDT318 ligand causes a uniform, nonspecific labeling due to ligand-mediated interactions with the cells, and the SERT specific labeling is only apparent at fluorescent intensities above this background.

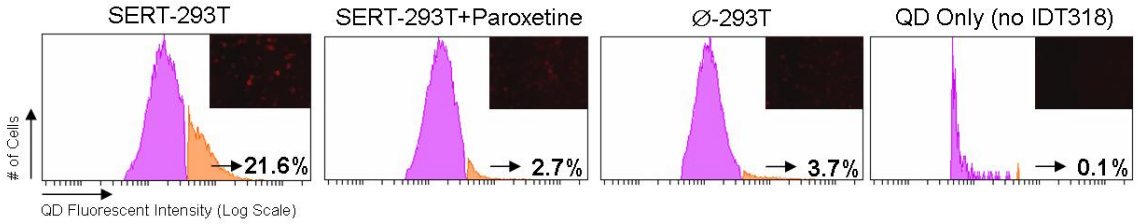

Figure 5-5. Flow cytometry analysis of different cell populations labeled with IDT318 targeted QDs. A population of cells specifically labeled for SERT is evident at higher fluorescent intensities for SERT expressing cells (left panel). This SERT-specific component can be blocked by pre-incubation with paroxetine and is not evident in sham-transfected populations (middle two panels). Control experiments using SA-QDs without the addition of IDT318 ligand indicates the presence of an added fluorescent background due to nonspecific, ligand-mediated cellular interactions. Fluorescent micrographs (inset) are in agreement with these findings.

Optimized Parameters for Targeting SERT in Cellular Assays

While the initial labeling conditions derived from successful labeling in *Xenopus* oocytes provided specific fluorescent imaging of SERT in a transiently transfected mammalian cell line, further modifications were required to optimize this SERT specific response of IDT318 in cellular assays. Two parameters in particular, ligand incubation time and ligand concentration, proved to differ significantly from the oocyte model to a mammalian cell system. Optimization of these two critical parameters minimized the ligand-mediated fluorescent background and improved sensitivity in SERT detection.

To assess the effect ligand incubation time has on specific SERT labeling, SERT-transfected HEK-293T cells were exposed to a 1 μM of IDT318 in PBS for specific time

intervals between five minutes and one hour. Sham-transfected HEK-293T cells were also exposed to identical conditions, and provided a suitable negative control for each time point. The results of this time-course experiment, summarized in Figure 5-6, illustrate specific labeling of SERT after only five minutes of exposure to the ligand, while a maximal fluorescent response is attained within 10-20 minutes of ligand incubation. The ligand-mediated nonspecific background is also increased at longer incubation times, as indicated by the sham transfected populations shifting to higher fluorescent intensities, allowing for minimized nonspecific background with shorter incubation times. Minimizing, or altogether eliminating, this ligand-mediated background will act to increase the sensitivity of SERT detection and acts to enhance the detection specific SERT labeling.

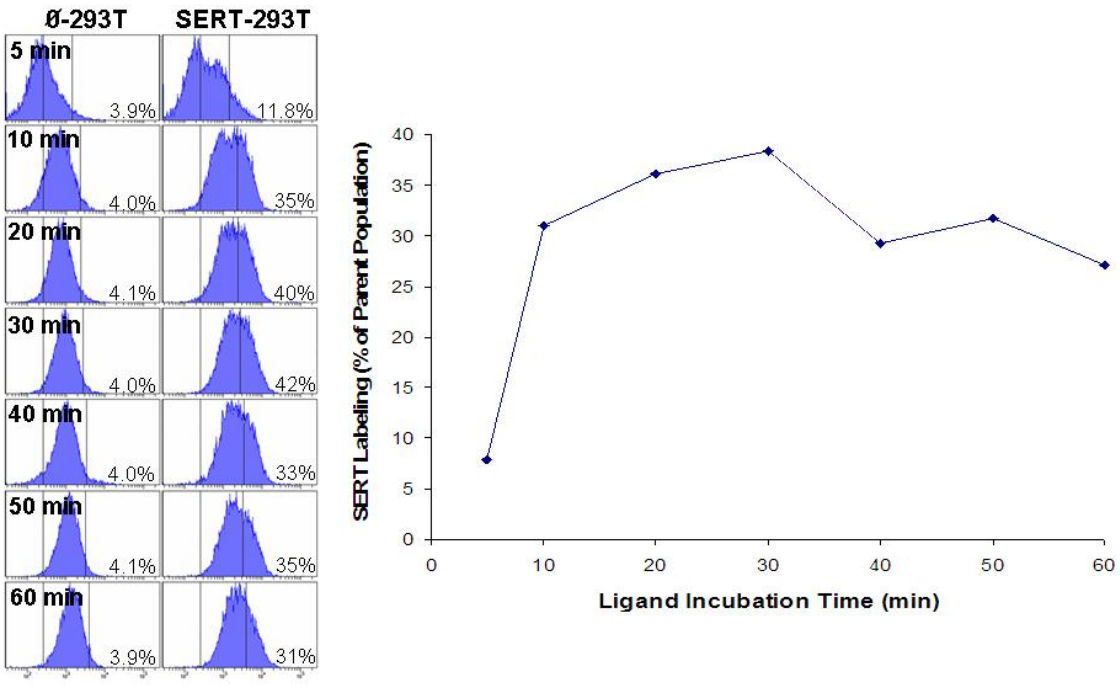

Figure 5-6. Determination of optimal incubation time for IDT318 labeling of SERT in cellular assays. Flow cytometry analysis of transiently transfected, SERT-expressing HEK-293T cells (SERT-293T, right column) demonstrate specific labeling of SERT at each time point as compared to sham-transfected cells lacking SERT (∅-293T, left column). Quantification of the SERT positive population was determined for each time point, and is expressed as a percentage of the parent population above a 4% threshold, established from each time's sham-transfected negative control. Graphical representation of these data after background subtraction (right) indicate maximal SERT labeling after only 10-20 minutes of ligand exposure. Longer incubation times cause an increase in the ligand-mediated background fluorescence which actually reduces detection of the SERT-positive population.

Having identified 20 minutes as a suitable incubation time for IDT318 labeling of SERT, an investigation of the concentration dependence of IDT318 labeling was then conducted. For this experiment, SERT-transfected HEK-293T cells were exposed to various concentrations of IDT318, each for 20 minutes. As in the time-course analysis, sham-transfected cells were exposed to identical labeling conditions to provide a negative control at each concentration point. The results, detailed in Figure 5-7, illustrate the concentration dependence for specific labeling of SERT with IDT318. SERT specific labeling is evident at 100 nM IDT318 concentrations, and peaks around 500 nM. At ligand concentrations above 1 μM however, the nonspecific ligand-mediated background

fluorescence once again overcomes the SERT-specific component, this time causing a dramatic decrease in SERT detection. This nonspecific background shows a strong dependence on IDT318 concentration, and can be minimized with lower concentrations of IDT318 to provide more sensitivity for SERT detection.

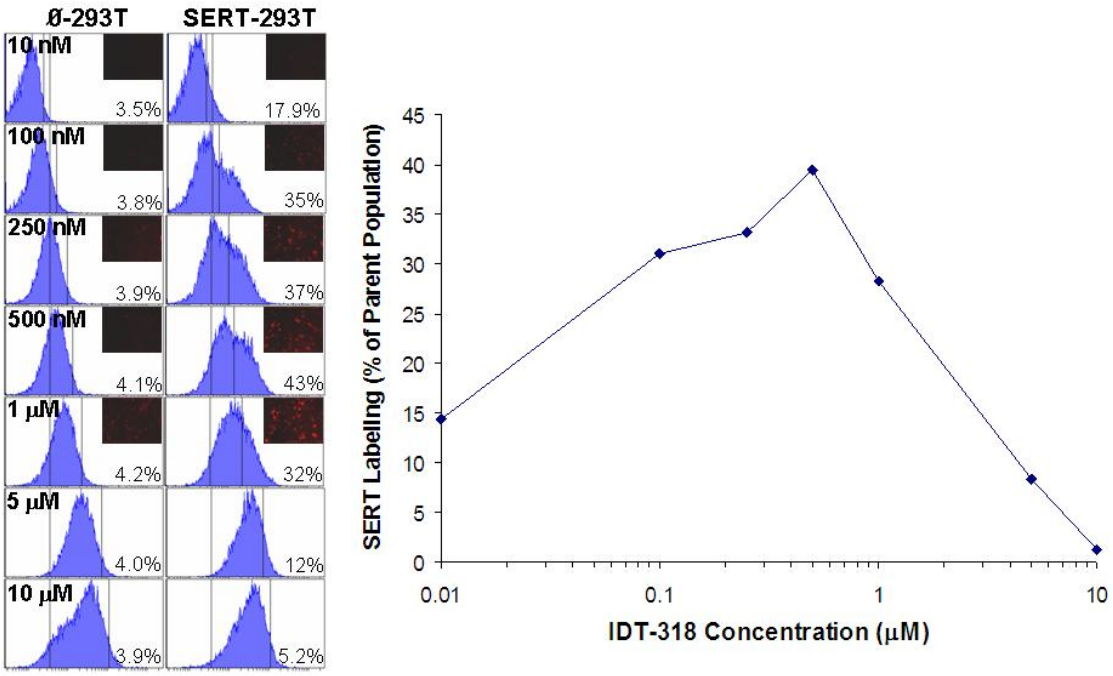

Figure 5-7. Determination of optimal IDT318 concentration for labeling of SERT in cellular assays. Flow cytometry analysis (left) as well as fluorescence imaging (inset) illustrates specific SERT labeling at specified concentrations. Sham-transfected cells (left column) have an increased nonspecific background with increasing ligand concentration, while specific SERT labeling is evident in SERT expressing cells (right column) as a discrete population above this nonspecific background. Quantification of the SERT positive population was determined for each concentration, and is expressed as a percentage of the parent population above a 4% threshold established from a sham-transfected negative control at each concentration. Graphical representation of these data after background subtraction (right) indicate maximal SERT labeling at an IDT318 concentration of 500 nM. At concentrations above 1 µM, however, the ligand-mediated background overtakes the SERT-specific signal, and compromises SERT detection.

The Importance of Alkyl Chain Length in Ligand Design

Previous competitive uptake assays with small molecule derivatives designed to target the dopamine transporter (DAT), an analogue of SERT which specifically transports the neurotransmitter dopamine, have indicated the importance of the alkyl

chain linker region which connects the bioactive drug derivative to the PEG backbone [*153*]. Consequently, analogues of IDT318 with varying alkyl chain lengths were utilized in cellular assays to assess the effect this linker arm length has on SERT labeling, and the results of this investigation are presented in Figure 5-8. A characteristic SERT-specific response is evident for IDT318 with roughly 28% of the cells exhibiting an increased fluorescent intensity due to specific labeling of SERT. This labeling is significantly diminished for the six-carbon IDT366 ligand, and altogether eliminated for the two-carbon IDT317 ligand. Thus, the length of this alkyl chain has a dramatic effect on each individual ligand's ability to specifically interact with SERT. This is likely due to the nature of the binding pocket for IDT318, with the added hydrophobicity somehow stabilizing IDT318's interaction with SERT. Additionally, it is apparent that the ligand-mediated nonspecific background increases with longer alkyl chain lengths, as indicated by a shift of the population to higher fluorescent intensities. Consequently, this ligand-mediated background is likely the result of hydrophobic interactions with the cell surface, and subsequent ligand design should take into account the trade-off between specific labeling and nonspecific background depending on the length of the alkyl linker.

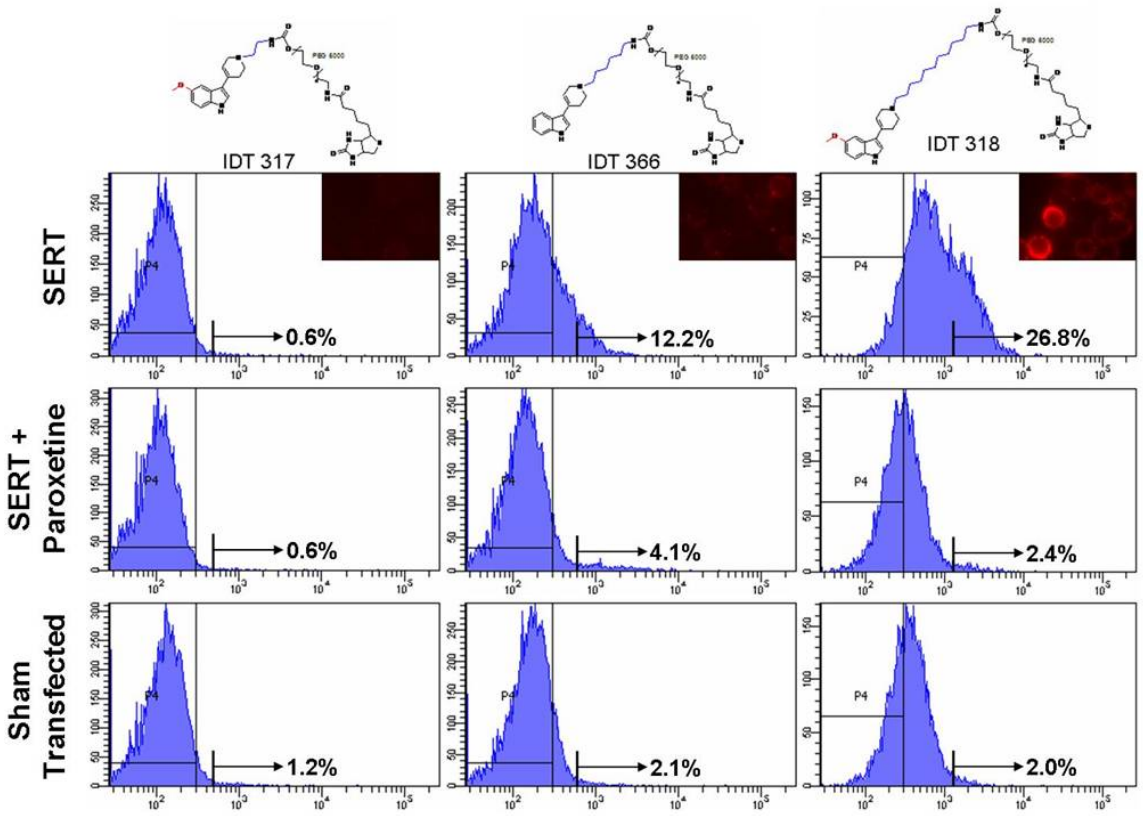

Figure 5-8. Alkyl chain length effect on SERT labeling in mammalian cell cultures. It is apparent that minor modification to ligand structure can have a dramatic effect on SERT labeling. Two carbon (IDT-317, left column), six carbon (IDT-366, middle column) and eleven carbon (IDT-318, right column) alkyl spacers result in differential labeling of SERT. Fluorescence images (inset) clearly demonstrate specific SERT labeling for the longer IDT-318, while this fluorescence intensity is diminished for both IDT-317 and IDT-366. Additionally, this increased SERT labeling is apparent in flow cytometry analyses, as indicated by an appreciable increase in fluorescent populations of SERT-expressing cells (top row) as compared to both paroxetine-blocked SERT cells (middle row) and sham transfected cells lacking SERT (bottom row).

Specificity of IDT318 for SERT

Fluorescent detection of SERT using IDT318-targeted QDs will eventually have to be performed in the presence of other monoamine transporters and cell surface receptors, especially considering one ultimate goal of multiplexed receptor detection in neuronal cultures. It was therefore crucial to further demonstrate SERT specificity even in the presence of similar transporter proteins. To assess the SERT-selectivity of IDT318, HEK-293T cells were transiently transfected with plasmid cDNA encoding for DAT as a means of generating a cellular system with expression of an alternate monoamine

transporter. IDT318 labeling experiments were subsequently performed on both cell lines and the results are presented in Figure 5-9. IDT307, which is transported by both SERT and DAT, was initially utilized to verify successful transporter expression in both instances. The characteristic green intracellular fluorescence was observed for both SERT and DAT cultures (Figure 5-9, top row), indicating successful transfection of both plasmids. Fluorescent imaging (middle row) and flow cytometry analysis (bottom row) following IDT318 labeling demonstrated specific labeling of SERT with no apparent selectivity for DAT. This finding highlights the feasibility of utilizing small molecule QD targeting for multiplexed transporter detection in clinically relevant neuronal cultures. Further investigations are undoubtedly warranted to further demonstrate the selectivity of IDT318 for SERT over alternate serotonin cell surface receptors, which could additionally interfere with selective SERT detection in native tissues.

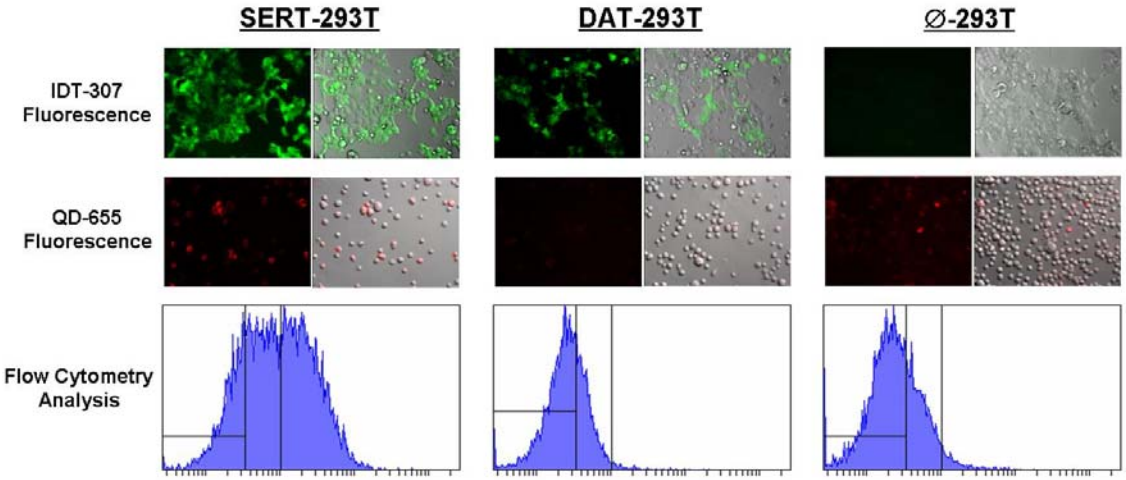

Figure 5-9. IDT-318 selectively labels SERT as compared to other monoamine transporters. HEK-293T cells transiently transfected with SERT (left), DAT (middle) or empty pcDNA3.0 vector (right) were initially exposed to 5 μM IDT307 in order to assess transfection efficiency. (A) IDT307 fluorescence is evident for SERT and DAT transfected cells, indicating successful transfection and expression of desired transporters, while no such fluorescence is apparent for sham-transfected cells. Specific QD labeling of SERT with IDT-318 is evident in fluorescent micrographs (B) and flow cytometry analysis (C), while no significant labeling is observed for either DAT-transfected or sham-transfected cells, highlighting the specificity of IDT-318 for SERT over other monoamine transporters.

Summary and Future Direction

IDT318 has been successfully utilized to specifically interact with SERT and facilitate its fluorescent detection with SA-QDs. The QD labeling protocol was developed to circumvent several potential interferences, namely: (1) biotinylated ligands and a two-step labeling were employed to eliminate the requirement of effectively presenting hydrophobic ligands at the QD surface, (2) serum proteins were eliminated from the protocol altogether to prevent protein adsorption to the QD surface, and (3) cells were labeled in suspension to reduce nonspecific QD interactions with the culture vessel. Ultimately, this labeling protocol provided negligible nonspecific binding due to QD interactions with cellular membranes, and SERT specific QD labeling was demonstrated using both fluorescence microscopy and flow cytometry. While IDT318 did cause an apparent nonspecific, ligand-mediated fluorescent background, the SERT-specific labeling was evident as an increased fluorescence above this background. Two critical parameters, ligand incubation time and concentration, were then investigated and a protocol incorporating a 20 minute incubation with 500 nM IDT318 provided the optimal fluorescent labeling conditions. The importance of the length of the alkyl chain connecting the bioactive drug derivative to the PEG backbone was also illustrated, and the eleven-carbon spacer of IDT318 is apparently required for SERT recognition. Finally, the selectivity of IDT318 for SERT was highlighted, with no apparent labeling of the alternate monoamine transporter DAT.

A fluorescent assay which permits facile and rapid determination of SERT expression can be immediately useful for numerous biochemical applications. These fluorescent probes can be utilized to replace existing radiographic methodologies for assessments of

processes such as SERT expression, function, and localization. Such a fluorescent assay would provide improved spatial and temporal resolution without any of the drawbacks associated with isotopic substrate handling. Additionally, a fluorescent probe specific for SERT could be employed in dynamic imaging experiments to determine whether or not patterns of regulation and surface trafficking in transfected cells are applicable to neurons. Similar dynamic imaging studies can also be performed to verify the role integrins play upon its formation of a complex with SERT [*154*]. Ultimately, IDT318 labeling of SERT expression in non-neuronal peripheral tissues, most notably in platelets, could eventually be utilized in the development of a routine diagnostic test to rapidly assess systemic levels of SERT expression or even identify mutational SERT variants. This screen could potentially aid in the diagnosis of disease states such as seasonal affective disorder or be utilized in determining a predisposed genetic susceptibility to diseases such as autism. A fluorescent assay to monitor SERT expression in platelets using IDT-318 targeted QDs could initially be developed to demonstrate differential SERT expression in platelets isolated from knockout ($SERT^{-/-}$), heterozygous ($SERT^{+/-}$) and wild type ($SERT^{+/+}$) mouse models. Identification of differential levels of SERT expression in platelets isolated from individuals with specific disease states could ultimately be utilized to verify the predictive feasibility of this particular assay, and eventually result in the establishment of specific diagnostic criteria.

CHAPTER VI

CONCLUSION

This research has been focused on the integration of highly fluorescent quantum dots into biological assays in an attempt to utilize their unique spectral properties to better understand complex cellular processes. Initial efforts incorporated antibody-QD conjugates to monitor IL-2 expression in activated populations of Jurkat T cells [*40*]. Similar antibody targeting approaches have been employed to introduce specificity for a wide variety of biological QD applications, and antibodies have frequently been the first option considered for generating bioactive QDs. Numerous labeling protocols had been developed to minimize nonspecific interactions for antibody-QD conjugates, and these probes were not prone to any interferences due to serum blocking conditions. Antibody conjugates, however, were not without associated drawbacks, such as added steric bulk resulting in an increased probe size, variable strength antibody-antigen interactions, and excessive purchasing costs. Additionally, no suitable antibodies exist for immunofluorescent imaging of certain cellular targets, most notably SERT. Subsequent research efforts were therefore focused on the development of a small molecule targeting strategy to alleviate some of the problems frequently encountered with antibody-QD conjugates, and to generate QD probes capable of specifically interacting with SERT.

Numerous technical challenges associated with the highly fluorescent AMP-QD platform had to be addressed prior to any successful demonstration of specific small molecule QD labeling. Preliminary investigations with AMP-QDs indicated that PEG modifications acted to reduce nonspecific cellular interactions [*24*], and subsequent

targeting ligands therefore utilized a PEG backbone to minimize any associated background fluorescence. It was then demonstrated for the first time that hydrophobic drug derivatives could self-assemble to the QD surface [*149*]. Attempts to utilize these conjugates in cellular assays ultimately failed to produce specific labeling, owing to the fact that the targeting functionality was associated with the QD surface and unable to interact with its intended target. Additionally, anomalous cellular imaging results led to the conclusion that proteins present in standard blocking solutions were adsorbing to the QD surface and causing artifact endosomal fluorescent staining. A better understanding of these unforeseen interferences ultimately permitted the development of a successful QD labeling protocol for SERT. Future investigators seeking to utilize small molecule QD conjugates for labeling membrane-associated receptors should undoubtedly be aware of these problematic interferences.

One frequently encountered problem in attempting to demonstrate specific QD labeling was associated with the assumption that various cellular systems were in fact expressing the desired targets. Control experiments should be performed, whenever possible, to confirm expression of a target protein before assuming that the QD conjugate is ineffective. Numerous IL-2R labeling attempts failed initially due to the fact that cellular activation was not occurring as a result of degraded PMA. Similarly, cell lines stably transfected with SERT were utilized for numerous failed QD labeling attempts before determining that the cells had been passaged to a point where they no longer expressed SERT. IDT307 eventually provided a convenient means to assess transporter expression, eliminating a great deal of experimental uncertainty with regards to questions

of transporter expression. Subsequent investigations will benefit from the use of IDT307 as a means of verifying successful transporter expression.

A better understanding of potential interferences combined with the emergence of improved analytical tools (i.e. IDT307) ultimately culminated in the demonstration of QD labeling of SERT expressed in mammalian cell cultures. A transient transfection resulted in higher expression levels of SERT which was easily detectable by fluorescent microscopy and flow cytometry, and IDT307 was used to confirm successful transporter transfection prior to imaging experiments. Successful imaging of SERT in an oocyte model system with IDT318 eliminated any uncertainty regarding the effectiveness of this ligand, and optimal incubation conditions were found to differ significantly from an oocyte system to mammalian cell cultures. Imaging experiments performed with similar ligands eventually demonstrated the dramatic effect alkyl chain linker length plays in efficient SERT labeling. Additionally, the selectivity of IDT318 for SERT even in the presence of alternate monoamine transporters seems to indicate the possibility to interrogate SERT expression in native tissues, perhaps even in a multiplexed format to detect multiple cellular targets.

APPENDIX A

FLUORESCENT IMAGING WITH IDT307: AN INTRACELLULARLY FLUORESCENT, MONOAMINE TRANSPORTER-SELECTIVE SMALL MOLECULE

Fluorescent imaging experiments characterizing the cellular response of IDT307 were also performed throughout the course of this research, in addition to the previously described investigations utilizing quantum dots in biological applications. Traditionally, isotopic methods have been widely employed to measure biogenic amine transporter expression and inhibition. However, despite the added cost and associated hazards of radioactive isotope handling and disposal, these methodologies generally suffer from poor temporal and spatial resolutions limiting their utility in high throughput screening applications. ASP^+, or 4-(4-diethylaminostyryl)-*N*-methylpyridinium iodide, a fluorescent analogue of the neurotoxin MPP^+, was initially identified as a suitable fluorescent substrate to facilitate a non-isotopic approach for the investigation of biogenic amine transporter localization, activity, and regulation [*155, 156*]. The search for improved fluorescent substrates based upon derivatives of ASP^+ and MPP^+ eventually resulted in the development of IDT307 (illustrated in Figure A-1), also referred to as 4-(4-(dimethylamino)phenyl)-1-methylpyridinium iodide. A previous report has demonstrated the ability of this particular compound to form a host-guest complex with β-cyclodextrin, resulting in a fluorescent species with an emission maximum at 500-520 nm due to the formation of a twisted intramolecular charge transfer (TICT) state upon excitation [*157*]. More recent cellular investigations with IDT307 have demonstrated its selective transport by the monoamine transporters for norepinephrine (NET), dopamine

(DAT), and serotonin (SERT), all resulting in a characteristic intracellular fluorescence [*152*].

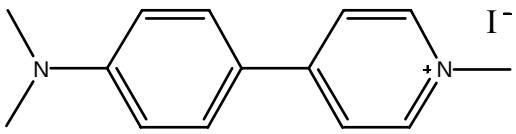

Figure A-1. Structure of IDT307, an intracellularly fluorescent small molecule selectively transported by monoamine transporters.

IDT307 has several intriguing characteristics which make it desirable for the development of a robust, non-isotopic platform to investigate monoamine transporters. Specifically, IDT307 is only fluorescent in specific environments, owing to the necessity of a TICT state for efficient fluorescence emission. Consequently, IDT307 has negligible fluorescence emission in aqueous environments without the addition of β-cyclodextrin, yet it is strongly fluorescent in specific intracellular environments. This unique fluorescent property permits IDT307 to be utilized without additional rinsing steps, as excess extracellular IDT307 does not result in an increased fluorescence background. Additionally, since IDT307 is specifically transported intracellularly by monoamine transporters, this characteristic intracellular fluorescence provides a useful signature to assess transporter expression and function. The intracellular fluorescent staining pattern observed upon addition of IDT307 to monoamine transporter expressing cell lines, illustrated Figure A-2 for hSERT-expressing HEK-293 cells, apparently results from interactions with distinct nuclear and cytosolic components. Finally, the intracellular accumulation of IDT307 can be blocked by traditional inhibitors of these monoamine transporters, highlighting the potential utility of this substrate for the development of a

high throughput drug discovery platform to identify clinically relevant transporter inhibitors.

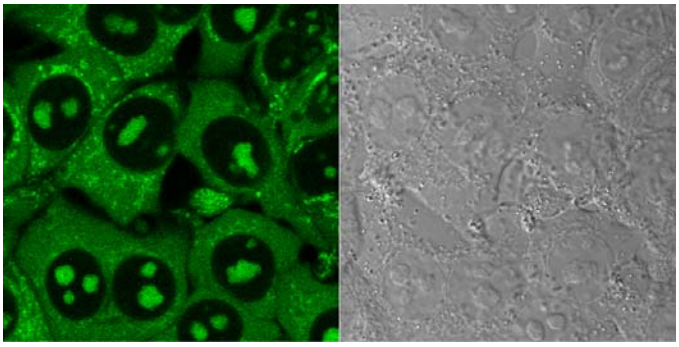

Figure A-2. Characteristic fluorescent staining pattern observed for monoamine transporter expressing cell lines upon exposure to IDT307. IDT307 is selectively delivered intracellularly by monoamine transporters, and its characteristic fluorescence consists of a nuclear component, a diffuse cytosolic component, with additional punctate cytosolic labeling.

Having demonstrated the specificity of this fluorescent substrate for the monoamine transporters SERT, DAT and NET, initial characterization efforts were focused both on determining the intracellular fate of IDT307 following transport as well as characterizing its fluorescent emission. Obtaining a fluorescent emission spectrum of IDT307, however, provided a unique technical challenge given that a TICT excited state is required for fluorescent emission. Fluorescent spectra were initially acquired in solution following the addition of β-cyclodextrin, but improved fluorescent detection would characterize the spectral properties of IDT307 *in vitro*. Consequently, LLC-PK1 cells stably transfected to express rDAT (dopamine transporter derived from rats) were incubated with a 10 μM IDT307 solution in KRH buffer for 30 minutes. Following one rinse with cold KRH, the cells were imaged on a Zeiss LSM 510 inverted confocal microscope using a specialized Meta detector. This Meta detector is capable of acquiring as many as 32 individual fluorescent images at distinct wavelength intervals (Figure A-3, left), ultimately allowing the determination of spectral information. ImageJ image analysis software was

subsequently used to determine the integrated intensity for each image and generate relevant emission spectra (Figure A-3, right). The fluorescent emission maxima in cell cultures occurs at ~510 nm, while the observed emission maxima for β-cyclodextrin-IDT307 host-guest complexes is at 485 nm. This shift in emission maxima is likely due to the solvochromatic nature of these TICT compounds.

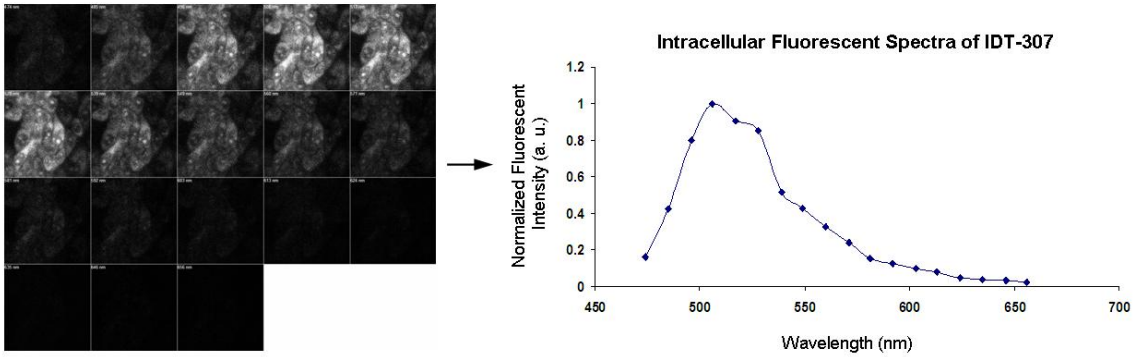

Figure A-3. Spectral analysis of IDT307 intracellular fluorescence. Spectral analysis could not be performed in solution due to the necessity of a TICT excited state for fluorescent emission. Therefore spectral analysis was performed using the Zeiss LSM 510 Meta detector which acquires a series of fluorescent images at 10 nm increments (left). These images can then be displayed as an emission spectrum by measuring the integrated fluorescent intensity for each image (ImageJ Software) and plotting it as a function of wavelength (right).

Fluorescent imaging analysis was also performed to characterize the intracellular fate of IDT307. The unique intracellular fluorescence of IDT307 consists of a nuclear component, a diffuse cytosolic component, with additional punctate cytosolic labeling (Figure A-1). Colocalization studies were therefore performed in an effort to determine specific cellular components corresponding to the fluorescence of IDT307. Specifically, the membrane-permient fluorescent dyes STYO-17, BODIPY-TR, MitoTracker Red, and LysoTracker Red (all from Invitrogen Corp.) were utilized to fluorescently stain for nucleic acids, the Golgi apparatus, mitochondria and lysosomes, respectively. Red fluorescent cellular dyes were specifically chosen to eliminate any potential spectral

overlap with the green fluorescence of IDT307. As such, HEK-293 cells stably transfected with hNET were initially exposed to a solution containing both the specified red-fluorescent cellular component dye and IDT307 (10 μM) for 30 minutes in KRH buffer. The labeling solution was then removed by aspiration, and the cells were subsequently rinsed once with cold KRH buffer. These fluorescently labeled cells were then imaged immediately on a Zeiss LSM 510 Meta confocal microscope, and representative dual color and colocalization images are displayed in Figure A-4. Dual color fluorescent images were acquired with appropriate band-pass (green channel) and long-pass (red channel) filter settings for optimized fluorescence detection, and dual excitation sources (488 nm excitation for green channel, and 543/633 nm excitation for red channel) were used to eliminate bleed-through from the green channel into the red channel.

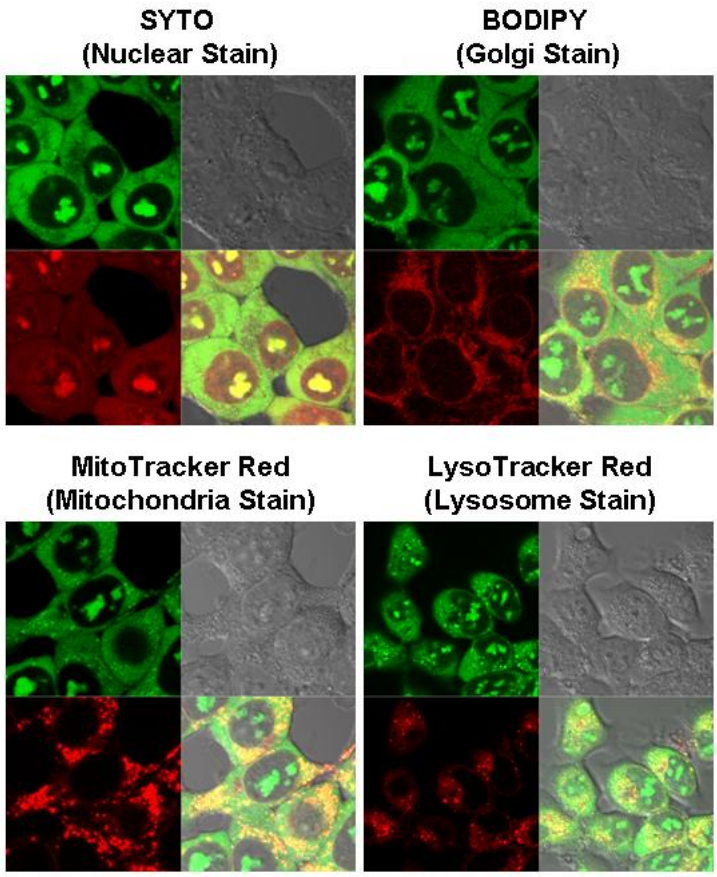

Figure A-4. Determining the intracellular localization of IDT307 using various fluorescent cellular organelle indicators. All images acquired on a Zeiss LSM-510 META confocal microscope using a 100× oil-immersion objective. A high degree of colocalization with a nucleic acid indicator (top left) is indicative of IDT307 localization to the nucleoli as well as the observed diffuse cytosolic staining. No appreciable accumulation at the Golgi apparatus as indicated by a BODIPY fluorescent indicator (top right). Additional punctant cytosolic labeling, not resulting from nucleic acid interactions, appears to be due to either mitochondrial association (bottom left) or lysosomal association (bottom right).

As anticipated, the intracellular fluorescence of IDT307 clearly colocalizes to a great extent with the nucleic acid stain SYTO-17 (Figure A-4, upper left). Therefore, both the diffuse cytosolic labeling and the nucleoli labeling of intracellular IDT307 can therefore be attributed to nucleic acid interactions. While IDT307 does not appear to colocalize with the Golgi apparatus (A-4, upper right), it is not immediately apparent whether the punctate cytosolic labeling component results from interactions with intracellular mitochondria (A-4, lower left) or lysosomes (A-4, lower right). It is likely that this

fluorescence is the result of interactions of IDT307 with mitochondrial DNA, having already demonstrated that nucleic acid interactions have an apparent effect on the fluorescence of IDT307. Indeed, closer examination of hNET expressing HEK-293 cells labeled with both MitoTracker Red and IDT307 clearly indicate an apparent mitochondrial colocalization (Figure A-5).

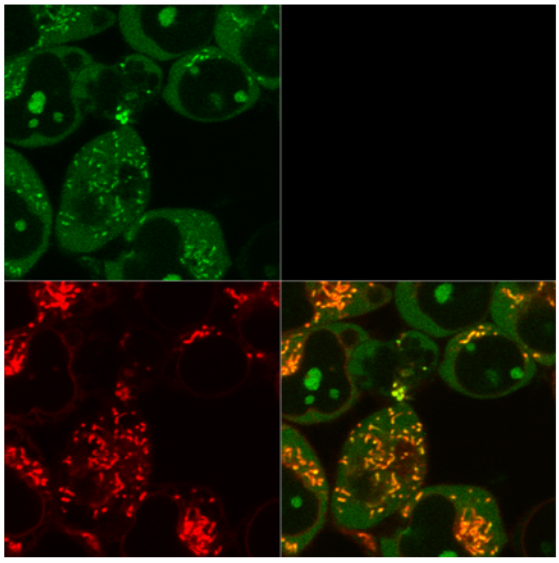

Figure A-5. Demonstrating colocalization of IDT307 intracellular fluorescence with mitochondria. Additional fluorescent imaging with MitoTracker Red provides convincing evidence that the punctate cytosolic fluorescent labeling observed for IDT307 is associated with mitochondria. (Note: the brightfield image has been eliminated to provide a clearer demonstration of colocalization.)

This appendix has described the microscopic approaches utilized to characterize the intracellular properties of IDT307, while a more detailed discussion of the unique cellular and fluorescent properties of this compound is currently in preparation [*152*]. The Zeiss LSM 510 Meta has proven to be a useful tool in determining the spectral properties of the fluorescent emission of IDT307 *in vitro*. The observed fluorescence emission spectrum of IDT307, with maximal emission at ~510 nm, permits its routine detection on standard fluorescence microscopes using any traditional GFP filter set. Additionally, the unique

fluorescent properties of IDT307 permit monoamine transporter analysis without required washes, owing to the fact that extracellular IDT307 does not significantly contribute to a fluorescence background signal. Routine analysis can therefore be performed simply by adding 1-10 μM IDT307 directly to the cell culture media, and subsequently imaging on a fluorescent microscope (equipped with a GFP filter set) after just 5-10 min incubation at 37 °C. As such, analyses utilizing IDT307 have proven to be extremely useful as a means of verifying monoamine transporter expression. Furthermore, dual color fluorescent imaging experiments have confirmed that the observed intracellular fluorescence for IDT307 is due to interactions with nucleic acids. The characteristic fluorescent staining pattern observed for IDT307 cells consists of both distinct labeling of the nucleoli and a diffuse cytosolic labeling as a result of these nucleic acid interactions, with an additional punctate cytosolic labeling due to an interaction with mitochondrial DNA.

REFERENCES

(1) *The material published in this chapter has largely been published in another source, which is under the copyright of Bentham Science Publishers Ltd.*

(2) Bruchez, M., Moronne, M., Gin, P., Weiss, S., and Alivisatos, A. P. Semiconductor nanocrystals as fluorescent biological labels. *Science* **1998**, *281*, 2013-2016.

(3) Chan, W. C. W., and Nie, S. M. Quantum dot bioconjugates for ultrasensitive nonisotopic detection. *Science* **1998**, *281*, 2016-2018.

(4) Michalet, X., Pinaud, F. F., Bentolila, L. A., Tsay, J. M., Doose, S., Li, J. J., Sundaresan, G., Wu, A. M., Gambhir, S. S., and Weiss, S. Quantum dots for live cells, in vivo imaging, and diagnostics. *Science* **2005**, *307*, 538-544.

(5) Fu, A. H., Gu, W. W., Larabell, C., and Alivisatos, A. P. Semiconductor nanocrystals for biological imaging. *Curr. Opin. Neurobiol.* **2005**, *15*, 568-575.

(6) Medintz, I. L., Uyeda, H. T., Goldman, E. R., and Mattoussi, H. Quantum dot bioconjugates for imaging, labelling and sensing. *Nature Mater.* **2005**, *4*, 435-446.

(7) Jaiswal, J. K., and Simon, S. M. Potentials and pitfalls of fluorescent quantum dots for biological imaging. *Trends Cell Biol.* **2004**, *14*, 497-504.

(8) Michalet, X., Pinaud, F., Lacoste, T. D., Dahan, M., Bruchez, M. P., Alivisatos, A. P., and Weiss, S. Properties of fluorescent semiconductor nanocrystals and their application to biological labeling. *Single Molecules* **2001**, *2*, 261-276.

(9) McBride, J., Treadway, J., Feldman, L. C., Pennycook, S. J., and Rosenthal, S. J. Structural basis for near unity quantum yield core/shell nanostructures. *Nano Lett.* **2006**, *6*, 1496-1501.

(10) Murray, C. B., Kagan, C. R., and Bawendi, M. G. Synthesis and characterization of monodisperse nanocrystals and close-packed nanocrystal assemblies. *Ann. Rev. Mater. Sci.* **2000**, *30*, 545-610.

(11) Peng, Z. A., and Peng, X. Formation of high-quality CdTe, CdSe, and CdS nanocrystals using CdO as precursor. *J. Am. Chem. Soc.* **2001**, *123*, 183-184.

(12) Gerion, D., Pinaud, F., Williams, S. C., Parak, W. J., Zanchet, D., Weiss, S., and Alivisatos, A. P. Synthesis and properties of biocompatible water-soluble silica-coated CdSe/ZnS semiconductor quantum dots. *J. Phys. Chem. B* **2001**, *105*, 8861-8871.

(13) Akerman, M. E., Chan, W. C. W., Laakkonen, P., Bhatia, S. N., and Ruoslahti, E. Nanocrystal targeting in vivo. *Proc. Natl. Acad. Sci. U.S.A.* **2002**, *99*, 12617-12621.

(14) Hanaki, K., Momo, A., Oku, T., Komoto, A., Maenosono, S., Yamaguchi, Y., and Yamamoto, K. Semiconductor quantum dot/albumin complex is a long-life and highly photostable endosome marker. *Biochem. Biophys. Res. Comm.* **2003**, *302*, 496-501.

(15) Mattoussi, H., Mauro, J. M., Goldman, E. R., Green, T. M., Anderson, G. P., Sundar, V. C., and Bawendi, M. G. Bioconjugation of highly luminescent colloidal CdSe-ZnS quantum dots with an engineered two-domain recombinant protein. *Phys. Status Solidi B* **2001**, *224*, 277-283.

(16) Jaiswal, J. K., Mattoussi, H., Mauro, J. M., and Simon, S. M. Long-term multiple color imaging of live cells using quantum dot bioconjugates. *Nature Biotechnol.* **2003**, *21*, 47-51.

(17) Mattoussi, H., Mauro, J. M., Goldman, E. R., Anderson, G. P., Sundar, V. C., Mikulec, F. V., and Bawendi, M. G. Self-assembly of CdSe-ZnS quantum dot bioconjugates using an engineered recombinant protein. *J. Am. Chem. Soc.* **2000**, *122*, 12142-12150.

(18) Dubertret, B., Skourides, P., Norris, D. J., Noireaux, V., Brivanlou, A. H., and Libchaber, A. In vivo imaging of quantum dots encapsulated in phospholipid micelles. *Science* **2002**, *298*, 1759-1762.

(19) Wu, X. Y., Liu, H. J., Liu, J. Q., Haley, K. N., Treadway, J. A., Larson, J. P., Ge, N. F., Peale, F., and Bruchez, M. P. Immunofluorescent labeling of cancer marker Her2 and other cellular targets with semiconductor quantum dots. *Nature Biotechnol.* **2003**, *21*, 41-46.

(20) Petruska, M. A., Bartko, A. P., and Klimov, V. I. An amphiphilic approach to nanocrystal quantum dot-titania nanocomposites. *J. Am. Chem. Soc.* **2004**, *126*, 714-715.

(21) Gao, X. H., Cui, Y. Y., Levenson, R. M., Chung, L. W. K., and Nie, S. M. In vivo cancer targeting and imaging with semiconductor quantum dots. *Nature Biotechnol.* **2004**, *22*, 969-976.

(22) Gerion, D., Parak, W. J., Williams, S. C., Zanchet, D., Micheel, C. M., and Alivisatos, A. P. Sorting fluorescent nanocrystals with DNA. *J. Am. Chem. Soc.* **2002**, *124*, 7070-7074.

(23) Ballou, B., Lagerholm, B. C., Ernst, L. A., Bruchez, M. P., and Waggoner, A. S. Noninvasive imaging of quantum dots in mice. *Bioconjugate Chem.* **2004**, *15*, 79-86.

(24) Bentzen, E. L., Tomlinson, I. D., Mason, J., Gresch, P., Warnement, M. R., Wright, D., Sanders-Bush, E., Blakely, R., and Rosenthal, S. J. Surface modification to reduce nonspecific binding of quantum dots in live cell assays. *Bioconjugate Chem.* **2005**, *16*, 1488-1494.

(25) Pathak, S., Cao, E., Davidson, M. C., Jin, S. H., and Silva, G. A. Quantum dot applications to neuroscience: New tools for probing neurons and glia. *J. Neurosci.* **2006**, *26*, 1893-1895.

(26) Zimmer, J. P., Kim, S. W., Ohnishi, S., Tanaka, E., Frangioni, J. V., and Bawendi, M. G. Size series of small indium arsenide-zinc selenide core-shell nanocrystals and their application to in vivo imaging. *J. Am. Chem. Soc.* **2006**, *128*, 2526-2527.

(27) Sehgal, D., and Vijay, I. K. A Method for the High-Efficiency of Water-Soluble Carbodiimide-Mediated Amidation. *Anal. Biochem.* **1994**, *218*, 87-91.

(28) Piran, U., and Riordan, W. J. Dissociation Rate-Constant of the Biotin-Streptavidin Complex. *J. Immunol. Methods* **1990**, *133*, 141-143.

(29) Lidke, D. S., Nagy, P., Heintzmann, R., Arndt-Jovin, D. J., Post, J. N., Grecco, H. E., Jares-Erijman, E. A., and Jovin, T. M. Quantum dot ligands provide new insights into erbB/HER receptor-mediated signal transduction. *Nature Biotechnol.* **2004**, *22*, 198-203.

(30) Courty, S., Luccardini, C., Bellaiche, Y., Cappello, G., and Dahan, M. Tracking individual kinesin motors in living cells using single quantum-dot imaging. *Nano Lett.* **2006**, *6*, 1491-1495.

(31) LeGac, S., Vermes, I., and vandenBerg, A. Quantum dots based probes conjugated to Annexin V for photostable apoptosis detection and imaging. *Nano Lett.* **2006**, *6*, 1863-1869.

(32) Howarth, M., Takao, K., Hayashi, Y., and Ting, A. Y. Targeting quantum dots to surface proteins in living cells with biotin ligase. *Proc. Natl. Acad. Sci. U.S.A.* **2005**, *102*, 7583-7588.

(33) O'Connell, K. M. S., Rolig, A. S., Whitesell, J. D., and Tamkun, M. M. Kv2.1 potassium channels are retained within dynamic cell surface microdomains that are defined by a perimeter fence. *J. Neurosci.* **2006**, *26*, 9609-9618.

(34) Dahan, M., Levi, S., Luccardini, C., Rostaing, P., Riveau, B., and Triller, A. Diffusion dynamics of glycine receptors revealed by single-quantum dot tracking. *Science* **2003**, *302*, 442-445.

(35) Bentzen, E. L., House, F., Utley, T. J., Crowe, J. E., and Wright, D. W. Progression of respiratory syncytial virus infection monitored by fluorescent quantum dot probes. *Nano Lett.* **2005**, *5*, 591-595.

(36) Giepmans, B. N. G., Deerinck, T. J., Smarr, B. L., Jones, Y. Z., and Ellisman, M. H. Correlated light and electron microscopic imaging of multiple endogenous proteins using Quantum dots. *Nature Methods* **2005**, *2*, 743-749.

(37) Li, Z. H., Wang, K. M., Tan, W. H., Li, J., Fu, Z. Y., Ma, C. B., Li, H. M., He, X. X., and Liu, J. B. Immunofluorescent, labeling of cancer cells with quantum dots synthesized in aqueous solution. *Anal. Biochem.* **2006**, *354*, 169-174.

(38) Sukhanova, A., Devy, M., Venteo, L., Kaplan, H., Artemyev, M., Oleinikov, V., Klinov, D., Pluot, M., Cohen, J. H. M., and Nabiev, I. Biocompatible fluorescent nanocrystals for immunolabeling of membrane proteins and cells. *Anal. Biochem.* **2004**, *324*, 60-67.

(39) Goldman, E. R., Anderson, G. P., Tran, P. T., Mattoussi, H., Charles, P. T., and Mauro, J. M. Conjugation of luminescent quantum dots with antibodies using an engineered adaptor protein to provide new reagents for fluoroimmunoassays. *Anal. Chem.* **2002**, *74*, 841-847.

(40) Warnement, M. R., Faley, S. L., Wikswo, J. P., and Rosenthal, S. J. Quantum dot probes for monitoring dynamic cellular response: Reporters of T cell activation. *IEEE Trans. Nanobiosci.* **2006**, *5*, 268-272.

(41) Tokumasu, F., and Dvorak, J. Development and application of quantum dots for immunocytochemistry of human erythrocytes. *Journal of Microscopy-Oxford* **2003**, *211*, 256-261.

(42) Winter, J. O., Liu, T. Y., Korgel, B. A., and Schmidt, C. E. Recognition molecule directed interfacing between semiconductor quantum dots and nerve cells. *Adv. Mater.* **2001**, *13*, 1673-1677.

(43) Stroh, M., Zimmer, J. P., Duda, D. G., Levchenko, T. S., Cohen, K. S., Brown, E. B., Scadden, D. T., Torchilin, V. P., Bawendi, M. G., Fukumura, D., and Jain, R. K. Quantum dots spectrally distinguish multiple species within the tumor milieu in vivo. *Nature Med.* **2005**, *11*, 678-682.

(44) Chen, F., and Gerion, D. Fluorescent CdSe/ZnS nanocrystal-peptide conjugates for long-term, nontoxic imaging and nuclear targeting in living cells. *Nano Lett.* **2004**, *4*, 1827-1832.

(45) Cai, W., Shin, D. W., Chen, K., Gheysens, O., Cao, Q., Wang, S. X., Gambhir, S. S., and Chen, X. Peptide-labeled near-infrared quantum dots for imaging tumor vasculature in living subjects. *Nano Lett.* **2006**, *6*, 669-676.

(46) Vu, T. Q., Maddipati, R., Blute, T. A., Nehilla, B. J., Nusblat, L., and Desai, T. A. Peptide-conjugated quantum dots activate neuronal receptors and initiate downstream signaling of neurite growth. *Nano Lett.* **2005**, *5*, 603-607.

(47) Sundara Rajan, S., and Vu, T. Q. Quantum dots monitor TrkA receptor dynamics in the interior of neural PC12 cells. *Nano Lett.* **2006**, *6*, 2049-2059.

(48) Young, S. H., and Rozengurt, E. Qdot Nanocrystal Conjugates conjugated to bombesin or ANG II label the cognate G protein-coupled receptor in living cells. *Am. J. Physiol., Cell Physiol.* **2006**, *290*, C728-C732.

(49) Pinaud, F., King, D., Moore, H. P., and Weiss, S. Bioactivation and cell targeting of semiconductor CdSe/ZnS nanocrystals with phytochelatin-related peptides. *J. Am. Chem. Soc.* **2004**, *126*, 6115-6123.

(50) Nan, X., Sims, P. A., Chen, P., and Xie, X. S. Observation of individual microtubule motor steps in living cells with endocytosed quantum dots. *J. Phys. Chem. B* **2005**, *109*, 24220-24224.

(51) Delehanty, J. B., Medintz, I. L., Pons, T., Brunel, F. M., Dawson, P. E., and Mattoussi, H. Self-assembled quantum dot-peptide bioconjugates for selective intracellular delivery. *Bioconjugate Chem.* **2006**, *17*, 920-927.

(52) Hoshino, A., Fujioka, K., Oku, T., Nakamura, S., Suga, M., Yamaguchi, Y., Suzuki, K., Yasuhara, M., and Yamamoto, K. Quantum dots targeted to the assigned organelle in living cells. *Microbiol. Immunol.* **2004**, *48*, 985-994.

(53) Lagerholm, B. C., Wang, M., Ernst, L. A., Ly, D. H., Liu, H., Bruchez, M. P., and Waggoner, A. S. Multicolor coding of cells with cationic peptide coated quantum dots. *Nano Lett.* **2004**, *4*, 2019-2022.

(54) Mattheakis, L. C., Dias, J. M., Choi, Y. J., Gong, J., Bruchez, M. P., Liu, J. Q., and Wang, E. Optical coding of mammalian cells using semiconductor quantum dots. *Anal. Biochem.* **2004**, *327*, 200-208.

(55) Shi, P., Chen, H. F., Cho, M. R., and Stroscio, M. A. Peptide-directed binding of quantum dots to integrins in human fibroblast. *IEEE Trans. Nanobiosci.* **2006**, *5*, 15-19.

(56) Tomlinson, I. D., Mason, J., Blakely, R. D., and Rosenthal, S. J. (**2005**) Peptide conjugated quantum dots: imaging the angiotensin type 1 receptor in living cells, in *Methods in Molecular Biology: Nanobiotechnology Protocols* (Rosenthal, S. J., and Wright, D. W., Eds.) pp 51-60, Humana Press, New York.

(57) Bentolila, L. A., and Weiss, S. Single-step multicolor fluorescence in situ hybridization using semiconductor quantum dot-DNA conjugates. *Cell Biochem. Biophys.* **2006**, *45*, 59-70.

(58) Ho, Y. P., Kung, M. C., Yang, S., and Wang, T. H. Multiplexed hybridization detection with multicolor colocalization of quantum dot nanoprobes. *Nano Lett.* **2005**, *5*, 1693-1697.

(59) Pathak, S., Choi, S. K., Arnheim, N., and Thompson, M. E. Hydroxylated quantum dots as luminescent probes for in situ hybridization. *J. Am. Chem. Soc.* **2001**, *123*, 4103-4104.

(60) Xiao, Y., and Barker, P. E. Semiconductor nanocrystal probes for human metaphase chromosomes. *Nucleic Acids Res.* **2004**, *32*, e28.

(61) Rosenthal, S. J., Tomlinson, I., Adkins, E. M., Schroeter, S., Adams, S., Swafford, L., McBride, J., Wang, Y., DeFelice, L. J., and Blakely, R. D. Targeting cell surface receptors with ligand-conjugated nanocrystals. *J. Am. Chem. Soc.* **2002**, *124*, 4586-4594.

(62) Gussin, H. A., Tomlinson, I. D., Little, D. M., Warnement, M. R., Qian, H., Rosenthal, S. J., and Pepperberg, D. R. Binding of muscimol-conjugated quantum dots to GABAc receptors. *J. Am. Chem. Soc.* **2006**, *128*, 15701-15713.

(63) Parak, W. J., Boudreau, R., Le Gros, M., Gerion, D., Zanchet, D., Micheel, C. M., Williams, S. C., Alivisatos, A. P., and Larabell, C. Cell motility and metastatic potential studies based on quantum dot imaging of phagokinetic tracks. *Adv. Mater.* **2002**, *14*, 882-885.

(64) Dahan, M., Laurence, T., Pinaud, F., Chemla, D. S., Alivisatos, A. P., Sauer, M., and Weiss, S. Time-gated biological imaging by use of colloidal quantum dots. *Opt. Lett.* **2001**, *26*, 825-827.

(65) Dixit, S. K., Goicochea, N. L., Daniel, M. C., Murali, A., Bronstein, L., De, M., Stein, B., Rotello, V. M., Kao, C. C., and Dragnea, B. Quantum dot encapsulation in viral capsids. *Nano Lett.* **2006**, *6*, 1993-1999.

(66) Makrides, S. C., Gasbarro, C., and Bello, J. M. Bioconjugation of quantum dot luminescent probes for Western blot analysis. *Biotechniques* **2005**, *39*, 501-506.

(67) Fountaine, T. J., Wincovitch, S. M., Geho, D. H., Garfield, S. H., and Pittaluga, S. Multispectral imaging of clinically relevant cellular targets in tonsil and lymphoid tissue using semiconductor quantum dots. *Mod. Pathol.* **2006**, *19*, 1181-1191.

(68) Chattopadhyay, P. K., Price, D. A., Harper, T. F., Betts, M. R., Yu, J., Gostick, E., Perfetto, S. P., Goepfert, P., Koup, R. A., De Rosa, S. C., Bruchez, M. P., and Roederer, M.

Quantum dot semiconductor nanocrystals for immunophenotyping by polychromatic flow cytometry. *Nature Med.* **2006**, *12*, 972-977.

(69) Hohng, S., and Ha, T. Near-complete suppression of quantum dot blinking in ambient conditions. *J. Am. Chem. Soc.* **2004**, *126*, 1324-1325.

(70) Lidke, K. A., Rieger, B., Jovin, T. M., and Heintzmann, R. Superresolution by localization of quantum dots using blinking statistics. *Opt. Express* **2005**, *13*, 7052-7062.

(71) Larson, D. R., Zipfel, W. R., Williams, R. M., Clark, S. W., Bruchez, M. P., Wise, F. W., and Webb, W. W. Water-soluble quantum dots for multiphoton fluorescence imaging in vivo. *Science* **2003**, *300*, 1434-1436.

(72) Kim, S., Lim, Y. T., Soltesz, E. G., De Grand, A. M., Lee, J., Nakayama, A., Parker, J. A., Mihaljevic, T., Laurence, R. G., Dor, D. M., Cohn, L. H., Bawendi, M. G., and Frangioni, J. V. Near-infrared fluorescent type II quantum dots for sentinel lymph node mapping. *Nature Biotechnol.* **2004**, *22*, 93-97.

(73) Voura, E. B., Jaiswal, J. K., Mattoussi, H., and Simon, S. M. Tracking metastatic tumor cell extravasation with quantum dot nanocrystals and fluorescence emission-scanning microscopy. *Nature Med.* **2004**, *10*, 993-998.

(74) Tada, H., Higuchi, H., Wanatabe, T. M., and Ohuchi, N. In vivo real-time tracking of single quantum dots conjugated with monoclonal anti-HER2 antibody in tumors of mice. *Cancer Res.* **2007**, *67*, 1138-1144.

(75) Mulder, W. J. M., Koole, R., Brandwijk, R. J., Storm, G., Chin, P. T. K., Strijkers, G. J., Donega, C. D., Nicolay, K., and Griffioen, A. W. Quantum dots with a paramagnetic coating as a bimodal molecular imaging probe. *Nano Lett.* **2006**, *6*, 1-6.

(76) van Tilborg, G. A. F., Mulder, W. J. M., Chin, P. T. K., Storm, G., Reutelingsperger, C. P., Nicolay, K., and Strijkers, G. J. Annexin A5-conjugated quantum dots with a paramagnetic lipidic coating for the multimodal detection of apoptotic cells. *Bioconjugate Chem.* **2006**, *17*, 865-868.

(77) Yang, H. S., Santra, S., Walter, G. A., and Holloway, P. H. Gd-III-functionalized fluorescent quantum dots as multimodal imaging probes. *Adv. Mater.* **2006**, *18*, 2890-2894.

(78) Samia, A. C. S., Chen, X. B., and Burda, C. Semiconductor quantum dots for photodynamic therapy. *J. Am. Chem. Soc.* **2003**, *125*, 15736-15737.

(79) Kim, Y., Lillo, A. M., Steiniger, S. C. J., Liu, Y., Ballatore, C., Anichini, A., Mortarini, R., Kaufmann, G. F., Zhou, B., Felding-Habermann, B., and Janda, K. D. Targeting heat shock proteins on cancer cells: Selection, characterization, and cell-penetrating properties of a peptidic GRP78 ligand. *Biochemistry* **2006**, *45*, 9434-9444.

(80) Zhang, Y., So, M. K., and Rao, J. H. Protease-modulated cellular uptake of quantum dots. *Nano Lett.* **2006**, *6*, 1988-1992.

(81) Hardman, R. A toxicologic review of quantum dots: Toxicity depends on physicochemical and environmental factors. *Environ. Health Perspect.* **2006**, *114*, 165-172.

(82) Zou, M. F., Kopajtic, T., Katz, J. L., Wirtz, S., Justice, J. B., and Newman, A. H. Novel tropane-based irreversible ligands for the dopamine transporter. *J. Med. Chem.* **2001**, *44*, 4453-4461.

(83) Shimada, S., Kitayama, S., Lin, C. L., Patel, A., Nanthakumar, E., Gregor, P., Kuhar, M., and Uhl, G. Cloning and Expression of a Cocaine-Sensitive Dopamine Transporter Complementary-DNA. *Science* **1991**, *254*, 576-578.

(84) Kilty, J. E., Lorang, D., and Amara, S. G. Cloning and Expression of a Cocaine-Sensitive Rat Dopamine Transporter. *Science* **1991**, *254*, 578-579.

(85) Xing, D. X., Chen, P., Keil, R., Kilts, C. D., Shi, B., Camp, V. M., Malveaux, G., Ely, T., Owens, M. J., Votaw, J., Davis, M., Hoffman, J. M., BaKay, R. A. E., Subramanian, T., Watts, R. L., and Goodman, M. M. Synthesis, biodistribution, and primate imaging of fluorine-18 labeled 2 beta-carbo-1 '-fluoro-2-propoxy-3 beta-(4-chlorophenyl) tropanes. Ligands for the imaging of dopamine transporters by positron emission tomography. *J. Med. Chem.* **2000**, *43*, 639-648.

(86) Jiang, S. C., Chang, A. C., Abraham, P., Kuhar, M. J., and Carroll, F. I. Synthesis and transporter binding properties of (R)-2 beta,3 beta- and (R)-2 alpha,3 alpha-diaryltropanes. *Bioorg. Med. Chem. Lett.* **1998**, *8*, 3689-3692.

(87) Meltzer, P. C., Blundell, P., Chen, Z. M., Yong, Y. F., and Madras, B. K. Bicyclo[3.2.1]octanes: Synthesis and inhibition of binding at the dopamine and serotonin transporters. *Bioorg. Med. Chem. Lett.* **1999**, *9*, 857-862.

(88) Prakash, K. R. C., Tamiz, A. P., Araldi, G. L., Zhang, M., Johnson, K. M., and Kozikowski, A. P. N-phenylalkyl-substituted tropane analogs of boat conformation with high selectivity for the dopamine versus serotonin transporter. *Bioorg. Med. Chem. Lett.* **1999**, *9*, 3325-3328.

(89) Xu, C., Coffey, L. L., and Reith, M. E. A. Translocation of Dopamine and Binding of 2 Beta-Carbomethoxy-3 Beta-(4-Fluorophenyl) Tropane (Win-35,428) Measured under Identical Conditions in Rat Striatal Synaptosomal Preparations - Inhibition by Various Blockers. *Biochem. Pharmacol.* **1995**, *49*, 339-350.

(90) Houlihan, W. J., Kelly, L., Pankuch, J., Koletar, J., Brand, L., Janowsky, A., and Kopajtic, T. A. Mazindol analogues as potential inhibitors of the cocaine binding site at the dopamine transporter. *J. Med. Chem.* **2002**, *45*, 4097-4109.

(91) Zhang, Y., Rothman, R. B., Dersch, C. M., de Costa, B. R., Jacobson, A. E., and Rice, K. C. Synthesis and transporter binding properties of bridged piperazine analogues of 1-{2-[bis(4-fluorophenyl)methoxy]ethyl}-4-(3-phenylpropyl)piperazine (GBR 12909). *J. Med. Chem.* **2000**, *43*, 4840-4849.

(92) Lewis, D. B., Matecka, D., Zhang, Y., Hsin, L. W., Dersch, C. M., Stafford, D., Glowa, J. R., Rothman, R. B., and Rice, K. C. Oxygenated analogues of 1-[2-(diphenylmethoxy)ethyl]- and 1-[2-[bis(4-fluorophenyl)methoxy]ethyl]-4-(3-phenylpropyl)piperazines (GBR 12935 and GBR 12909) as potential extended-action cocaine-abuse therapeutic agents. *J. Med. Chem.* **1999**, *42*, 5029-5042.

(93) Choi, S. W., Elmaleh, D. R., Hanson, R. N., and Fischman, A. J. Novel 3-aminomethyl- and 4-aminopiperidine analogues of 1-[2-(diphenylmethoxy)ethyl]-4-(3-phenylpropyl)piperazines: Synthesis and evaluation as dopamine transporter ligands. *J. Med. Chem.* **2000**, *43*, 205-213.

(94) Rothman, R. B., Mele, A., Reid, A. A., Akunne, H. C., Greig, N., Thurkauf, A., Decosta, B. R., Rice, K. C., and Pert, A. Gbr12909 Antagonizes the Ability of Cocaine to Elevate Extracellular Levels of Dopamine. *Pharmacol. Biochem. Behav.* **1991**, *40*, 387-397.

(95) Dutta, A. K., Fei, X. S., Vaughan, R. A., Gaffaney, J. D., Wang, N. N., Lever, J. R., and Reith, M. E. A. Design, synthesis, and characterization of a novel, 4-[2-(diphenylmethoxy)ethyl]-1-benzyl piperidine-based, dopamine transporter photoaffinity label. *Life Sciences* **2001**, *68*, 1839-1849.

(96) Hsin, L. W., Dersch, C. M., Baumann, M. H., Stafford, D., Glowa, J. R., Rothman, R. B., Jacobson, A. E., and Rice, K. C. Development of long-acting dopamine transporter ligands as potential cocaine-abuse therapeutic agents: Chiral hydroxyl-containing derivatives of 1[2-[bis(4-fluorophenyl)methoxy]ethyl]-4-(3-phenylpropyl) piperazine and 1-[2-(diphenylmethoxy)ethyl]-4-(3-phenylpropyl)piperazine. *J. Med. Chem.* **2002**, *45*, 1321-1329.

(97) Benedetti, P., Mannhold, R., Cruciani, G., and Pastor, M. GBR compounds and mepyramines as cocaine abuse therapeutics: Chemometric studies on selectivity using grid independent descriptors (GRIND). *J. Med. Chem.* **2002**, *45*, 1577-1584.

(98) Dutta, A. K., Davis, M. C., Fei, X. S., Beardsley, P. M., Cook, C. D., and Reith, M. E. A. Expansion of structure-activity studies of piperidine analogues of 1-[2-(diphenylmethoxy)ethyl]-4-(3-phenylpropyl)piperazine (GBR 12935) compounds by altering substitutions in the N-benzyl moiety and behavioral pharmacology of selected molecules. *J. Med. Chem.* **2002**, *45*, 654-662.

(99) Dutta, A. K., Coffey, L. L., and Reith, M. E. A. Highly selective, novel analogs of 4-[2-(diphenylmethoxy)ethyl]-1-benzylpiperidine for the dopamine transporter: Effect of different aromatic substitutions on their affinity and selectivity. *J. Med. Chem.* **1997**, *40*, 35-43.

(100) Matecka, D., Lewis, D., Rothman, R. B., Dersch, C. M., Wojnicki, F. H. E., Glowa, J. R., DeVries, A. C., Pert, A., and Rice, K. C. Heteroaromatic analogs of 1-[2-(diphenylmethoxy)ethyl]- and 1-[2-[bis(4-fluorophenyl)methoxy]ethyl]-4-(3-phenylpropyl)piperazines (GBR 12935 and GBR 12909) as high-affinity dopamine reuptake inhibitors. *J. Med. Chem.* **1997**, *40*, 705-716.

(101) Sallee, F. R., Fogel, E. L., Schwartz, E., Choi, S. M., Curran, D. P., and Niznik, H. B. Photoaffinity-Labeling of the Mammalian Dopamine Transporter. *FEBS Lett.* **1989**, *256*, 219-224.

(102) Zimmermann, K., and Hengerer, B. Design and synthesis of a biotinylated dopamine transporter ligand for the purification and labeling of dopaminergic neurons. *Bioorg. Med. Chem. Lett.* **1998**, *8*, 261-266.

(103) Tomlinson, I. D., Mason, J., Burton, J. N., Blakely, R., and Rosenthal, S. J. The design and synthesis of novel derivatives of the dopamine uptake inhibitors GBR 12909 and GBR 12935. High-affinity dopaminergic ligands for conjugation with highly fluorescent cadmium selenide/zinc sulfide core/shell nanocrystals. *Tetrahedron* **2003**, *59*, 8035-8047.

(104) Wada, M., Nakai, H., Sato, Y., Hatanaka, Y., and Kanaoka, Y. Photochemistry of the Phthalimide System .33. a Removable Functional-Group in a Photochemical Macrocyclic Synthesis - Remote Photocyclization with a Pair System of Phthalimide and 1,3-Dithiolanyl Groups. *Tetrahedron* **1983**, *39*, 2691-2698.

(105) Mitsunobu, O. The Use of Diethyl Azodicarboxylate and Triphenylphosphine in Synthesis and Transformation of Natural-Products. *Synthesis-Stuttgart* **1981**, 1-28.

(106) Invitrogen Corporation. Qdot® streptavidin conjugates user's manual, Appendix 3: extinction coefficients. http://probes.invitrogen.com/media/pis/mp19000.pdf (accessed May 2008).

(107) Walker, J. M. (**2002**) Nondenaturing polyacrylamide gel electrophoresis of proteins., in *The protein protocols handbook* (Walker, J. M., Ed.) pp 57-60, Humana Press, Totowa, NJ.

(108) Weiss, A., Imboden, J., Shoback, D., and Stobo, J. Role of T3 Surface Molecules in Human T-Cell Activation - T3-Dependent Activation Results in an Increase in Cytoplasmic Free Calcium. *Proc. Natl. Acad. Sci. U.S.A., Biol. Sci.* **1984**, *81*, 4169-4173.

(109) Perantoni, A., and Berman, J. J. Properties of Wilms Tumor Line (Tuwi) and Pig-Kidney Line (Llc-Pk1) Typical of Normal Kidney Tubular Epithelium. *In Vitro* **1979**, *15*, 446-454.

(110) Gu, H. H., Ahn, J., Caplan, M. J., Blakely, R. D., Levey, A. I., and Rudnick, G. Cell-specific sorting of biogenic amine transporters expressed in epithelial cells. *J. Biol. Chem.* **1996**, *271*, 18100-18106.

(111) Pear, W. S., Nolan, G. P., Scott, M. L., and Baltimore, D. Production of High-Titer Helper-Free Retroviruses by Transient Transfection. *Proc. Natl. Acad. Sci. U.S.A.* **1993**, *90*, 8392-8396.

(112) Abbas, A. K., Lichtman, A. H., and Pillai, S. (**2007**) *Cellular and Molecular Immunology*, 6th ed., Saunders Elsevier, Philadelphia, PA.

(113) Spizizen, J., Reilly, B. E., and Evans, A. H. Microbial Transformation and Transfection. *Ann. Rev. Microbiol.* **1966**, *20*, 371-&.

(114) *The material published in this chapter has largely been published in another source, which is under the copyright of IEEE.*

(115) Coudronniere, N., Villalba, M., Englund, N., and Altman, A. NF-kappa B activation induced by T cell receptor/CD28 costimulation is mediated by protein kinase C-theta. *Proc. Natl. Acad. Sci. U.S.A.* **2000**, *97*, 3394-3399.

(116) Kvanta, A., Kontny, E., Jondal, M., Okret, S., and Fredholm, B. B. Mitogen Stimulation of T-Cells Increases C-Fos and C-Jun Protein-Levels, Ap-1 Binding and Ap-1 Transcriptional Activity. *Cell. Signalling* **1992**, *4*, 275-286.

(117) Baier, G. The PKC gene module: molecular biosystematics to resolve its T cell functions. *Immunol. Rev.* **2003**, *192*, 64-79.

(118) Truneh, A., Albert, F., Golstein, P., and Schmittverhulst, A. M. Early Steps of Lymphocyte-Activation Bypassed by Synergy between Calcium Ionophores and Phorbol Ester. *Nature* **1985**, *313*, 318-320.

(119) Paccani, S. R., Tonello, F., Ghittoni, R., Natale, M., Muraro, L., D'Elios, M. M., Tang, W. J., Montecucco, C., and Baldari, C. T. Anthrax toxins suppress T lymphocyte activation by disrupting antigen receptor signaling. *J. Exp. Med.* **2005**, *201*, 325-331.

(120) Ringerike, T., Ulleras, E., Volker, R., Verlaan, B., Eikeset, A., Trzaska, D., Adamczewska, V., Olszewski, M., Walczak-Drzewiecka, A., Arkusz, J., van Loveren, H., Nilsson, G., Lovik, M., Dastych, J., and Vandebriel, R. J. Detection of immunotoxicity using T-cell based cytokine reporter cell lines ("Cell Chip"). *Toxicology* **2005**, *206*, 257-272.

(121) Wikswo, J. P., Prokop, A., Baudenbacher, F., Cliffel, D., Csukas, B., and Velkovsky, M. Engineering challenges of BioNEMS: the integration of microfluidics, micro- and nanodevices, models and external control for systems biology. *IEE Proc., Nanobiotech.* **2006**, *153*, 81-101.

(122) Chang, D. Z., Wu, Z. N., and Ciardelli, T. L. A point mutation in interleukin-2 that alters ligand internalization. *J. Biol. Chem.* **1996**, *271*, 13349-13355.

(123) *The material published in this chapter has largely been published in another source, which is under the copyright of The American Chemical Society.*

(124) Tomlinson, I. D., Gies, A. P., Gresch, P. J., Dillard, J., Orndorff, R. L., Sanders-Bush, E., Hercules, D. M., and Rosenthal, S. J. Universal polyethylene glycol linkers for attaching receptor ligands to quantum dots. *Bioorg. Med. Chem. Lett.* **2006**, *16*, 6262-6266.

(125) Choi, H. S., Liu, W., Misra, P., Tanaka, E., Zimmer, J. P., Ipe, B. I., Bawendi, M. G., and Frangioni, J. V. Renal clearance of quantum dots. *Nature Biotechnol.* **2007**, *25*, 1165-1170.

(126) Wang, S. P., Mamedova, N., Kotov, N. A., Chen, W., and Studer, J. Antigen/antibody immunocomplex from CdTe nanoparticle bioconjugates. *Nano Lett.* **2002**, *2*, 817-822.

(127) Wang, Q., Kuo, Y. C., Wang, Y. W., Shin, G., Ruengruglikit, C., and Huang, Q. R. Luminescent properties of water-soluble denatured bovine serum albumin-coated CdTe quantum dots. *J. Phys. Chem. B* **2006**, *110*, 16860-16866.

(128) Orndorff, R. L., Warnement, M. R., Mason, J. N., Blakely, R. D., and Rosenthal, S. J. Quantum Dot Ex Vivo Labeling of Neuromuscular Synapses. *Nano Lett.* **2008**, *8*, 780-785.

(129) Liu, W., Choi, H. S., Zimmer, J. P., Tanaka, E., Frangioni, J. V., and Bawendi, M. Compact Cysteine-Coated CdSe(ZnCdS) Quantum Dots for in Vivo Applications. *J. Am. Chem. Soc.* **2007**, *129*, 14530-14531.

(130) Liu, W., Howarth, M., Greytak, A. B., Zheng, Y., Nocera, D. G., Ting, A. Y., and Bawendi, M. G. Compact Biocompatible Quantum Dots Functionalized for Cellular Imaging. *J. Am. Chem. Soc.* **2008**, *130*, 1274-1284.

(131) Giljohann, D. A., Seferos, D. S., Patel, P. C., Millstone, J. E., Rosi, N. L., and Mirkin, C. A. Oligonucleotide Loading Determines Cellular Uptake of DNA-Modified Gold Nanoparticles. *Nano Lett.* **2007**, *7*, 3818-3821.

(132) Amara, S. G., and Kuhar, M. J. Neurotransmitter Transporters - Recent Progress. *Ann. Rev. Neurosci.* **1993**, *16*, 73-93.

(133) Blakely, R. D., Defelice, L. J., and Hartzell, H. C. Molecular Physiology of Norepinephrine and Serotonin Transporters. *J. Exp. Biol.* **1994**, *196*, 263-281.

(134) Miller, G. W., Gainetdinov, R. R., Levey, A. I., and Caron, M. G. Dopamine transporters and neuronal injury. *Trends Pharmacol. Sci.* **1999**, *20*, 424-429.

(135) Murphy, D. L., Lerner, A., Rudnick, G., and Lesch, K. P. Serotonin transporter: Gene, genetic disorders, and pharmacogenetics. *Molecular Interventions* **2004**, *4*, 109-123.

(136) Tatsumi, M., Groshan, K., Blakely, R. D., and Richelson, E. Pharmacological profile of antidepressants and related compounds at human monoamine transporters. *European Journal of Pharmacology* **1997**, *340*, 249-258.

(137) Barker, E. L., and Blakely, R. D. (**1995**) Norepinephrine and serotonin transporters: Molecular targets of antidepressant drugs, in *Psychopharmacology: The Fourth Generation of Progress* (Bloom, F. E., and Kupfer, D. J., Eds.) pp 321-333, Raven Press, New York.

(138) Federal Trade Commission. Analysis of Proposed Consent Order to Aid Public Comment In the Matter of Pfizer Inc., and Warner-Lambert Company. http://www.ftc.gov/os/2000/06/pfizeranalysis.htm (accessed June 2008)

(139) Schroeter, S., Levey, A. I., and Blakely, R. D. Polarized expression of the antidepressant-sensitive serotonin transporter in epinephrine-synthesizing chromaffin cells of the rat adrenal gland. *Mol. Cell. Neurosci.* **1997**, *9*, 170-184.

(140) Qian, Y., Galli, A., Ramamoorthy, S., Risso, S., DeFelice, L. J., and Blakely, R. D. Protein kinase C activation regulates human serotonin transporters in HEK-293 cells via altered cell surface expression. *J. Neurosci.* **1997**, *17*, 45-57.

(141) Ramamoorthy, S., Giovanetti, E., Qian, Y., and Blakely, R. D. Phosphorylation and regulation of antidepressant-sensitive serotonin transporters. *J. Biol. Chem.* **1998**, *273*, 2458-2466.

(142) Lesch, K. P., Bengel, D., Heils, A., Sabol, S. Z., Greenberg, B. D., Petri, S., Benjamin, J., Muller, C. R., Hamer, D. H., and Murphy, D. L. Association of anxiety-related traits with a polymorphism in the serotonin transporter gene regulatory region. *Science* **1996**, *274*, 1527-1531.

(143) Koldzic-Zivanovic, N., Seitz, P. K., Cunningham, K. A., Thomas, M. L., and Hughes, T. K. Serotonin regulation of serotonin uptake in RN46A cells. *Cell Mol. Neurobiol.* **2006**, *26*, 979-87.

(144) Zhou, F. C., Xu, Y., Bledsoe, S., Lin, R., and Kelley, M. R. Serotonin transporter antibodies: production, characterization, and localization in the brain. *Mol. Brain Res.* **1996**, *43*, 267-278.

(145) Sur, C., Betz, H., and Schloss, P. Immunocytochemical detection of the serotonin transporter in rat brain. *Neuroscience* **1996**, *73*, 217-231.

(146) Kohls, M. D., Majer, K. A., Russell, B. J., Han, Q., Blakely, R. D., and Lappi, D. A. A monoclonal antibody to an extracellular domain of the serotonin transporter: Characterization and targeting properties. *Soc. Neurosci. Abstr.* **2001**, *27*, 2153.

(147) Tomlinson, I. D., Mason, J. N., Blakely, R. D., and Rosenthal, S. J. High affinity inhibitors of the dopamine transporter (DAT): Novel biotinylated ligands for conjugation to quantum dots. *Bioorg. Med. Chem. Lett.* **2006**, *16*, 4664-4667.

(148) Tomlinson, I. D., Warnement, M. R., Mason, J. N., Vergne, M. J., Hercules, D. M., Blakely, R. D., and Rosenthal, S. J. Synthesis and characterization of a pegylated derivative of 3-(1,2,3,6-tetrahydro-pyridin-4yl)-1H-indole (IDT199): A high affinity SERT ligand for conjugation to quantum dots. *Bioorg. Med. Chem. Lett.* **2007**, *17*, 5656-5660.

(149) Warnement, M. R., Tomlinson, I., Chang, J. C., Luckabaugh, C. M., and Rosenthal, S. J. Controlling the reactivity of ampiphilic quantum dots in biological assays through hydrophobic assembly of custom PEG derivatives. *Bioconjugate Chem.* **2008**, *In Press*.

(150) Gordon, J., and Barnes, N. M. Lymphocytes transport serotonin and dopamine: agony or ecstasy? *Trends Immunol.* **2003**, *24*, 438-443.

(151) Schifferli, K. P., and Ciccarone, V. Optimization of cationic lipid reagent-mediated transfection for suspension cell lines. *Focus* **1996**, *18*, 45-47.

(152) Mason, J. N., Tomlinson, I. D., Iwamoto, H., Warnement, M. R., DeFelice, L. J., Blakely, R. D., and Rosenthal, S. J. Novel fluorescent substrates for the serotonin, dopamine, and norepinephrine transporters. **In Preparation**.

(153) Warnement, M. R., Tomlinson, I. D., and Rosenthal, S. J. Fluorescent imaging applications of Quantum Dot probes. *Curr. Nanosci.* **2007**, *3*, 273-284.

(154) Carneiro, A. M. D., Cook, E. H., Murphy, D. L., and Blakely, R. D. Interactions between integrin alpha IIb beta 3 and the serotonin transporter regulate serotonin transport and platelet aggregation in mice and humans. *J. Clin. Invest.* **2008**, *118*, 1544-1552.

(155) Schwartz, J. W., Blakely, R. D., and DeFelice, L. J. Binding and Transport in Norepinephrine Transporters. Real-Time, Spatially Resolved Analysis in Single Cells Using a Fluorescent Substrate. *J. Biol. Chem.* **2003**, *278*, 9768-9777.

(156) Mason, J. N., Farmer, H., Tomlinson, I. D., Schwartz, J. W., Savchenko, V., DeFelice, L. J., Rosenthal, S. J., and Blakely, R. D. Novel fluorescence-based approaches for the study of biogenic amine transporter localization, activity, and regulation. *Journal of Neuroscience Methods* **2005**, *143*, 3-25.

(157) Lyapustina, S. A., Metelitsa, A. V., Bulgarevich, D. S., Alexeev, Y. E., and Knyazhansky, M. I. The twisted-intramolecular-charge-transfer-state-forming compound as a guest for cyclodextrins. *J. Photochem. Photobiol., A* **1993**, *75*, 119-123.